attoAPPLICATIONS
Where Ideas Become Results

Application Notes

Where Ideas Become Results

attocube
pioneers of precision

attoMICROSCOPY
Sophisticated Tools for Science

attoMOTION
Piezo-based Nanopositioners

attoSENSORICS
Ultra Precision Sensors

attoMICROSCOPY
Sophisticated Tools for Science

attoMICROSCOPY
Sophisticated Tools for Science

MFM imaging of a Skyrmion lattice and a helimagnetic phase in the attoDRY1000

Balázs Sipos, Thomas Scheler
attocube systems, Munich, Germany

Introduction

Currently, magnetic skyrmions are one of the most studied phenomena in magnetic materials. The structure was originally proposed in particle physics by Tony Skyrme in 1962 [1] as a result of his unified field theory. However, it turned out that these topological objects exist in many more areas than just in high-energy physics. Similar structures have been reported in liquid crystals, superconductors, and magnetic materials.

A skyrmion can be best pictured as a magnetic frozen tornado. However, in a magnetic material they consist of local spins that form the whirl rather tQhan wind (Figure 1). Like tornados, magnetic skyrmions are exceptionally stable through their geometric construction. This topological stability enables them to be a candidate for magnetic storage. A commercial hard disc drive (HDD) is an array of 2D topological magnetic structures, i.e. the domain walls. However, there are size limitations to how small a magnetic domain can be. Following the discovery of skyrmions by neutron scattering [2], skyrmions as small as 1 nm have been observed [3,4], promising storage densities far beyond the current limitations. Furthermore, in a magnetic structure the energy required to change its state is proportional to the number of spins it contains. The reduced size of a skyrmion not only allows for higher storage densities but also more energy-efficient writing. Recently, N. Romming and co-workers reported on the first artificial creation and annihilation of a single skyrmion [5]. This manifested in effect the first writing experiment, confirming their potential for applications in information-technology.

The potential use of skyrmions in magnetic storage is just one of the many reasons why studying their dynamics and individual properties are of the upmost interest. To achieve more insight into these questions, it is important to be able to study them in real space. Select one, see how

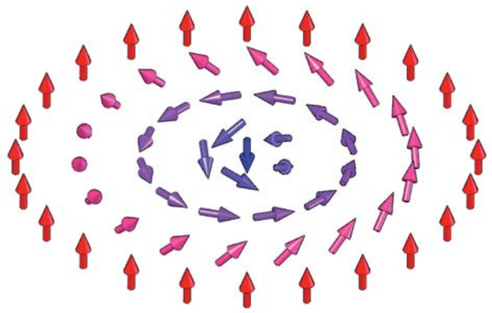

Figure 1: *Spin arrangement in a single skyrmion.*

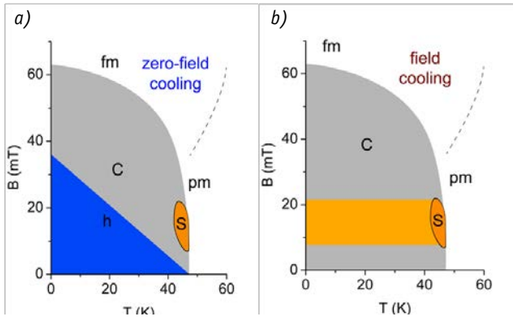

Figure 2: *a) Phase diagram of $Fe_{0.5}Co_{0.5}Si$ in zero field cooling (zfc). The location of the pocket where the skyrmions are present (S) is very small and its boundaries are strongly sample dependent. h denotes the helimagnetic phase, C is a conical phase, fm is ferromagnetic and pm is paramagnetic. b) The phase diagram under field cooling for field values in the range of the skyrmion lattice phase. It is important to see that contrary to the zfc case, under field cooled conditions the skyrmion lattice is extended to the lowest temperatures. Figure adapted from [3].*

they move, appear, and disappear. In this application note we show the observation of the skyrmion lattice and its dynamics in a bulk $Fe_{0.5}Co_{0.5}Si$ crystal with a low temperature MFM in a cryogen-free environment similar to the first real space observations shown on this material by Peter Milde and co-workers [6].

$Fe_{0.5}Co_{0.5}Si$ is a material without an inversion symmetry. This property is important because it allows the formation of skyrmions. The measurements reported in this application note were performed on a single crystal sample of this material (courtesy of A. Bauer and C. Pfleiderer, Technical University of Munich, Germany). The sample, despite being a bulk crystal, exhibits exceptional surface quality with a surface roughness of less than 1 nm. From the phase diagram (see Figure 2), one can see that the skyrmion lattice phase, stable only under certain B–T–conditions, can be transferred into a metastable state at lower temperatures by field-cooling. This not only makes it easier to find the interesting phases, but lowering the temperature also increases the magnetic signal, due to reduced fluctuations in the sample.

Experimental Setup

The measurements were carried out in an attoDRY1000. The attoDRY1000 is attocube's answer to the continuously shrinking helium supplies and skyrocketing He prices. It is a cryogen-free measurement platform specially designed for scanning probe experiments. For the measurement a standard attoAFM/MFM I was used. To have the best possible lateral resolution, we chose a Nanosensors SSS-type magnetic tip.

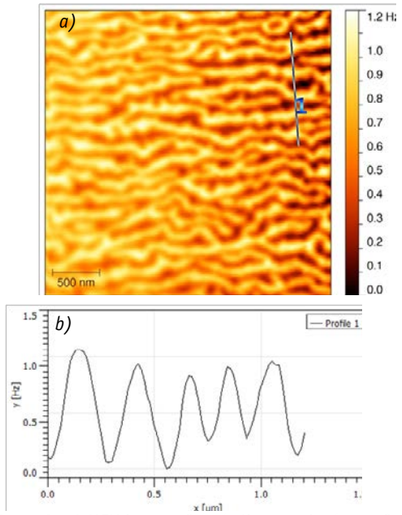

Figure 3: *a) MFM image of the helimagnetic phase of $Fe_{0.5}Co_{0.5}Si$. The measurement was carried out at 3.2 K under zero magnetic field. b) Line profile of the MFM phase shift along the line cut 1. The periodicity of the stripes is between 100 and 250 nm.*

Measurement Results

We measured both the helimagnetic and the skyrmion lattice phase. For the former, we cooled the sample in zero magnetic field to 3.22 K. The results are shown in Figure 3. The periodicity of the magnetic structure is between 100 and 250 nm as it can be seen from the line cut.

After measuring the helimagnetic phase the sample was warmed up to 60 K, the magnetic field raised to 15 mT, and the sample cooled again to 3.44 K. At this temperature several images were taken at varying magnetic fields to see the effect of the field on the metastable skyrmion lattice (Figure 4). As the magnetic field decreases, a few skyrmions start to fuse into larger structures. Furthermore, at -30 mT, the helimagnetic phase is abruptly restored. We did not observe the gradual transition described by Milde et al. [6]. This may be due to the significantly lower temperature, where reduced magnetic fluctuations make the skyrmions more stable.

In a subsequent series of measurements, the magnetic field was reduced to zero and temperature increased to 10 K to induce thermal effects and increase magnetic fluctuations. A series of 28 images on the same area was taken over time. The time between frames was approximately 30 min with 15 min frame time. From frame to frame, a slight reordering of the helimagnetic lines can be seen, usually in the form of two previously separated lines snapping into contact.

Summary

In this application note we showed the very first real space observation of skyrmions with MFM in a cryogen free cryostat. The setup used is a standard commercially available

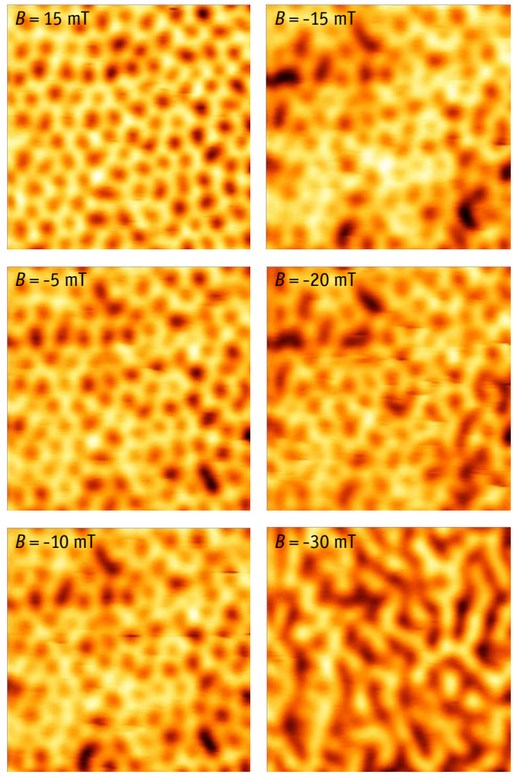

Figure 4: *MFM image of the skyrmion phase of $Fe_{0.5}Co_{0.5}Si$ (scan size is 1.5 µm x 1.5 µm). The sample was first cooled down from 60 K under 15 mT magnetic field to 3.4 K. Then the field was gradually changed to 5 mT, -10 mT, -15 mT, -20 mT and -30 mT in that order, and a new image was acquired at each field. On the figures one can see the skyrmions starting to merge already at -5 mT and they abruptly disappear at -30 mT.*

attoAFM/MFM in an attoDRY1000. We hope that this will greatly facilitate the understanding of these exotic magnetic structures and accelerate their introduction into commercial applications.

We would like to thank Jan Seidel, University of New South Wales, Sydney, Australia for communicating the sample and fruitful discussions. We gratefully acknowledge A. Bauer and C. Pfleiderer, Technical University of Munich, Garching, Germany for preparing and providing the $Fe_{0.5}Co_{0.5}Si$ sample.

References

[1] T. H. R. Skyrme, Nucl. Phys. **31**, 556-560 (1962).
[2] S. Mühlbauer et al., Science **323**, 915 (2009).
[3] X. Z. Yu et al., Nature **465**, 901 (2010).
[4] S. Heinze et al Nature Physics **7**, 713 (2011)
[5] N. Romming et al., Science **341**, 636 (2013).
[6] P. Milde et al., Science **340**, 1076 (2013).

pioneers of precision

Cryogenic Raman and Electronic-Raman Scattering Measurements using the attoRAMAN at High Magnetic Fields

Claudio Dal Savio, Khaled Karraï
attocube systems AG, Munich, Germany

Clement Faugeras, Piotr Kossacki, Marek Potemski
LMCMI-Grenoble, CNRS-UJF-UPS-INSA, France

Introduction

The electronic properties of graphene are very much reminiscent of high quality layered semiconductors devices. Such two dimensional layered systems do exhibit striking electrical and optical properties at cryogenic temperatures and under strong magnetic fields.

Very pure graphene can be obtained in form of tiny flakes of few µm² by exfoliating the surface of high quality natural single crystal of graphite. In many cases the flakes are however so small that a micro-Raman setup is necessary to localize them and to measure their properties. We have designed and built a high resolution confocal microscope capable of Raman spectroscopy of surfaces at low temperature and high magnetic fields.

Experimental Setup

The attocube cryogenic Raman spectroscopy system combines a high resolution, low temperature confocal microscope with an ultra-sensitive Raman spectrometer (see Figure 1 and 2). This innovative product enables state-of-the-art confocal Raman measurements at cryogenic environments and can be combined with liquid Helium cryostats (magnetic fields up to 16 T) or cryogen-free cryostats (magnetic fields up to 9 T). The attoRAMAN is a ready-to-use system and comes typically with a Raman laser source (frequency doubled or tripled Nd:YAG [532 nm, 355 nm] or HeNe [632.8 nm]), an ultra-high throughput spectrometer including a Peltier-cooled, back-illuminated CCD, and a state-of-the-art Raman controller/ software package.

The microscope uses a set of attocube xyz-positioners for coarse positioning of the sample over a range of several mm. Developed particularly for cryogenic applications, the piezo scanner ANSxy100 provides a scan range of 30 x 30 µm² even at liquid helium temperature.

Measurement Results

Raman spectra have been acquired on a single exfoliated graphene flake with a 532 nm laser source at 7 K. A typical result is presented in Figure 3: the green spectrum was acquired at $B = 0$ T field and shows the characteristic E_{2g} and D bands. With high magnetic field applied ($B = 9$ T) an electronic Raman band appears at around 1800 cm^{-1}, the energy of which depends on the field strength.

In the presence of magnetic field the continuous spectrum of electronic excitations becomes discrete and splits into excitonic Landau levels characteristic of a 2D system. By sweeping the magnetic field, optically active inter-Landau level transitions are tuned in resonance with the E_{2g} phonon excitation, resulting in avoided crossings in the field evolution of the graphene Raman spectra. The signature of electron-phonon hybridization is presented in the following measurements.

Field evolution of Raman spectra on graphene

We map the Raman scattering signal over an area of 7 x 7 µm² centered onto a single graphene flake with 0.5 µm spatial resolution. Figure 4 shows different scattering bands – namely red-shifted (left), centered (center) and blue-shifted (right) from the E_{2g} phonon peak at $B = 4.3$ T and $B = 5.3$ T. These two magnetic fields are chosen to be just below and just above the resonant condition for hybridization. As expected, at $B = 4.3$ T the graphene flake appears bright in the blue shifted image (lower right), it appears bright in the red shifted image at $B = 5.3$ T, while it is dark in the Raman scattering mapping centered on the E_{2g} (both center images).

© attocube systems AG, 2014. All rights reserved.

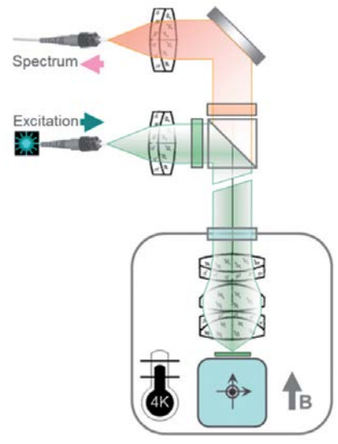

Figure 1: *Schematics of the confocal microscope.*

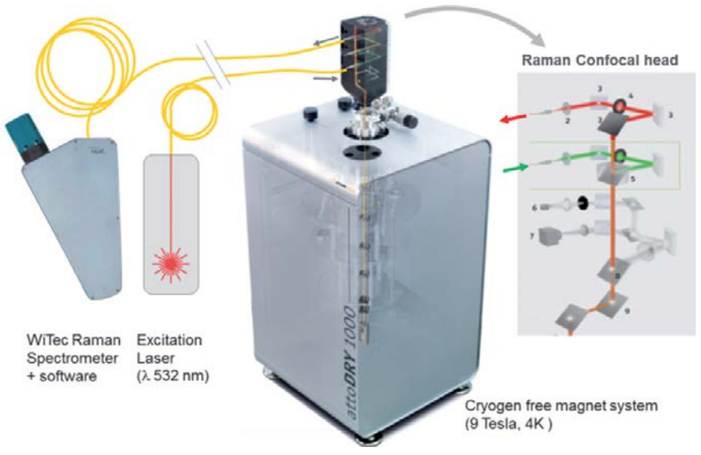

Figure 2: *Low temperature and high magnetic field Raman setup in the configuration with a 9 T cryogen-free cryostat.*

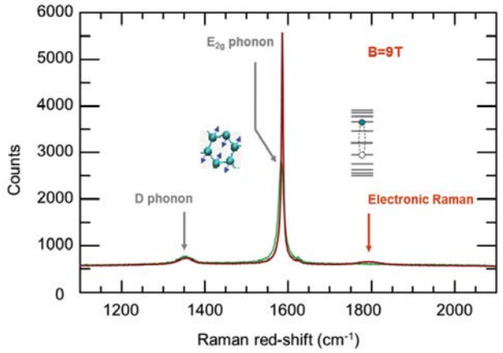

Figure 3: *Raman spectra of graphene acquired at 7 K and at B=0 T (red) and B=9 T (green) showing a magnetic field dependent band at 1800 cm^{-1}.*

The lower right side of Figure 4 shows the magnetic field evolution of Raman spectra recorded in the center of the graphene flake where the hybridization of E_{2g} phonon and (-2, +1) and (-1,+2) magneto-exciton takes place. For comparison, the E_{2g} phonon band on the graphite substrate just a few micrometers away doesn't show any dependence on the magnetic field (left side).

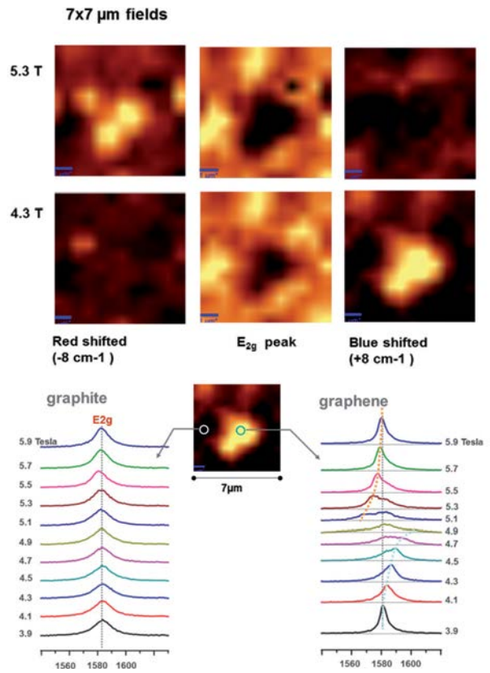

Figure 4: *Raman mapping of a graphene flake on graphite. The magnetic fields values (B=4.3 T and B=5.3 T) are chosen to be just below and just above the resonant condition for electron-phonon hybridization.*

The evolution of the E_{2g} band while sweeping the magnetic field from -9 T to +9 T is shown in Figure 5. As expected the data show a series of avoided crossing when the E_{2g} phonon energy is resonant with the electron-hole separation between the valence and conduction Landau levels (-N, +M) of the Dirac cone. Furthermore, the field dependent electronic Raman features in the spectra and their field dependence are clearly resolved.

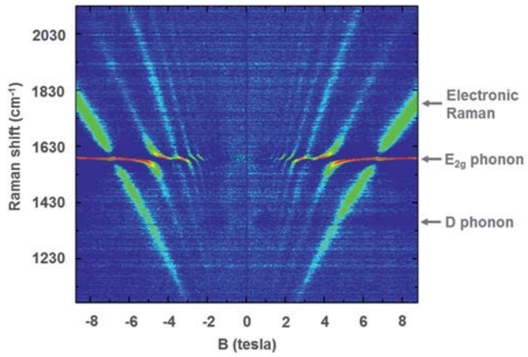

Figure 5: *Micro-Raman spectra of a graphene flake as function of the magnetic field. The spectrum at B=0 T has been subtracted.*

Summary

Magneto-Raman measurements were performed with unprecedented spatial resolution (0.5 µm) on an exfoliated single crystal of natural graphite, exposed to magnetic fields of up to 9 T at 7 K. The data were recorded on a single graphene flake and clearly show electron-phonon resonances in the spectra. Resonant hybridization of the E_{2g} phonon with excitons is a specific signature of graphene flakes which display very rich Raman scattering spectra varying strongly as a function of magnetic field [1].

The measurements were performed in the attocube application labs (2011), in cooperation with C. Faugeras, P. Kossacki, and M. Potemski, LNCM I - Grenoble, CNRS-UJF-UPS-INSA France.

References

[1] C. Faugeras, M. Amado, P. Kossacki, M. Orlita, M. Kühne, A.A.L. Nicolet, Yu. I. Latyshev, and M. Potemski, *„Magneto-Raman Scattering of Graphene on Graphite: Electronic and Phonon Excitations"*, Phys. Rev. Lett. **107**, 036807 (2011).

Resonance Fluorescence Spectroscopy of a single quantum dot with the attoCFM I

Elena Kammann[1], Sebastian H. E. Müller[1], Katja Puschkarsky[2], Matthias Hauck[2], Sarah Beavan[2], Alexander Högele[2], and Khaled Karraï[1]
[1]attocube systems AG, Munich, Germany
[2]Ludwig Maximilian Universität, Munich, Germany

I. Introduction

Resonance fluorescence spectroscopy of semiconductor quantum dots (QDs) [1, 2, 3, 4, 5] and other single photon emitters, such as vacancy centers [6] often yields more information about the emitters than the more commonly used non-resonant excitation. However it is a technically challenging measurement to perform. The difficulty lies within the separation of the excitation laser photons from the re-emitted and scattered photons. One way in which this can be achieved is by means of polarization suppression: in a geometry where the scattered laser photons have a well-defined polarization, they can be filtered from the detected signal facilitating the detection of resonance fluorescence (RF). The confocal microscope presented in section II is designed to combine a high polarization extinction ratio (ER) for efficient RF measurements with low temperature and high magnetic field compatibility. In particular we present the first low temperature microscope with apochromatic performance in the near-infrared spectral range. Such a setup allows for convenient switching between resonant and non-resonant excitation without the need for re-alignment, as shown in II.3.

In order to demonstrate the functionality of the instrument in high spatial and spectral resolution spectroscopy, we performed measurements on single gate-voltage controlled QDs, such as described in section III. Section IV describes the first observation of RF, as well as the associated Mollow triplet [7], obtained with a commercially available system.

II. The cryogenic confocal optical microscope

In this section, the measurement setup and its basic characteristics are described. The cryo-compatible microscope head is outlined in sub-section II.1 and subsequently the excitation lasers and the detectors used for the experiments are presented in II.2 and II.3 respectively. The characteristics of the low temperature apochromatic objectives are discussed in subsection II.4 and details on the polarization suppression can be found in subsection II.5.

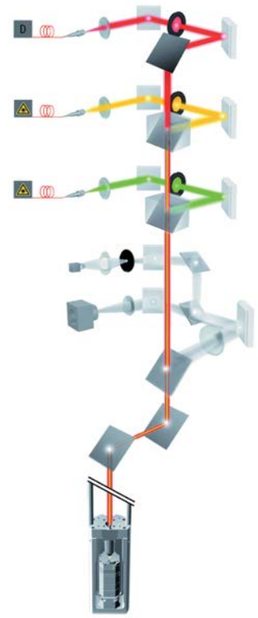

Figure 1: *3D-Scheme of the attoCFM I consisting of two excitation channels (green and yellow) and one detection channel (red), the inspection optics (light grey), for wide field imaging of the sample. The housing comprised of the objective and the 3D positioning system, which carries the sample, is located in the cryogenic space.*

Figure 2: *Schematic of the polarization suppression option. An excitation laser (1.) is coupled into the microscope by a single mode fiber (2.) and a collimation lens (3.). The polarization is defined by a nanoparticle plate polarizer on a rotator (4.) such that the excitation light is reflected by the polarizing beam splitter cube (5.). A quarter-wave plate (6.) allows for switching between suppression and transmission mode. The cold space is separated by an optical window (7.) and the light is focused by an apochromatic low temperature objective (8.) onto a sample mounted on a piezo positioning stack (9.). The p-polarized fraction of the collected light passes to the detection channel and is recorded with a photodetector (10.).*

II.1. The optical microscope

The optical setup is based on the attoCFM I, attocube's commercial confocal microscope designed specifically for applications at low temperature and high magnetic field. The microscope head, shown in Figures 1 and 2 includes several excitation and detection channels, as well as an inspection unit allowing for wide field imaging of the sample. We took particular care during the design of the microscope head to achieve high mechanical rigidity of the structure, resulting in unprecedented stability against drift [8]. Furthermore, the excitation and collection paths can be aligned separately, which facilitates a straight-forward and systematic alignment procedure. The head is mounted onto a microscope stick which is inserted in a thin wall stainless steel vacuum tube. This vacuum tube, filled with low pressure, pure helium exchange gas, in turn is cooled in a top loading ultra-low vibration closed cycle cryostat (attoDRY1000) to temperatures in the lower Kelvin range. Alternatively, the microscope and its insert can be plunged in a bath of liquid helium in a standard dewar.

The objective and the sample position handling are rigidly mounted in a common compact housing of 49 mm in diameter and placed at the bottom of the microscope stick. The compact microscope head experiences a homogeneous temperature at all times, preventing drifts due to temperature gradients. The excitation light is collimated in the head assembly, enters through a vacuum sealed window on the top of the stick and propagates freely to the objective's back aperture. The re-emitted or scattered light traces back the same pathway back to the detection unit. The sample is held by a piezo-positioner stack, allowing for precise positioning and focusing at cryogenic temperatures.

II.2. Laser excitation sources

A single mode laser diode, tunable from 920 - 980 nm (Sacher Lion Metcalf Laser System TEC500) is used for resonant spectroscopy. For the non-resonant excitation a laser diode at 850 nm (Roithner Lasertechnik GmbH, LJ-series) is used. Both lasers are coupled into single mode fibers and launched into the fiber ports of the microscope. In order to retain the collimation, excitation and collection, fibers are permanently attached to the microscope head and the different lasers were coupled by using fiber connectors.

II.2. Detection system

The emission is collected through a single mode fiber and detected with a spectrometer or an avalanche photo diode (APD, <100 dark counts by Excelitas) connected to a gated photon counter. A home-made Fabry-Pérot tunable filter is used in order to spectrally resolve the emission with a resolution of 100 MHz. Beneath the sample the transmitted intensity is recorded on a photodiode. The gate voltage applied on the sample was modulated around the average voltage value at 77 Hz with a square wave form. The signal demodulated by a lock-in amplifier yielded the differential transmission of the quantum dot [9]. The average gate voltage value was swept continuously. This in turn tunes the QD optical transition through the resonance with the excitation laser by means of the quantum confined Stark Effect.

II.3. The apochromatic objective

The mapping, localization and characterization of an appropriate single quantum emitter prior to the resonant experiment were performed under non-resonant excitation. In this context, the use of a standard aspheric lens is problematic [10] because of chromatic aberrations that yields different focal planes for the non-resonant excitation laser and the resonant laser/emission. While achromatic performance is generally assumed as given in confocal microscopy at room temperature, this is not trivial for cryogenically cooled microscopes. To eliminate this problem, low temperature-compatible objectives with an apochromatic range in the near infrared (700 - 1010 nm) were designed. The apochromatic range is defined as the range of wavelengths that focus within the depth of focus, given by $n\lambda_{ref}/NA^2$, where λ_{ref} is chosen to maximize the apochromatic range and n is the index of refraction. This range is relevant for a number of applications, including cryogenic spectroscopy of III-V alloy QDs.

Figure 3 shows the calculated focal shift as a function of wavelength for the three apochromatic objectives currently available from attocube systems. The focal shift of an aspheric lens typically used in RF experiments [2] is also shown for comparison. In our experiments the QDs emit at around 960 nm and the non-resonant excitation is performed at 850 nm. The chromatic focal shift between those two wavelengths of the aspheric lens amounts to 8 µm, whilst the shift for the LT-APO/IR/0.75 remains below the depth of focus of 1.7 µm, which demonstrates the superiority of the apochromatic objectives.

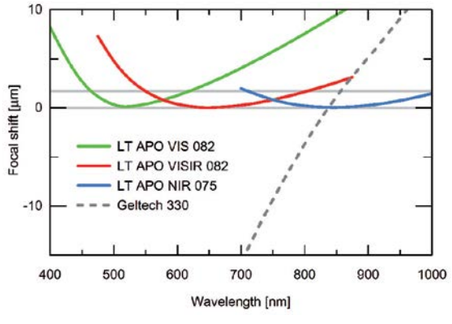

Figure 3: *Calculated focal plane shift as a function of wavelength for the 3 apochromatic objectives available at attocube systems. The Geltech 330 is often used in RF measurements [2] but shows extremely poor achromatic behavior making it very difficult to use for combined luminescence and resonant spectroscopy. For the LT-APO/IR/075 the calculated focal displacement remains within the diffraction limited depth of focus of 1.7 µm indicated by the grey line for the LT-APO/NIR/075 (for λ_{ref} = 955 nm).*

APPLICATION NOTE
Resonance Fluorescence Spectroscopy of a single quantum dot with the attoCFM I
attoMICROSCOPY
Sophisticated Tools for Science
pioneers of precision
© attocube systems AG, 2014. All rights reserved.

The effective focal length of the LT-APO/IR/0.75 is 3.13 mm, the working distance of 0.65 mm is compatible with the use of solid immersion lenses, and the clear aperture of 4.7 mm is adapted to the collimation optics.

II.4. Polarization suppression

The key parameter of a polarization darkfield microscope is the extinction ratio, namely $ER = I_{max}/I_{min}$, where I_{max} corresponds to the intensity of photons reflected from the sample and detected in a collinear configuration of the polarizer and the analyzer, and I_{min} is obtained in a cross-polarized configuration. In an ideal system I_{min} is zero and the ER diverges, but in reality it corresponds to the imperfection of the cross-polarization scheme and is called the leakage signal. For an RF measurement on a single semiconductor QD the extinction ratio ER should exceed 10^5 in order to detect a reasonable ratio of the weak QD signal relative to the shot-noise inherent to the laser leakage background.

In the confocal microscope the polarization optics are integrated according to the scheme in Figure 2. A polarizing beam splitter cube is placed into the lower unit (excitation unit), which reflects the *s*-polarized light towards the sample. The laser reflected back from the sample is directed back into the excitation channel such that only residual laser light enters the collection optics. The back-scattered laser light in this configuration is suppressed by about 3 orders of magnitude. In order to increase the extinction, plate polarizers are inserted into the excitation and the detection channels where they support the action of the cube polarizer (4. in Figure 2). Precision attocube stepping piezo rotators (ECR4040AP) are crucial for the sensitive alignment of the polarizers along the axes of the polarizing cube [2]. The configuration of the microscope can be switched from maximum extinction to maximum transmission by rotating a quarter-wave plate beneath the microscope on a second attocube rotator. The quarter-wave plate also reverses ellipticities that are unintentionally induced along the beam path in the microscope, which requires ultra-precise alignment facilitated by ECR4040AP rotator. The system is aligned in the maximum transmission configuration and the ratio of the minimum and maximum values measured in the two configurations correspond to the extinction ratio.

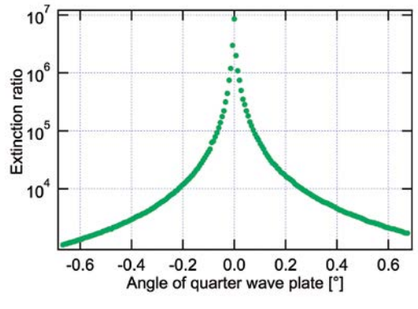

Figure 4: *The extinction ratio plotted as a function of the angle of the quarter wave plate. In a narrow angular region of about 30 m° the extinction exceeds six orders of magnitude ultimately demonstrating the need for high resolution piezo-driven rotators.*

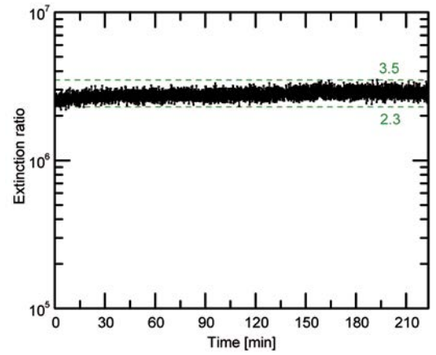

Figure 5: *The extinction ratio tracked over a period of 3.5 hours.*

For maximization of the *ER* the rotators carrying the polarizers and the waveplate are rotated until the ratio between I_{max} und I_{min} is maximized. In Figure 3 the evolution of the extinction ratio as a function of the orientation of the wave-plate is shown. It is observed that for a very small angular range within 30 m° only, the extinction ratio is adjusted to exceed 10^6 rendering piezo-driven rotators, such as the ECR4040AP, essential for reaching extreme extinctions.

Further, we observed that these extremely high extinctions ratio can only be reached when the tunable narrow band external cavity laser diode is used (Sacher Metcalf). In a comparison experiment using a standard laser diode (Roithner Lasertechnik GmbH, 960 nm) a dependency of the extinction

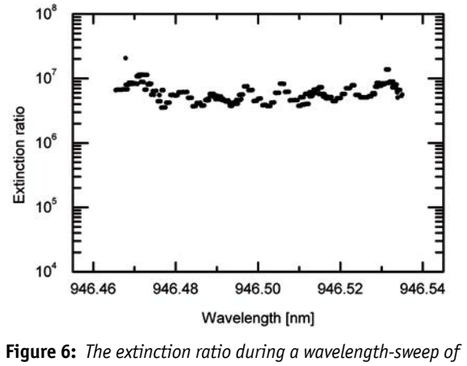

Figure 6: *The extinction ratio during a wavelength-sweep of ~70 pm.*

on the quality of the laser is observed. Using the narrowband source an extinction of 3 x 10^7 was reached, whilst using the diode laser the extinction was limited to 1.8 x 10^6, with the exact same optical alignment. Using a 905 nm laser diode, the extinction is limited to the 10^5 range. This observation can be attributed to the excess non lasing background photons in diode lasers used without internal spectral filtering, such as the latter two laser diodes. In general it is found that the extinction ratio that can be achieved varies between 10^6 and 10^8, when the tunable diode laser is employed.

In order to carry out long and demanding experiments on single photon emitters the stability of the *ER* over time is of utmost importance. The stability of the extinction is demonstrated by tracking the counts on the APD over more than 3 hours. The *ER* during this period remains strictly above 10^6 (see Fig. 5).

Finally we show that the setup can also be used for single quantum emitters without a gate-tunable resonance, where instead of the gate voltage the wavelength can be swept across the resonance. In Figure 6 the *ER* is shown as a function of wavelength for a narrow band wavelength-sweep of ~70 pm. For comparison the linewidth of a QD resonance is of the order of 5 pm. We observe that for this range the *ER* remains well above 10^6.

III. The sample

The sample under investigation contains self-assembled InGaAs QDs grown by molecular beam epitaxy [11] embedded inside a field effect device [12] (see Fig. 7) grown at UC Santa Barbara in the group of P. M. Petroff. The QD heterostructure can be controlled by a semitransparent top electrode formed by a thin semi-transparent layer of NiCr, which is evaporated on the surface of the sample. The gate voltage which can be applied to the top electrode shifts the QD resonances with respect to the Fermi level. This allows for charge carriers to be loaded one by one into the QD [13]. Furthermore the exciton emission energy can be tuned by means of the quantum confined Stark effect [14].

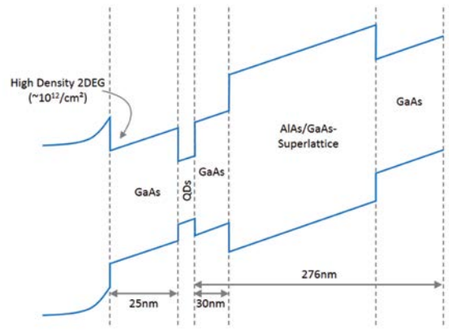

Figure 7: *Band-structure schematic of the sample.*

IV. Resonance fluorescence measurements

In this section the measurement strategy to obtain RF data with a gate tunable QD sample is outlined and the results from the different steps are discussed.

In the first step an appropriate QD for the RF investigation is selected by mapping the photoluminescence spectrum as a function of the gate voltage. The sample is excited off-resonantly by the 850 nm laser diode and the emission is directed to the grating spectrometer. At this stage the microscope should already be roughly adjusted to the suppression mode, such that the laser does not enter the collection fiber and the fluorescence thereof is minimized. The QD modes are easily identifiable in a PL-map (Fig. 8), according to reference 13.

For the RF experiments we chose to investigate the negatively charged exciton X^{1-} as the transition is unpolarized at zero magnetic field [15]. Consequently the resonant fluorescence has significant emission with a polarization orthogonal to the excitation laser. Furthermore the X^{1-} emission is not expected to depend on the crystallographic orientation of the QD, as it would for an X^0.

Next the gate voltage is tuned to favor X^{1-} stable photoluminescence and the resonant laser is adjusted on the spectrometer to the X^{1-} emission wavelength. The *ER* can now be conveniently maximized by minimizing the laser background counts on the spectrometer. At this point the microscope is adjusted to the suppression mode and ready for the RF measurements.

Simultaneously with the RF differential transmission is also acquired [9] for the sake of direct comparison. To this end the gate voltage is modulated with amplitude of 200 mV whilst scanned and the differential transmission is recorded by means of the transmission photodiode and demodulated, using a lock-in amplifier. At the same time the fluorescence photons, which are collected through the collection path of the microscope are recorded on the avalanche photodi-

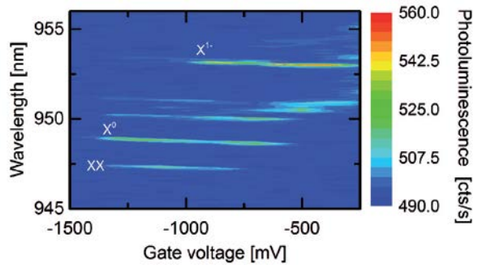

Figure 8: *The photoluminescence spectra as a function of the gate voltage. Here, three different charge states of the quantum dot is revealed through its various exciton emission lines (Neutral exciton X^0, negatively charge exciton X^{1-}, and biexciton XX)*

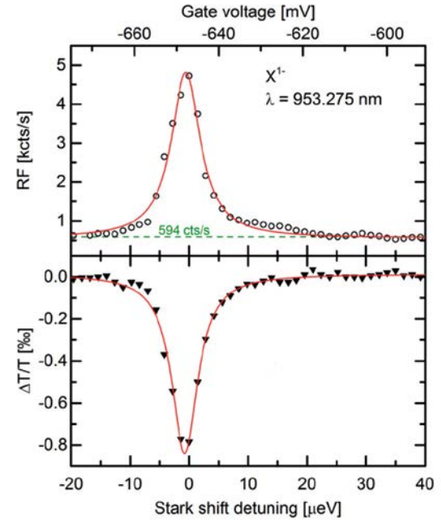

Figure 9: *Simultaneously taken RF (empty circles in the upper panel) and differential transmission spectra (filled triangles in the lower panel) with the corresponding Lorentzian fits. The extinction ratio amounts to 10^6.*

ode. Taking both measurements simultaneously allows for a direct comparison between the two techniques. Figure 8 displays the simultaneously taken differential transmission and RF spectra.

Both the resonant transmission and fluorescence were measured and analyzed over a broad range of powers. The detection counts of the resonant emission signal are displayed in Figure 10 (a). A clear saturation of the fluorescence counts can be observed. The linewidth (Fig. 10 (b)) increases monotonically due to power broadening, which can be monitored in both resonant measurements. A larger range of powers is accessible to the RF, as the differential transmission contrast fades in the noise level at high laser powers (Fig. 10 (c)). The largest signal to noise ratio (Fig. 10 (d)) in transmission and in fluorescence is marked by the vertical dotted line and it coincides with the inflection point of the differential transmission contrast. We find that the signal to noise ratio is about three times higher in RF measurements, as it is in transmission, making the RF a powerful high resolution spectroscopy technique.

It should be pointed out that the impressive high light emission rates of several hundred thousands of counts per second that has been achieved in ref. 2, was not observed in the present measurements due to the sample quality. First, the low power linewidth limit amounts to ~6 μeV being much broader than the usual 1 to 2 μeV measured on better QDs[2]. We noticed that the low fluorescence yield of the sample is already present in PL measurements where the counts saturate at ~1000 cts. This number is far from the estimated counts according to the cycling rate correspond-

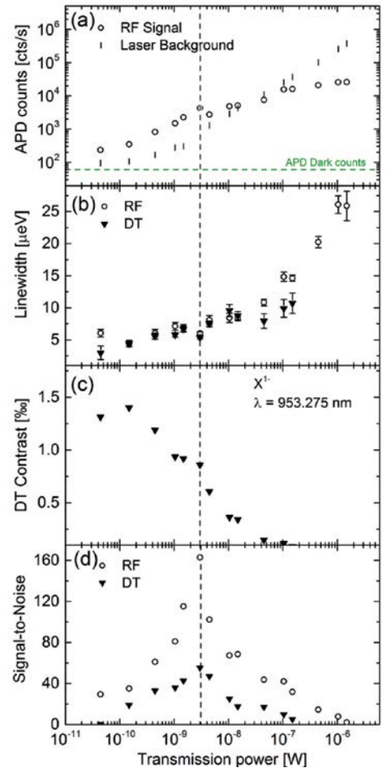

Figure 10: *Power dependence of a single quantum dot resonant transmission and resonance fluorescence. (a) The RF counts (circles) and the background counts from the laser (vertical lines). (b) Line-widths at half maximum extracted from a Lorentzian fit to the data. (c) Signal contrast of the resonant transmission measurements. (d) Signal to noise ratio of RF and transmission measurements. The vertical line marks the power where the best signal to noise ratio is obtained.*

ing to a lifetime of ~1 ns (~100 000 cts/s after correction for collection and detector efficiencies), which is typical for gate-tunable InGaAs QDs [16]. The low count rates are consistent with previously obtained results taken with a microscope constructed according to the descriptions in ref. 2. The collection efficiency, and therefore the RF counts, could further be improved by using a solid immersion lens, which is expected to increase the number of counts by a factor of four to five [17]. In any case choosing to test our setup on poorly emitting QDs is the perfect "stress-test" for our instrument showing that it can be easily used on poorer single quantum emitters.

Finally, the resonant measurements just shown previously are obtained by sweeping the exciton emission wavelength in resonance with the probing laser wavelength. In the next step, the gate voltage is fixed such that the laser directly coincides with the maximum of the RF. The emission is filtered through a Fabry-Perot spectral filter. This allows for the res-

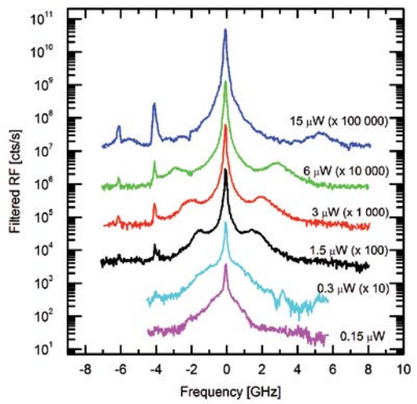

Figure 11: *The resonant quantum dot emission filtered through a high finesse scanning Fabry-Pérot spectral filter reveals a central and two side peaks (Mollow triplet), which move away from the central resonance with increasing excitation power. (The sharp peaks at -4 and -6 GHz correspond to the laser leaking through higher order Fabry-Pérot modes).*

olution of the side bands at high excitation power, referred to as the Mollow triplet [7], which is shown in Figure 10. This triplet is a pure quantum optical signature of the hybridization of the photon-exciton fields. It has previously been observed in QDs [19] and was interpreted as a characteristic feature of a quantum optical solid-state two-level system in close analogy to atoms [18] or molecules [19].

V. Summary

In summary we presented a setup for low temperature high resolution laser spectroscopy. The unique feature of this setup is the apochromatic performance that permits alignment free switching between off-resonant PL measurements and RF. This feature is fully enabled by our novel cryogenic compatible apochromatic objectives designed to hold the focus plane at the same position on the sample independently from the photon wavelength.

The commercially available polarization extinction option of the attoCFM I confocal head combines for the first time the use of high precision rotators within the flexible beam-management. This enabled us to achieve extinction ratios of 10^7, a factor just 10 away from world record in research labs [2] while allowing an unprecedented flexibility of use. We conducted the first RF measurements on a single quantum emitter obtained with a commercial system and demonstrated the simultaneity of the measurement with resonant transmission laser spectroscopy confirming the full correlation between the two forms of measurements. The RF is found to have a signal to noise advantage of 300%. High resolution spectroscopy reveals the splitting of the QD mode at high excitation powers, known as the Mollow-Triplet.

Finally, we would like to stress that the application of our instrument is not limited to the study of gate-controlled quantum dots, but can also be employed for quantum dots or other single photon emitters with a fixed resonance, by scanning the resonant laser excitation at constant extinction.

References

[1] A. N. Vamivakas *et al.*, Nature Physics **5**, 198 (2009).
[2] A. V. Kuhlmann *et al.*, Review of Scientific Instruments **84**, 073905 (2013).
[3] A. V. Kuhlmann *et al.*, Nature Physics **9**, 570 (2013).
[4] A. Ulhaq *et al.*, Nature Photonics **6**, 238 (2012).
[5] M. Munch *et al.*, Nature Nanotechnology **9**, 671 (2014).
[6] T. Müller *et al.*, Nature Communications **5**, 3328 (2014).
[7] B. R. Mollow, Physical Review **188** (1969).
[8] http://attocube.com/attomicroscopy/high-performance/confocal-microscopy-attocfmi/
[9] K. Karrai and R. Warburton, Superlattices and Microstructures **33**, 311 (2003).
[10] A. Högele *et al.*, Review of Scientific Instruments **79**, 023709 (2008).
[11] D. Leonard *et al.*, Applied Physics Letters **63**, 3203 (1993).
[12] H. Drexler *et al.*, Physical Review Letters **73**, 2252 (1994).
[13] R. Warburton *et al.*, Nature **405**, 926 (2000).
[14] R. Warburton *et al.*, Physical Review B **11**, 113303 (2002).
[15] A. Högele *et al.*, Phys. Rev. Lett. **93**, 217401 (2004).
[16] P. A. Dalgarno *et al.*, Physical Review B **77**, 245311 (2008).
[17] B. D. Gerardot *et al.*, Applied Physics Letters **90**, 221106 (2007).
[18] F. Wu *et al.*, Physical Review Letters **35**, 1426 (1975).
[19] G. Wrigge *et al.*, Nature Physics **4**, 60 (2008).

Valley polarization dynamics of monolayer WSe_2 measured by time-resolved PL in an attoDRY700

Gang Wang, Louis Bouet, Delphine Lagarde, Maël Vidal, Andréa Balocchi, Thierry Amand, Xavier Marie, and Bernhard Urbaszek
Université de Toulouse, INSA-CNRS-UPS, LPCNO, Toulouse, France

Introduction

The transition metal dichalcogenide (TMDC) monolayers (MLs) have been extensively studied in recent years because of their unique electronic and optical properties. The band structures of these TMDC materials undergo a crossover from indirect to direct gap semiconductors in the visible region when thinned to one ML, with potential applications in e.g. electronics as transistors or optoelectronics as LEDs [1]. An important feature of these TMDCs is that the band edge is located at the *K*-valleys of the hexagonal Brillouin zone. In TMDC MLs the crystal inversion symmetry breaking (see Fig. 1(a)) and the strong spin-orbit interaction result in the unique coupling of carrier spin and the *K*-valley index in momentum space. Therefore two types of nonequivalent K^+ and K^- valleys are associated with σ+ and σ- circularly polarized light in the interband transition process. This allows to address individual valley carriers, so called valley polarization, by circularly polarized optical excitation as shown in Figure 1(c), which makes TMDC MLs an especially promising candidate for studies on the emerging field "valleytronics".

It is essential to examine the stability of the created valley polarization for the implementation of valleytronics applications. The optically generated initial valley polarization is expected to be stable, as the large spin-orbit interaction will suppress the valley-spin relaxation. However, strong Coulomb interactions between charge carriers, excitonic effects, dominate the optical properties in these systems with ideal 2D confinement of TMDC and lead to very intricate valley dynamics.

Our target is to investigate the stability of the valley polarization experimentally. Two different cases need to be investigated: First, the neutral exciton (X^0), a Coulomb bound electron-hole pair, for which strong Coulomb exchange effects are expected to lead to a fast loss of valley polarization [2]. Second, the charged exciton, an X^0 with an additional electron forming a trion. This state is expected to have a more robust valley polarization.

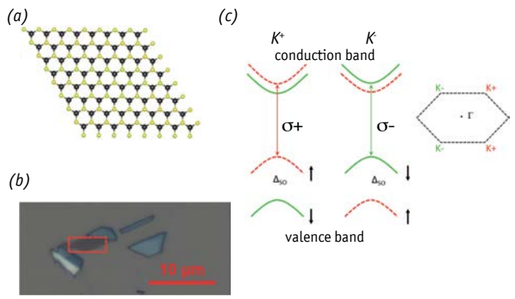

Figure 1: *(a) Schematic of TMDC MLs structures with inversion symmetry breaking. Transition metal atoms are shown in black, chalcogen atoms in yellow [1]. (b) ML WSe_2 samples are identified by optical contrast. The flake used for this note is marked with a red box. (c) Valley-contrast optical selection rules under circularly polarized laser excitation in ML WSe_2.*

In the well-explored ML MoS_2, spectrally broad transitions make the distinction between the valley dynamics of the X^0 and the trion currently very difficult. In this application note we employed time-resolved photoluminescence (TRPL) in another very promising material, namely monolayer WSe_2. In this 2D semiconductor with strong light-matter interaction, the X^0 and trion are spectrally well-separated. Thanks to the high sample quality and the stability of our set-up, we were able to reveal for the first time a striking difference between X^0 and trion valley dynamics [3]. The stable valley polarization of the trion lasting over nano-seconds makes this complex an excellent candidate for the valley Hall research and valleytronics devices.

High quality TMDC MLs samples can be obtained through mechanical exfoliation from bulk materials. The sample we used in this application note is shown in Figure 1(b). The ML flake is identified by its optical contrast and further confirmed by strong PL emission, as flakes with thicknesses >1 ML are inefficient emitters due to their indirect band-gap. The typical diameter of exfoliated TMDC ML samples is around 10 μm, therefore micro-PL and an accurate positioners with at least sub μm resolution are needed to locate the sample and perform optical measurements. Based on the attoDRY700 and the ANP positioners, we have designed and built a confocal microscope PL system with high stability and temperature control, working in a range from 4 K to 300 K.

Experimental Setup

The measurement system consists of the micro-PL head combined with the attoDRY700 cryostat and the excitation/detection optical system as illustrated in Figure 2. The micro-PL head is mounted inside the attoDRY700 chamber, as shown in the zoom out in Figure 2. The ML sample is loaded onto an XYZ stack of ANP positioners whose one end is fixed to the cold head of the cryostat. The objective is mounted on to the cold head providing the microscopic resolution and is used to focus the excitation laser as well as to collect the PL signal. For the TRPL measurements, ps pulses are generated from a frequency-doubled optical parametric oscillator (OPO) synchronously pumped by a mode-locked Ti:Sa laser. For the time-integrated PL measurements, continuous wave lasers with 633 nm and/or 532 nm wavelength are used. The excitation/detection spot is around 1 μm in diameter. The PL signal can be detected by a Hamamatsu streak camera with an overall time resolution of 4 ps for the TRPL or by a Si-CCD camera for the time-integrated PL.

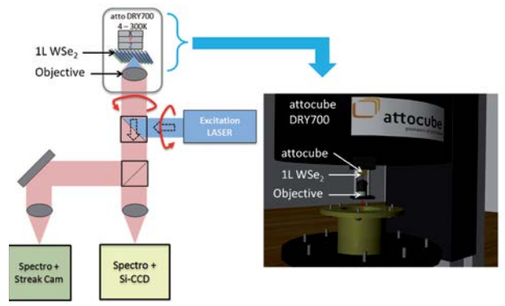

Figure 2: *Schematics of the micro-PL setup.*

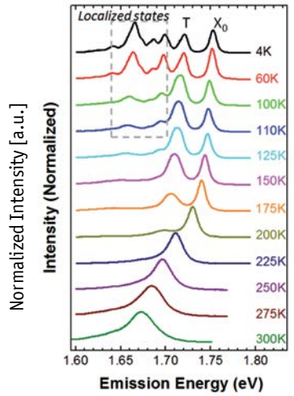

Emission Energy [eV]

Figure 3: *Temperature dependence of PL emission. Localized states can be seen up to a temperature of 110 K.*

The co- (cross-) circular polarization component of the PL emission (with respect to the excitation laser) can be chosen by a quarter-wave plate placed in front of a linear polarizer. In this application note, right circularly polarized laser excitation (σ+) will be used. The circular polarization is defined as $P_C = (I_{\sigma+} - I_{\sigma-})/(I_{\sigma+} + I_{\sigma-})$, where $I_{\sigma+}$ ($I_{\sigma-}$) denotes the intensity of σ^+ (σ^-) components of the PL emission. The time evolution of P_C indicates the *K* valley dynamics of ML WSe_2.

Measurement Results

Integrated PL has been acquired from ML WSe_2 flake at different temperatures, as depicted in Figure 3. At low temperature (T = 4 K), the PL contains emissions from neutral exciton X^0, trion and localized states. The narrow PL peak around 1.752 eV originate from the X^0 and the trion energy is at 1.722 eV. This gives a larger trion binding energy of around 30 meV, which also demonstrates the strong Coulomb interaction inside 2D ML WSe_2. PL emission from localized states, located at lower energy than the trion, vanishes when the temperature is raised to 110 K.

By fitting the TRPL results of the ML WSe_2 emission, we can extract the emission times of X^0, trion and localized states. Here we focus on the X^0 and the trion emissions. The X^0 emission decays so fast that it cannot be resolved by our setup. We infer a PL emission time shorter than 4 ps. Very different to the X^0 the trion emission exhibits a first decay with a characteristic time of around 18 ps and a second decay with a characteristic time 30 ps.

Next we discuss the evolution of the circular polarization of the X^0 and trion emissions, which is due to the initial valley population decay. Limited by the time resolution of our setup, we cannot extract the X^0 valley depolarization time. As shown in Figure 4(a), the fast polarization decay happens already within the first 4 ps range. This is further confirmed in time-resolved Kerr rotation experiments with a femto-second laser [4]. The efficient X^0 depolarization can be attributed to a strong Coulomb exchange coupling between the neutral excitons in *K*+ and *K*- valleys. The valley depolarization therefore does not dependent on single carrier spin flips. These are strongly suppressed by the conduction and valence band spin splittings in the meV and hundreds of meV range, respectively.

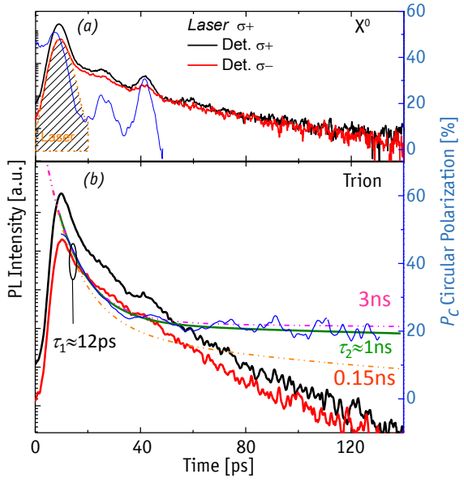

Figure 4: *Time-resolved PL under σ+ polarized laser excitation. Left axis: PL emission intensity. Right axis: circular polarization of PL emission. (a) Measured on X^0. (b) Measured on trion. Biexponential decay with τ_1=12 ps, τ_2=1 ns (solid green line) is shown. Two other decay lines with τ_2=0.15 ns (dotted orange line) and τ_2=3 ns (dotted purple line) are plotted for comparison [5].*

The valley polarization of the trion decays partially within 12 ps and then a stable plateau of 20% polarization is reached as depicted in Figure 3(b). The first, fast polarization decay has its origin possibly in the coexistence of the trion and the depolarized X^0. For the decay of the remaining, stable trion polarization a characteristic time as long as 1 ns can be inferred. In the trion case, the depolarization relies on the single particle spin flips and the scattering between the nonequivalent valleys, which is energetically too costly due to the large spin splittings. Stable valley polarization is clearly observed in the TRPL experiments on trions in monolayer WSe_2.

Summary

In this application note we show time-integrated, as well as time-resolved PL results for monolayer WSe_2 in a homemade micro-PL setup based on an attoDRY700 cryostat and ANP positioners. The time evolution of the circular polarization of the PL allows to probe the *K*-valley dynamics of the neutral and charged excitons (trions). Our results demonstrate the robustness of the optically generated valley polarization through the ns decay time of the trion polarization. This stable valley polarization will allow to further progress our understanding of the interaction between monolayer TMDCs and polarized light for applications and fundamental research.

References

[1] Wikipedia: http://en.wikipedia.org/wiki/Transition_metal_dichalcogenide_monolayers
[2] M. M. Glazov *et al.*, Phys. Rev. B **89**. 201302 (2014).
[3] G. Wang *et al.*, Phys. Rev. B **90**, 075413 (2014).
[4] C. R. Zhu *et al.*, Phys. Rev. B **90**, 161302 (2014).
[5] Figure reprinted with permission from G. Wang *et al.*, Phys. Rev. B **90**, 075413 (2014). Copyright 2014 by the American Physical Society.

Imaging fractional incompressible stripes in integer quantum Hall systems using the attoAFM III

Nicola Paradiso, Stefan Heun, Stefano Roddaro, Lucia Sorba, and Fabio Beltram
NEST, Istituto Nanoscienze-CNR and Scuola Normale Superiore, Pisa, Italy

Giorgio Biasiol
Istituto Officina dei Materiali CNR, Laboratorio TASC, Basovizza (TS), Italy

Loren N. Pfeiffer and Ken W. West
Department of Electrical Engineering, Princeton University, Princeton, USA

Introduction

Transport experiments provide conflicting evidence on the possible existence of fractional order within integer quantum Hall systems. In fact, integer edge states sometimes behave as monolithic objects with no inner structure, while other experiments clearly highlight the role of fractional substructures. Recently developed low-temperature scanning probe techniques offer today an opportunity for a deeper-than-ever investigation of spatial features of such edge systems. In our work we used the attocube attoAFM III in an attoLiquid3000 ^{3}He cryostat system to demonstrate that fractional features were unambiguously observed in every integer quantum Hall constriction studied [1]. We present also an experimental estimate of the width of the fractional incompressible stripes corresponding to filling factors 1/3, 2/5, 3/5, and 2/3. Our results compare well with predictions of the edge-reconstruction theory.

Setup Description

The attoLiquid3000 allows for AFM and transport measurements at low temperature and high magnetic field. The only customization that we made in our lab was to add a special sample holder, which now can receive a chip carrier with 20 contacts, allowing to combine LT-AFM operation with transport studies, i.e. AFM can be performed on a device in operation.

The ^{3}He part of the attoLiquid3000 cryostat is inserted in a liquid helium bath reservoir which is suspended by means of springs in a soundproof box, in order to damp vibrations induced by the lab floor and acoustical noise. The cryostat is a ^{3}He-closed cycle refrigerator that can reach a base temperature of 300 mK at the cold finger. The dewar is equipped with a superconducting coil which provides magnetic fields up to 9 T. The AFM head of our setup is constructed with a stack of actuators for both the coarse and fine control of the tip-sample position. The sample, mounted on a leadless chip carrier, is positioned on top of the piezo scanner, while the tip is glued to a tuning fork. The sample topography is obtained by controlling the oscillation amplitude damping of the tuning fork due to the tip-sample shear force (non-contact mode).

The scheme of our transport experiment is shown in Fig. 1a. Our samples (indicated as A and B) are obtained starting from AlGaAs-GaAs heterojunctions with an embedded two-dimensional electron gas (2DEG). The 2DEG depth, electron density, and mobility are d = 80 (80) nm, n = 1.77 (1.99) x 10^{11} cm^{-2}, μ = 4.2 (4.5) x 10^6 cm^2/Vs, for the A (B) sample, respectively. By optical lithography we fabricated a Hall bar with source and drain contacts. A quantum point contact (QPC) was fabricated by thermal evaporation of Schottky split gates (10 nm Ti / 20 nm Au bilayer), defined by electron beam lithography. The gap between the split gates is 300 nm (400 nm).

At very low temperature and high magnetic field (the so-called quantum Hall regime) the bulk 2DEG is insulating whenever the chemical potential lies between two consecutive Landau levels. In such condition the electron transport between source and drain contacts is mediated by 1D edge channels. The number of edge channels equals the number of filled Landau levels (called filling factor, ν). Each edge channel has a counter-propagating partner on the opposite side of the Hall bar. Due to their macrosco-

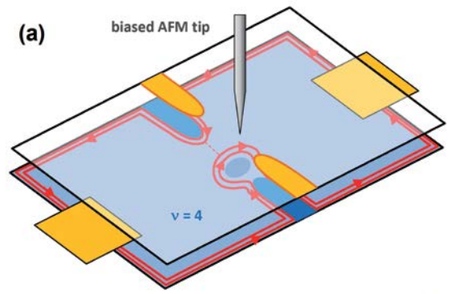

Figure 1: *(a) Sketch of the SGM operation mode. The AFM tip is used to perturb the edge confining potential and selectively bring the edges into interaction. (b) Map of G_{sd} as a function of the position of the tip (V_{tip} = -5 V) with respect to the split-gates (dashed line). The plateau ν* = 2 corresponds to the backscattering of the inner edge channel.*

pic spatial separation, the backscattering between them is suppressed. Therefore, since each channel carries e^2/h units of conductance, the source-drain conductance is $G_{sd}=\nu\ e^2/h$. At the QPC center, however, the separation between the counter-propagating edge channels is much smaller. It is therefore possible to intentionally induce backscattering using the electrostatic potential of the tip. This mode of operation of the AFM, in which the tip is used as a local gate, is called Scanning Gate Microscopy (SGM).

Fig. 1a shows the SGM configuration for measurements in the quantum Hall regime at bulk filling factor $\nu=4$ (sample A, magnetic field B = 3.04 T, temperature T = 300 mK). In these conditions the source drain current is carried by two pairs of spin degenerate edge channels at the sample edge, each carrying $2e^2/h$ units of conductance [2]. We apply a negative bias (-5 V) to the AFM tip and we scan it (in non-contact mode) over the QPC. SGM maps are obtained by plotting G_{sd} as a function of the tip position. As shown in Fig. 1b, when the tip is far from the QPC center there is no backscattering, i.e. the conductance takes the unperturbed value ($G_{sd}=4e^2/h$). As the tip is moved towards the center, the confinement potential is modified, so that the counter-propagating edges are put in interaction and backscattering occurs. Therefore the transmitted conductance decreases, until a complete pinch-off occurs when the tip is placed exactly at the QPC center (inner black area in Fig. 1b).

The attoLiquid3000 allows us to perform SGM measurements at the temperature and magnetic field conditions required to observe the fractional quantum Hall effect. Our goal is to image for the first time the presence of fractional incompressible stripes, i.e. the existence of an inner structure within the integer edge channel. We repeated the same measurements described above on the sample B at bulk filling factor $\nu=1$ (B = 8.23 T, T = 300 mK). The corresponding SGM map in the region close to the QPC center is depicted in Fig. 2a. Analogously to the $\nu=4$ case, we expect to find plateaus when the local electron phase is gapped, i.e. when the local filling factor ν^*equals a robust fraction. The scan profile depicted in Fig. 2b reveals a clear shoulder for $G_{sd}=e^2/3h$ (corresponding to points where $\nu^*=1/3$). A more careful analysis [1] allows to determine the occurrence of incompressible phases for $\nu^*=1/3$, 2/5, 2/3, and 3/5, i.e. the two most robust fractions and their hole-particle conjugates, respectively. The SGM maps allow us not only to reveal the fractional incompressible stripes, but also to measure their width and correlate it with the local electron density slope. With this data we were able to test directly the predictions of the reconstruction theory [3]. The agreement between the data and the reconstruction model is remarkable, especially in light of the uncertainty on the fractional-gap value, which is known to be rather sensitive to the details of disorder potential. Notably, data globally follow the expected dependence on the electron density gradient.

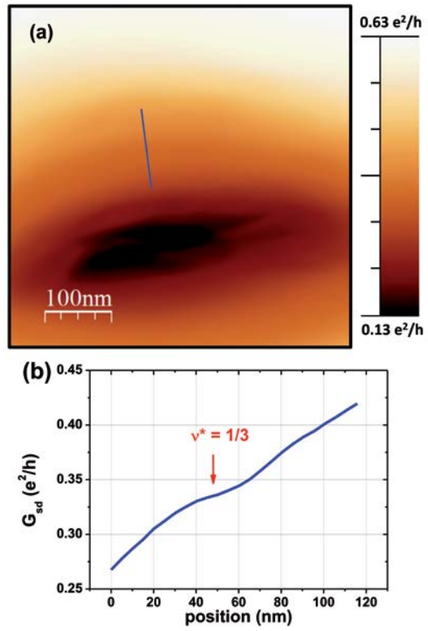

Figure 2: *(a) SGM scan at the center of a QPC in a $\nu=1$ QH system (V_{tip}=-6 V). The map shows the transmitted differential conductance G_{sd} as a function of the tip position. (b) Profile of G_{sd} along the light blue line in the top panel.*

Summary

In conclusion, we exploited the attocube attoLiquid3000 setup to perform a spatially resolved study of the edge structure. Our findings shed a new light on quantum Hall physics, and in particular on the complex phenomena recently reported in transport experiments [4]. In fact, the role of fractional phases in quantum interferometry is still not clear and this knowledge may open up exciting developments, as for instance the implementation of a Mach-Zehnder interferometer for fractional quasiparticles.

References

[1] N. Paradiso, S. Heun, S. Roddaro, L. Sorba, F. Beltram, G. Biasiol, L. N. Pfeiffer, K. W. West. Phys. Rev. Lett. **108**, 246801 (2012). See also the Supplemental Material.
[2] N. Paradiso, S. Heun, S. Roddaro, D. Venturelli, F. Taddei, V. Giovannetti, R. Fazio, G. Biasiol, L. Sorba, F. Beltram, Physica E **42**, 1038 (2010).
[3] D. B. Chklovskii, B. I. Shklovskii, and L. I. Glazman, Phys. Rev. B **46**, 4026 (1992).
[4] A. Bid, N. Ofek, H. Inoue, M. Heiblum, C. L. Kane, V. Umansky, and D. Mahalu, Nature **466**, 585 (2010).

pioneers of precision
© attocube systems AG, 2014. All rights reserved.

Magnetic Force Microscopy Specifications in attoDRY1100 on par with Liquid Cryostats

Christoph Bödefeld, Dieter Andres, Florian Otto
attocube systems AG, Munich, Germany

Introduction

As supplies of liquid helium are getting ever more expensive and less reliable, the importance of cryogen-free cooling systems grows. While such alternatives have been around for quite some time, they usually failed to meet the requirements of researchers in need of low vibration environments, such as those working in the field of scanning probe microscopy. It is in this field of research in particular, where the attoDRY1100 cryogen-free magnet system determines the state of the art. In this application note, we show examples of magnetic force microscopy measurements performed in a pulse-tube based cooling system, with specifications close to those reached in a regular liquid bath cryostat.

attoDRY1100

The attoDRY1100 (see Figure 1) builds the cryogen-free basis of the attoDRY LAB platform, offering a truly unique low temperature measurement platform with a fully automated gas handling system. The integrated touchscreen allows for conveniently setting the desired field (B) and temperature (T) without even using a PC. More elaborate measurement schemes such as programmable sweeps of B and T are easily possible via a USB/Ethernet connection and a LabVIEW interface.

The top-loading design enables quick and easy sample exchange while offering a generous sample space of 49.7 mm in diameter, which makes it compatible with a whole variety of different measurement options offered by attocube. The unmatched cooling performance via exchange gas coupling enables probe cooldown times as fast as 1-2 hours, with the initial cooldown time of the complete system being around 10-12 hours including a 9 T magnet. The temperature stability was measured to be better than ±5 mK over 14 hours at 4 K.

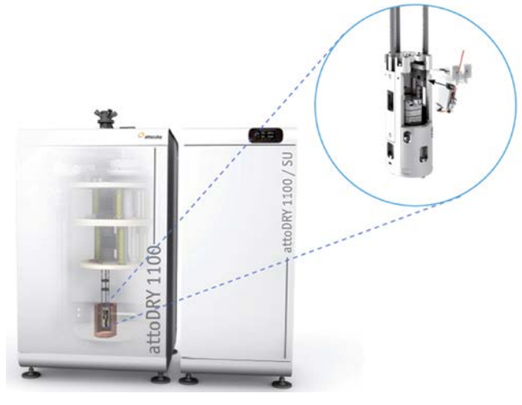

Figure 1: *The attoDry1100 platform. The inset shows the attoAFM/MFM setup.*

attoAFM/MFM I

Magnetic force microscopy (MFM) is a technique derived from atomic force microscopy (AFM), in which an etched silicon cantilever/ tip combined with optical deflection detection is used to precisely measure local interactions such as van der Waals or Coulomb forces. MFM takes advantage of tips with magnetic coatings, typically NiCr or cobalt, making them sensitive to the magnetic interaction between tip and sample. Figure 2 below shows a schematic of attocube's cantilever-based attoMFM, designed particularly for low temperature and high magnetic field applications. The attoMFM uses a single-mode, fiber-based interferometer to detect the tip deflection. As with most MFMs, the attoMFM applies an AC modulation technique to achieve highest detection sensitivity. More details can be found in [1].

Example MFM measurements

Single magnetic vortices in superconducting materials such as freshly cleaved $Bi_2Sr_2CaCu_2O_{8+x}$ (Bi-2212), a cuprate superconductor, represent reproducible features with low moment. A vortex consists of a circular supercurrent, which allows for a quantized flux of exactly one flux quantum to penetrate the superconductor. Hence, these substrates are ideal candidates for MFM characterization measurements.

The measurements in Figure 3 show how the density of vortices varies with applied magnetic field when changing it from -40 Oe to +50 Oe. For each field value, the sample was field-cooled in the respective field. In these images, the orientation of the vortices with respect to the moment of the tip is indicated by the color of the vortices: Bright (dark) colors indicate repulsive (attractive) forces. Here, the tip was scanned in a constant height of about 30 nm above the surface of a freshly cleaved piece of Bi-2212 [2].

Note that the applied field was always much lower than the coercitivity of the hard-magnetic tip (≈400 Oe), hence the orientation of the tip moment was kept unchanged. While at low vortex densities pinning effects are comparable, one can see at higher densities the hexagonal Abrikosov pattern [3].

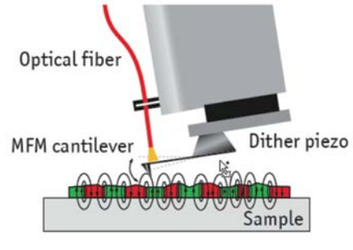

Figure 2: *Sketch of the AFM/MFM setup. An AFM tip (here: magnetically coated), is brought into close vicinity of the sample. The deflection of the cantilever due to forces on the tip can be read using a built-in fiber interferometer.*

Performance characterization

In order to further test and quantify the performance of the microscope, certain key specifications are measured for every attoAFM/MFM I. The most important are:

(a) RMS z-noise: this number characterizes the level of vertical vibrations experienced between the AFM/MFM tip and the sample surface during a typical measurement. While the tip is in contact with the sample surface, a so-called noise-scan (at 4 K) is performed, in which the scanner is practically scanning only one and the same point (the scan size is below detectable limits). In this way, vibration data of the fully enabled system are acquired over time without any topographic influence. This 100 x 100 pixel noise scan hence acquires noise statistics of the tip deflection over 10,000 points. The sample time is set to 5 ms, which corresponds to a measurement bandwidth of 200 Hz. After subtracting slow drifts (using a line-by-line filter), the RMS z-noise value can now be easily determined from the image or the respective histogram. For the attoDRY systems attocube systems expects a z-noise value < 100 pm RMS and guarantees < 150 pm RMS, while for liquid helium systems these numbers are < 50 pm RMS (expected) and < 120 pm RMS (guaranteed).

(b) Signal-to-noise ratio (SNR): the SNR in MFM measurements on standard samples is also an indicator for the performance of the system. The SNR can easily be determined from the relative peak height of the visible structures and the noise determined in a separate noise scan with otherwise same conditions. attocube systems expects the SNR on such standard sample to exceed 20:1 and guarantees 10:1, measured in a bandwidth of 10 ms.

Performance Test Results in the attoDry1100

(a) The result of a respective performance test done in attocube Application Labs is shown in form of a histogram in Figure 4, which demonstrates a measured value of 65 pm RMS (5 ms sample time, feedback loop enabled). This value is close to what is being achieved in attocube's liquid systems and demonstrates the superior performance of the attoDRY product line.

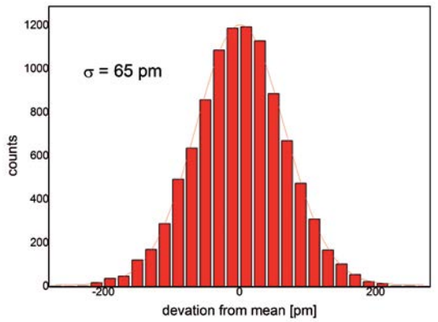

Figure 4: *Histogram of z-height values over 10,000 points (or 50 s) measured with a bandwidth from 1 to 200 Hz. The standard deviation results in 65 pm.*

(b) The typical SNR in the attoDRY LAB MFM can be determined from the MFM measurements discussed above and shown in Fig. 3. The S/N ratio was determined from the peak height of isolated vortices (e.g. at B = 10 Oe) to be above 20:1. In low noise liquid helium cryostats for comparison, the SNR is expected to exceed 20:1 as well.

Summary

In this application note, we demonstrate that extremely sensitive scanning probe techniques such as magnetic force micros-copy are now routinely possible inside the cryogen-free attoDRY1100. Most remarkably, the specifications reached are close to those achieved in liquid systems, hence opening the door to a whole new class of experiments without the need for liquid helium.

References

[1] M. Zech, C. Bödefeld, F. Otto, and D. Andres, Microscopy Today **19**, pp. 34-38 (2011). doi: 10.1017/S1551929511001180.
[2] Sample courtesy of A. Erb, TU Munich.
[3] A. A. Abrikosov, Zh. Eksp. i Teor. Fiz. **32**, 1442 (1957); Soviet Phys. JETP **5**, 1174 (1957).

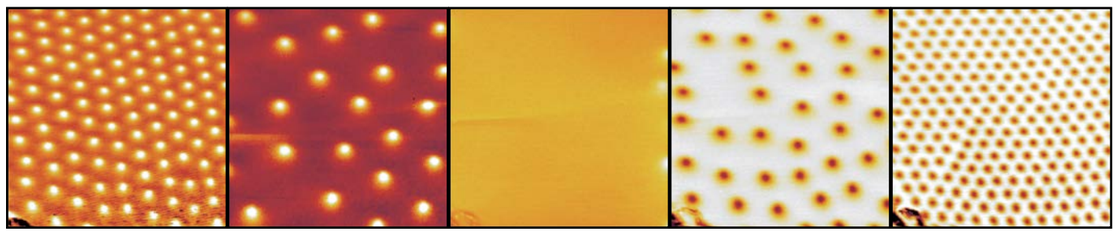

Figure 3: *MFM measurements at different magnetic fields: Left to right: B = -40 Oe, -10 Oe, 0 Oe, +10 Oe, +50 Oe. Scan size is 10 x 10 µm², color span is 2 Hz for all images.*

Material composition and strain analysis of single semiconductor quantum dots using the attoCFM I

Jorge Puebla
University of Sheffield, Sheffield, UK
attocube systems AG, Munich, Germany

Introduction

Often for material structure analysis, invasive techniques such as e.g. neutron scattering or energy dispersive X-ray spectroscopy inside a focussed ion beam microscope are used to obtain information. Unfortunately, such techniques may generate permanent perturbations to the sample under study. Hence, a non-invasive tool for structural material analysis is usually more desirable. Nuclear Magnetic Resonance (NMR) is a non-invasive technique which extracts information using the fundamental properties of nucleus for different materials. The basic principle of this technique relies on a strong applied magnetic field which induces precession of the atom spins around the magnetic field direction. When a radiofrequency excitation perpendicular to the strong magnetic field is in resonance with the spin precessions, the nuclear spins can be flipped, which can then be detected as a change in the overall nuclear polarization. The frequency of the spin precessions depends on the type of nucleus which hence allows structural analysis.

Electron-nuclear hyperfine interaction is an efficient and widely employed method for polarizing nuclear spins under optical excitation. Initially, the angular momentum is transferred from the polarized excitation light to electron spins, which is then transmitted to the nuclear spins. Any fluctuation of the nuclear spin polarization is finally transferred back to the electron spin and can hence be detected optically. This process is better known as Optically Detected NMR (ODNMR). However, since a single nuclear spin induces only a small net nuclear polarization P_N, a large ensemble of nuclear spins is typically required to obtain measurable values.

For ODNMR, an external magnetic field B_z normal to the sample induces a Zeeman splitting of the nuclear spin levels. If a nucleus with non-zero quadrupole moment experiences an electric gradient parallel to B_z, an extra energy splitting of the spin levels will appear allowing observation of all dipole active transitions at different frequencies (quadrupole moments).

The first ODNMR measurement on a single Quantum Dot (QD) was realized in GaAs interface QDs more than one decade ago by D. Gammon and co-workers [1]. Here, the electron spin of one localized exciton interacts with the nuclei that build up the quantum dot. The QDs they used were strain-free nanostructures that typically contain ≈ 10^5 nuclei – a fact that facilitated the measurements in this case.

Now, when ODNMR is applied to strained nanostructures, a major difficulty arises: the strain-induced quadrupole interaction significantly broadens, hence reducing the sensitivity of the NMR spectra. This is because in standard saturation NMR spectroscopy, the sample is excited with a set of frequencies W_f, inducing a change of nuclear polarization P_N. It is important that W_f is in resonance with one transition between two quadrupole moments, yet has no effect on other dipole transitions. Still, the contribution of just one transition makes it difficult to resolve the net change of P_N.

Only recently, researchers at the University of Sheffield developed an elegantly modified ODNMR technique, which allows structural analysis of strained QDs [2]. E.A. Chekhovich and his colleagues' approach employs a continuous-wave, broadband radiofrequency excitation not containing the frequencies W_{gap} (see schematic graph in Figure 1). This method represents an inversion pattern of the radiofrequency excitation used previously – hence the term "inverse" is used. When the gap W_{gap} is in resonance with a transition between two quadrupole moments, the overall change on P_N will be the contribution of all the transitions below and above the gap W_{gap}. This approach proved to significantly enhance the detected

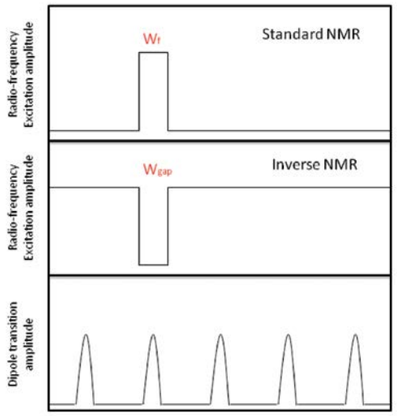

Figure 1: *Schematic of radiofrequency patterns for Standard-NMR and Inverse-NMR.*

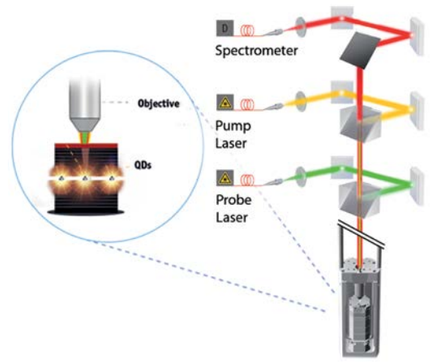

Figure 2: *Schematic diagram of the ODNMR setup. The sample is placed inside an insert, filled with low-pressure helium gas with optical access from the top. The insert is immersed in a liquid helium bath cryostat. Photoluminescence is excited by diode lasers. All experiments are performed in Faraday geometry, with the magnetic field normal to the sample surface.*

signal. This inverse ODNMR technique enables obtaining information about the strain distribution and the chemical composition of strained QDs, and can potentially enable precise control of nuclear spins for quantum information processing [3]. Further reviews and comments on this technique can also be found in [4,5].

Experimental Conditions and Setup

The experiments were performed by placing the sample in an attocube cryostat at $T = 4.2$ K, and using an external magnetic field B_z normal to the sample surface. The measured samples are InP/GaInP quantum dots, nominally grown by metal organic chemical vapor deposition (MOCVD) and InAs/GaAs quantum dots grown by molecular beam epitaxy (MBE). Due to the growth conditions, Ga atoms incorporate to the dot substituting *P* and *As* atoms; this process is more pronounced for InAs QDs which are usually referred as InGaAs dots.

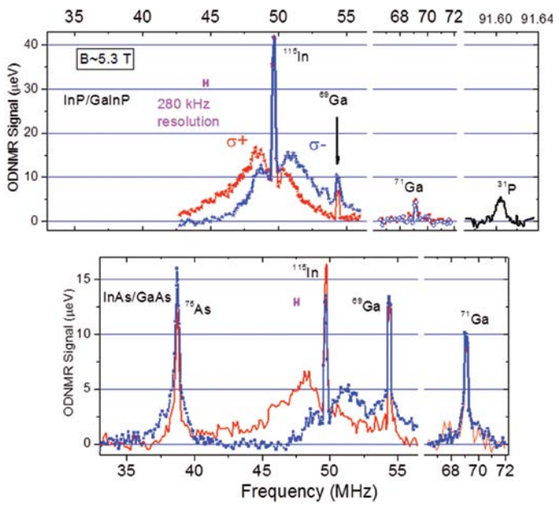

Figure 3: *Inverse NMR spectra of strained quantum dots. ODNMR spectra measured at $B_z \approx 5.3$ T in self-assembled InP/GaInP (top) and InAs/GaAs (bottom) quantum dots using the inverse method.*

In order to detect the nuclear polarization in the single quantum dots, a high resolution micro-photoluminescence spectroscopy setup was used (see experimental setup scheme in Figure 2). The photoluminescence is excited with non-resonant laser light and is analyzed with a double-grating spectrometer coupled to a CCD. Polarization-resolved excitation and detection of the light is used to manipulate and probe nuclear spin polarization. The waveform of the radiofrequency excitation is produced by a digital waveform generator and delivered by a small coil which can be positioned with ultra-high stability using an xyz attocube positioner (see Figure 2).

ODNMR measurements were carried out using a pump–probe type of experiment. The dot is first excited with a circularly polarized laser pulse of duration T_{pump}. Afterwards, radio-frequency (rf) excitation is applied under non-light excitation for a duration T_{rf}. Finally, a short laser pulse (T_{probe}) is applied to measure the photoluminescence spectrum and to probe the effect of the rf-field on the nuclear polarization. This allows the NMR signal to be obtained as the absolute magnitude of the Overhauser shift, which is proportional to the degree of nuclear spin polarization.

Measurement Results

Figure 3 shows ODNMR spectra measured on single InP (top) and In(Ga)As (bottom) quantum dots at $B_z = 5.3$ T. In the nominally InP dots grown in GaInP barriers (top caption in Figure 3), the inverse technique allows contributions from quadrupole nuclei ^{115}In, ^{69}Ga and ^{71}Ga within the volume probed by a single electron wave-function to be resolved, which is not possible for standard NMR techniques.

The ^{115}In peak dominating the spectrum consists of a sharp central line (corresponding to the $-½ \rightarrow +½$ central transition, CT) with amplitude ~40 meV at ~49.7 MHz, and two broad bands of satellite transitions (STs) to lower and higher frequencies each stretching up to ±7 MHz. These sidebands are due to strain-sensitive, quadrupole shifted transitions involving spin levels with $|Iz| > ½$.

The ODNMR spectra of a single In(Ga)As/GaAs quantum dot were measured using the inverse method ($W_{gap} = 280$ kHz) and are shown in the lower part of Figure 3. The CTs have similar amplitudes for the four isotopes present in the dot, revealing significant substitution of In-atoms by Ga-atoms in the nominally grown InAs dots. From the amplitudes of the ^{115}In and ^{71}Ga central peaks one can now obtain numerical estimates for the relative gallium and indium concentrations in these In(Ga)As dots.

Another important physical property of the nanostructures that can be accessed by NMR is the magnitude and distribution of the elastic strain. Quadrupole effects are insensitive to isotropic (hydrostatic) strain, but can provide information on biaxial and shear strains, due to non-uniform changes of induced electric gradients.

Summary

The innovative Optically Detected NMR methods presented here prove to be an important non-invasive spectroscopy method for structural analysis of strained nanostructures, and requires no special preparation of the sample. Furthermore, the technique allows detailed studies of electron and hole spins for qubit applications under strong quadrupole interactions [3]. A future challenge will be the development of nano-NMR techniques, sensitive to smaller numbers of nuclei in solid state materials for diverse applications including imaging.

References

[1] D. Gammon, *et al.*, Science **277**, no. 5322 (1997).
[2] E.A. Chekhovich, *et al.*, Nature Nanotechnology **7**, 646 (2012).
[3] E.A. Chekhovich, *et al.*, Nature Physics **9**, 74 (2013).
[4] B. Urbaszek, Nature Physics **9**, 65 (2013).
[5] D. Gammon, Nature Nanotechnology **7**, 621 (2012).

pioneers of precision
© attocube systems AG, 2014. All rights reserved.

Magnetoresistance of self-assembled GaMnAs based nanowires using the atto3DR

Christian H. Butschkow, Dieter Weiss
Institute of Experimental and Applied Physics
University of Regensburg, Germany

Tobias Lindenberg, Florian Otto
attocube systems AG, Munich, Germany

Introduction

Dilute magnetic semiconductors promise to offer a rich playground for designing spintronics devices, i.e. solid state based electronics, which not only make use of the electron's charge, but also the spin degree of freedom. In particular the relatively new class of self-assembled ferromagnetic nanowires could potentially be used for producing e.g. one-dimensional spin valve transistors or ferromagnetic single electron transistors, while maintaining a high flexibility in the choice of material as well as the axial and radial degrees of freedom. Due to the arbitrary orientation inherent to self-assembled materials on the substrate, typical characterization techniques such as magnetoresistance measurements conducted at cryogenic temperatures greatly benefit from the possibility to freely change the mutual orientation of external magnetic field and sample. Although this is easily possible e.g. by using a 3D vector magnet setup, the associated costs (>> 100 k$) are often prohibitive. Single axis sample rotator setups on the other hand not only require choosing either an out-of-plane or in-plane configuration prior to cooldown, but also put firm restrictions on certain measurements which rely on a precise orientation of the field e.g. perpendicular or parallel to an initially unknown direction along a sample structure. The perfect solution to such applications is now available (at moderate costs) by the new atto3DR, attocube's 3-dimensional rotator [1].

Experimental Setup

The atto3DR setup is shown above as well as sketched in Figure 1. The module consists of two piezo based 'slip-stick' rotators, which by their combination allow for arbitrary mutual orientations of an external magnetic field vector (e.g. from a standard single solenoid superconducting magnet as present in most low temperature cryostats) and the sample plane. The first rotator essentially controls the out-of-plane (θ) component, whereas the second rotator revolves around an axis perpendicular to the sample plane, and thus affects the in-plane component. The atto3DR comes fully wired with 20 measurement lines as twisted pairs, a convenient leadless ceramic chip carrier (LCCC) mount for quick and easy sample exchange of wire bonded sample structures (based on non-magnetic pogo pins), and two resistive encoders for the rotators so that full closed loop operation is possible.

The corresponding electronics ANC350 can easily be integrated with automated measurement routines via a LabVIEW® interface or a DLL.

Figure 1: *Working principle. The first rotation axis controls the orientation of the sample plane with respect to the fixed external magnetic field (θ: ±90°), whereas the second rotator actuates the in-plane component (ϕ: ±90°). Combining both axes allows for arbitrary mutual orientations of the magnetic field vector with regards to the sample plane.*

Measurements

Similar to a recent publication by C. H. Butschkow and coworkers from the group of Prof. Dieter Weiss (Univ. of Regensburg) [2], magnetotransport measurements on individual GaAs/(Ga,Mn)As core-shell nanowires have been conducted. The nanowires were grown self-assembled via molecular-beam-epitaxy (MBE) and the vapor-liquid-solid technique (VLS) using gold as catalyst. The (Ga,Mn)As shell was grown

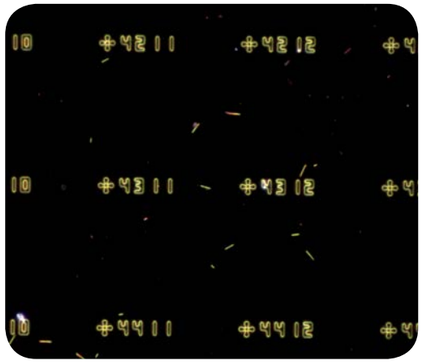

Figure 2: *Dark field microscope image of randomly distributed GaAs/(Ga,Mn)As core-shell nanowires on a SiO_2 substrate with pre-patterned marker structures.*

epitaxially on the side facettes with a Mn concentration of approximately 5% [3]. In order to contact individual nanowires (diameter ≈ 100 nm, length ≈ 4 µm) electrically, they were transferred by casting a droplet of nanowire suspension onto a SiO_2 substrate, leading to a random distribution of nanowires (see Figure 2). Gold contacts (width ≈ 300 nm, thickness ≈ 200 nm) were fabricated on selected nanowires (see Figure 3) using electron beam lithography.

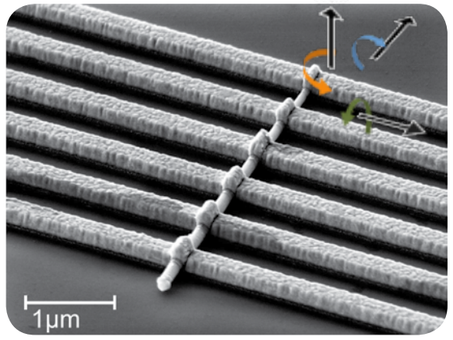

Figure 3: *Tilted scanning electron micrograph of a contacted nanowire. Black arrows indicate the sample coordinate system. Coloured arrows indicate the rotational directions as used in the measurements in Figure 5 (blue: transverse, orange: in-plane, green: perpendicular rotation).*

A detailed description of the sample-preparation can be found in [2]. For this experiment, we measured the resistance in a two-terminal configuration at a cryogenic temperature of 4 K. From previous measurements, it is known that the contact resistances can be considered as negligible and two terminal resistance measurements are in many cases sufficient.

The (Ga,Mn)As shell shows a ferromagnetic transition temperature of ~20 K and strong uniaxial magnetic anisotropy with the magnetic easy axis pointing along the nanowire axis. The external magnetic field needed to force the magnetization entirely into the magnetic hard axis, usually referred to as anisotropy field H_a, is in the range of $\mu_0 H_a$ = 1.3 T to 2 T. This value exceeds the anisotropy field of comparable (Ga,Mn)As nanostructures by a factor of 10 [4,5]. As described in [2], this large anisotropy field leads to a significant dependency of the charge-carrier magnon scattering resistance contribution on the direction of the magnetization. In particular, we found that the magnetoresistance of the nanowires is for relatively small magnetic fields at least to the first order linearly proportional to the internal effective magnetic field H_{eff}, rather than the external field H_0:

$$R \sim -|H_{eff}| \qquad (1)$$

This effective magnetic field contains, additionally to the external field, any molecular fields. Since the saturation magnetization in (Ga,Mn)As is low, the demagnetizing field can be neglected and only the anisotropy field has to be considered. It can be shown, that H_{eff} is approximately described in our case by:

$$H_{eff} = H_0 \cos(\phi_M - \phi_H) + H_0 \cos(2\phi_M) \qquad (2)$$

with ϕ_M and ϕ_H denoting the directions of the magnetization and the external magnetic field H_0 with respect to the magnetic easy axis, respectively. Together with eq. 1, the angular dependence of H_{eff} leads to a dependency of the magnetoresistance on the direction of the magnetization and thus enables us to gain knowledge of the magnetic anisotropy by means of (longitudinal) resistance measurements.

This dependency can be measured by rotating the nanowire in a large affixed magnetic field, thus varying ϕ_H and forcing the internal magnetization roughly into the direction of the external field. Figure 4 shows such measurements for 3 different values of H_0, revealing very pronounced magnetoresistance. It can be seen that the amplitude of the magnetoresistance on the scale of Figure 4 decreases with increasing external magnetic field, since then the first term in eq. 2, which can be regarded for high magnetic fields as a constant offset, becomes dominant.

The homogeneity and pureness of the uniaxial magnetic anisotropy of a nanowire can be examined by performing this measurement for different rotation planes. However due to the random distribution of the nanowires on the substrate, the implementation of such an experiment is in general not straight forward. Using the convenience of a double rotator as the atto3DR, this is easily realizable in this setup.

APPLICATION NOTE
Magnetoresistance of self-assembled GaMnAs based nanowires using the atto3DR
attoMICROSCOPY
Sophisticated Tools for Science

pioneers of precision

We performed magnetoresistance measurement as a function of the field angle for three different rotation planes (see Figure 5):

(i) in-plane rotation, referring to the SiO_2 substrate plane

(ii) out of plane (perpendicular) rotation with the long nanowire axis entirely in the rotation plane

(iii) out of plane (transversal) rotation with the rotation plane transversal to the nanowire axis

The in-plane and the perpendicular magnetoresistance traces exhibit approximately the same amplitude, which is an indication that only the uniaxial anisotropy along the nanowire axis is present. The shift of 20° of the in-plane trace along the angular scale compared to the perpendicular trace is related to the random orientation of the nanowire.

While the in-plane and the perpendicular measurements show rather pronounced magnetoresistance, the resistance change for transverse rotation is almost negligible. This is expected, as then the magnetization is always forced in the magnetic hard direction (ϕ_M = 90°) resulting in a constant effective magnetic field.

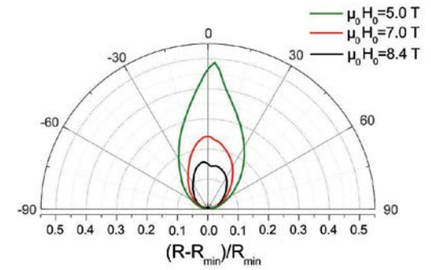

Figure 4: *Normalized magnetoresistance as a function of the angle between externally applied magnetic field and the nanowire axis for various magnitudes of the external magnetic field.*

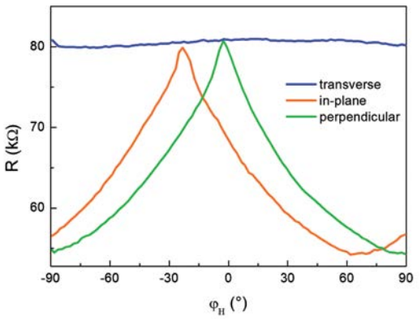

Figure 5: *Magnetoresistance at 5 T as a function of the angle between externally applied magnetic field and the nanowire axis for different rotation planes: (orange) in-plane rotation, referring to the SiO_2 substrate plane, (green) out of plane (perpendicular) rotation with the long nanowire axis entirely in the rotation plane, and (blue) out of plane (transversal) rotation with the rotation plane transversal to the nanowire axis.*

References:

[1] www.attocube.com/attoCRYO/atto3DR.html
[2] C.H. Butschkow, E. Reiger, S. Geißler, A. Rudolph, M. Soda, D. Schuh, G. Woltersdorf, W. Wegscheider, D. Weiss, arXiv:1110.5507v1
[3] A. Rudolph, M. Soda, M. Kiessling, T. Wojtowicz, D. Schuh, W. Wegscheider, J. Zweck, C. Back, and E. Reiger, Nano Lett. **9**, 3860 (2009).
[4] S. Hümpfner, K. Pappert, J. Wenisch, K. Brunner, C. Gould, G. Schmidt, L. Molenkamp, M. Sawicki, and T. Dietl, Appl. Phys. Lett. **90**, 102102 (2007).
[5] J. Wenisch, C. Gould, L. Ebel, J. Storz, K. Pappert, M.J. Schmidt, C. Kumpf, G. Schmidt, K. Brunner, and L.W. Molenkamp, Phys. Rev. Lett. **99**, 1 (2007).

The sample was prepared by C.H. Butschkow et al. The measurements were performed in attocube application labs by C.H. Butschkow and F. Otto, 2012.

© attocube systems AG, 2014. All rights reserved.

Piezo-Response Force Measurements on Ferroic Oxide Films using the attoAFM I

Karim Bouzehouane, Stephane Fusil
Unité Mixte de Physique CNRS/Thales, Paris, France

The renaissance of multiferroics in which at least two ferroic or antiferroic orders coexist, is motivated by fundamental aspects as well as by their possible applications in the field of spintronics. Magnetoelectric coupling allows for instance the reversal of the ferroelectric polarization by a magnetic field or the control of the magnetic order by an electric field. Most of the ferromagnetic-ferroelectric compounds exhibit both orders at low temperature.

Piezo-response Force Microscopy (PFM) is a variant of contact mode AFM. While the tip is in contact to the sample, AC voltages are applied to the conducting AFM tip, which result in height changes at the frequency of the excitation thanks to the inverse piezoelectric effect. The sample surface vibration is detected by de-modulating the recorded tip height. The vibration amplitude is related to the vertical projection of the ferroelectric polarization, the vibration phase lag is 0° or 180°, depending on whether the polarization is pointing up or down. The PFM mode gives an image of the ferroelectric structure at nanoscale.

In the measurements presented here, K. Bouzehouane and S. Fusil from the CNRS Unité mixte de Physique CNRS/Thales show PFM data taken on a layered heterostructure (150 nm $BiFeO_3$-Mn on top of 35 nm of $SrRuO_3$ on a $SrTiO_3$ (001) substrate) recorded at 82 K with a standard attoAFM I. The multiferroic material $BiFeO_3$ (also BFO) is both magnetic and strongly ferroelectric even at room temperature. It is therefore an ideal candidate for PFM measurements.

While the topography scan of the sample shows a fairly flat sample (see Figure 1), the simultaneous PFM signals show clearly ferroelectric domains. The external part of these images corresponds to the pristine state and the center part to written square shaped domains (see Figure 2). A 1 x 1 µm² and a second, 45° rotated square were written with an applied DC tip voltage of ±15 V. The recorded phase shows the different orientations of the domains with approximately 180° phase difference, as expected in parasitic free acquisition conditions. In the right image, one can see that the PFM amplitude goes to zero at the intersection of these structures, as expected for vibration nodes between two antiparallel domains corresponding to domain walls. Figure 3 is a typical piezo-response hysteretic cycle acquired with an AC+DC bias applied to the tip and giving the coercive switching biases at 82 K. Note that the piezo-response of BFO is a few tens of picometers, attesting for the low noise sample environment.

Images and data courtesy of K. Bouzehouane and S. Fusil, Unité Mixte de Physique CNRS/Thales, Paris, France.

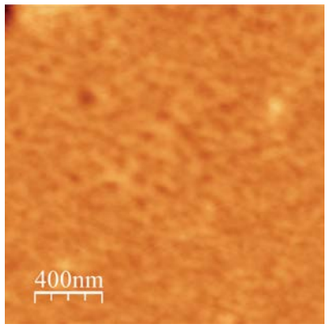

Figure 1: *Topography image of the sample surface. The height contrast (black to white) is 15 nm.*

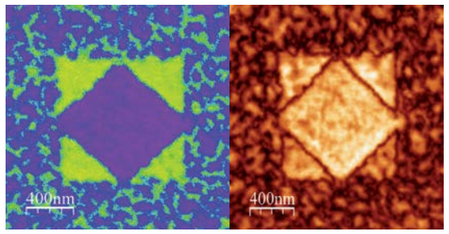

Figure 2: *Piezo-response phase (left, 0-180° contrast) and amplitude (right, a.u.) map of the sample at 82 K. Two squares have been written, a 1 x 1 µm² and a smaller, rotated one with ±15 V tip voltage. Note that the amplitude goes to zero in the domain walls. The outside area shows natural domains.*

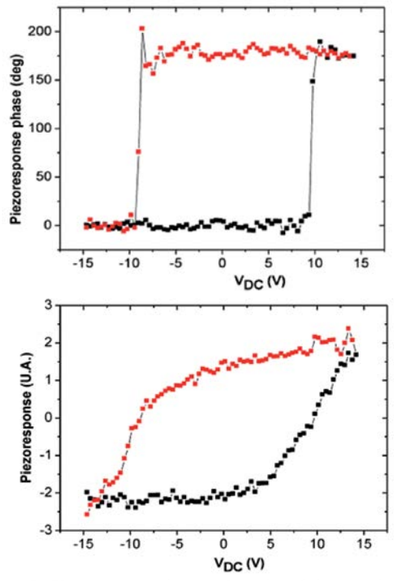

Figure 3: *Piezo-response hysteretic cycles of the sample at 82 K: phase (left) and amplitude behavior (right graph).*

Vortex Imaging on Iron Pnictides using the attoMFM Ixs

Huang Yang, Hai-Hu Wen
Center for Superconducting Physics and Materials
National Laboratory of Solid State Microstructures and
Department of Physics, Nanjing University, China

Christoph Bödefeld
attocube systems AG, Munich, Germany

Introduction

In their latest publication [1], H. Yang and co-workers from the group of Prof. Hai-Hu Wen, from Nanjing University, present results on vortex studies on $Ba_{1-x}K_xFe_2As_2$ - a potassium-doped superconductor of the pnictide family. Since their discovery in 2008, the iron-pnictides have drawn intensive attention, not only because they have broken the monopoly of the cuprates but also because of strong pinning effects observed in certain pnictide-compounds. A vortex consists of a circular supercurrent, which allows for exactly one flux quantum each to penetrate the superconductor. Through the mutual repulsion of neighboring circular currents, a vortex lattice forms, which in the easiest case is hexagonal [2]. In contrast to e.g. a cuprate superconductor such as $Bi_2Sr_2CaCu_2O_{8+x}$ (Bi-2212), the pnictide samples show strong pinning leading to significantly disordered vortex lattices.

In the measurements shown here, the authors present magnetic force microscopy (MFM) images on pnictide samples at different magnetic fields as recorded with an attocube attoMFM Ixs inside a Quantum Design PPMS.

As demonstrated by H. Yang *et al.*, the vortex arrangement in their samples evolves from strong disorder at very low fields (several Oe) to more uniform patterns at higher field (100 Oe) as the density increases and vortex-vortex interactions overcome the pinning forces.

Experimental Setup

The attoMFM Ixs setup is shown on the right as well as sketched in Figure 1. On top of an ANPxyz51 positioner stack (3 x 3 x 2.5 mm³ range), an ANSxy50 (here 19 x 19 µm² scan range @ 4 K) and an ANSz50 scanner (2 µm scan range @ 4 K) are mounted, together with a heater / temperature sensor element and the sample holder. The interferometric sensor head is mounted to the top of a rigid housing while the sample is scanned. For the MFM measurements, standard hard magnetic point probes from NanoWorld were used. For each field, the sample was first heated to above its transition temperature, field-cooled to 2 K, and subsequently imaged by MFM.

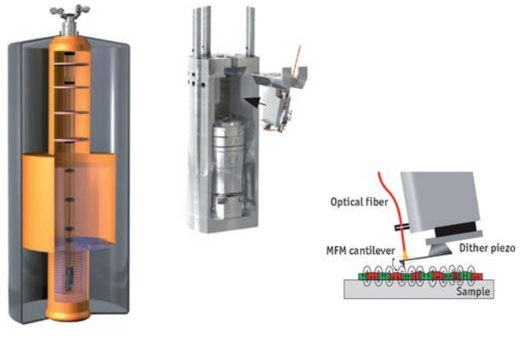

Figure 1: *The attoMFM Ixs (left) and the measurement head. On the right, the MFM measurement principle and the interferometric deflection detection is shown.*

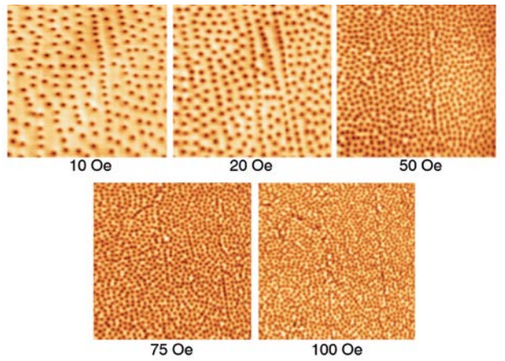

Figure 2: *MFM scans of 19 x 19 µm² size at 2 K and different magnetic fields ranging from 10 to 100 Oe.*

As the sample surface was well prepared by cleaving, the surface was extremely flat. After slope compensation utilizing a tapping mode scan, the MFM images are scanned with a constant lift height of only 10-20 nm (see Figure 2).

The open-loop xy-scanners ANSxy50 do show the typical artifacts known from piezo scanners, as e.g. non-linearities and hysteresis. In the measurements presented here, the authors performed calibration scans on a known grating sample, thus achieving distorted images of this standard pattern. By using a non-linear afitting procedure as shown below, the parameters for linearizing identical scan images were found (identical in temperature, scan size, and speed). The vortex images measured in a separate cooling cycle were then post-corrected for linearity and hysteresis using these parameters.

Correction of Scanner Hysteresis and Non-linearity

To discuss the linearization procedure in detail, an example scan is shown in the upper image of Figure 3. Here, a 32 x 32 µm² area of a calibration grating was scanned using a different scanner. The image can now be linearized using additional software. The following steps were performed to find out the linearization parameters:

- First, the image was flattened,
- then the coordinates of selected (equidistant) features were identified,
- and finally fitted using a third order polynomial.
- The so received correction parameters can now be used in a polynomial distortion routine.

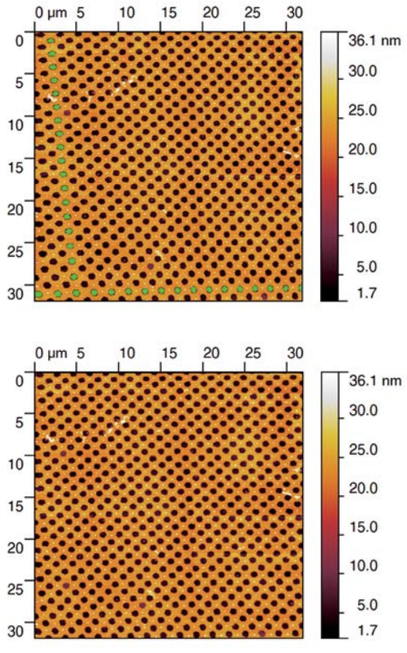

Figure 3: *Upper: Scan of a known calibration grating. The dots have been marked using a threshold criterion, while only one representative line and column was chosen.*
Lower: Resulting image after distortion correction.

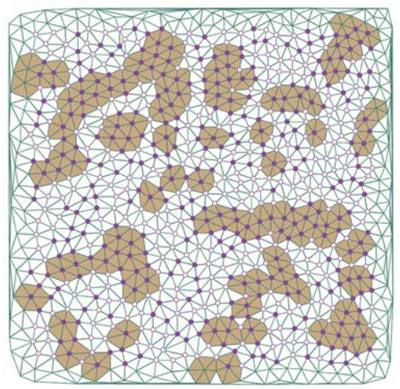

Figure 4: *Delaunay triangulation of the vortex centers at 100 Oe. Filled purple dots mark six-neighbored vortices. The brown areas show the area of the distorted triangle lattice.*

The final image is shown in the Figure 3 (lower image). Note that this procedure can also be done in an automated way using the hysteresis correction tool of commercial software [3].

Measurements

After the correction procedure, the authors took the coordinates of all the vortex centers and used a Delaunay triangulation to find the vortex distribution (see Figure 4) as well as looked at self-correlation images. The statistics (not presented here) show that square and hexagonal structures coexist, with a more random distribution governed by pinning at low fields. At intermediate fields of 20-50 Oe a mostly square pattern dominates, while the six-neighbored structure is clearly favored at higher magnetic fields (≥100 Oe), due to higher forces and lower distances between the vortices. In addition to these findings, vortex chains are observed in underdoped samples with nearly randomly distributed vortices between the chains.

Moreover, in Figure 5 surface steps are found to behave as pinning centers. It is worth pointing out that this image was achieved already during the initial installation and training on the attoMFM Ixs.

Summary

The authors observed a cooperative pinning induced by the large-scale twin boundaries and the weak local disorders, which may be a common picture to describe the vortex dynamics in iron pnictide superconductors.

References

[1] H. Yang, B. Shen, Z. Wang, L. Shan, C. Ren, and H.H. Wen, Phys. Rev. B **85**, 014524 (2012).
[2] A. A. Abrikosov, Zh. Eksp. i Teor. Fiz. **32**, 1442 (1957); Soviet Phys. JETP **5**, 1174 (1957).
[3] www.imagemet.com

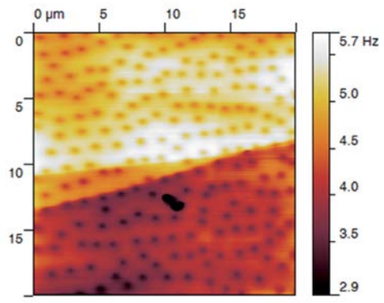

Figure 5: *Vortex image in the presence of two steps on the surface at 10 Oe and 2 K. From a topography scan one can see that the heights of the two steps are about 10 nm each. Image dimension is 19 x 19 µm². The vortices near the steps are pinned along the edge of the steps.*

pioneers of precision

Low Temperature Surface Piezoelectricity in $SrTiO_3$ using an attoAFM I for Piezo-Response Force Microscopy

Natalia Andreeva, Semyon Plyastov
NCM group, St. Petersburg State Polytechnical University, Russia

$SrTiO_3$ (STO) is one of the most investigated materials from the ferroelectric perovskite titanates family due to the variety of physical phenomena ranging from incipient ferroelectricity to superconductivity. Nowadays, considerable interest to STO is conditioned by the observations of additional anomalies in the quantum paraelectric regime of STO, which could be described in terms of a coherent quantum state occurring below $T \approx 37$ K [1]. It is supposed that these anomalies are related to the existence of large polarization clusters. Visualizing the dynamic of ferroelectric nanoscale structure at low temperatures may shed light on the mechanisms of the $T \approx 37$ K anomaly.

To observe the ferroelectric structure at nanoscale, a sample of STO ceramics was scanned in vertical piezo-response force microscopy (PFM) mode with an attocube systems attoAFM I microscope. The purpose of the experiment was to find out the dynamic of piezo-response from STO with changing temperatures from 8 K to ambient. It should be noted here that the effective vertical piezoelectric coefficient for STO ceramics never exceeded 1 pm/V, making PFM measurements quite challenging.

At room temperature, a good contrast on STO sample in PFM mode was obtained. Then the system was cooled down and the PFM data were taken from 8 K to ambient temperature with steps of 10 K. A slight enhancement of the piezo-response signal from STO at 8 K was observed. Further on, the PFM contrast remained on the same level up to 130 K. At $T \approx 130$ K though, a sharp enhancement on both PFM amplitude and phase signals was recorded (see Figure 2 and 3). This point in temperature can be associated with an antiferro-distortive phase transition (cubic --> tetragonal) in STO.

All measurements have been done by N. Andreeva and S. Plyastsov from the Research and Educational Center "Physics of Nanocomposite Materials" of the Saint Petersburg State Polytechnical University. The sample is courtesy of A. Kholkine, University of Aveiro, Portugal.

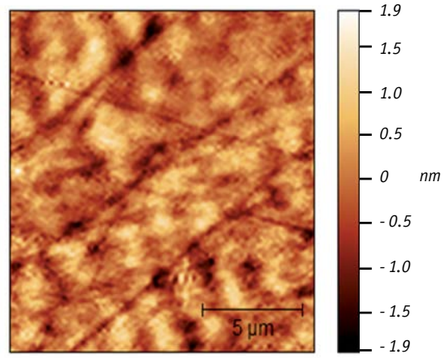

Figure 1: *Topography of STO ceramics at 130 K. Scan size is 15 x15 µm.*

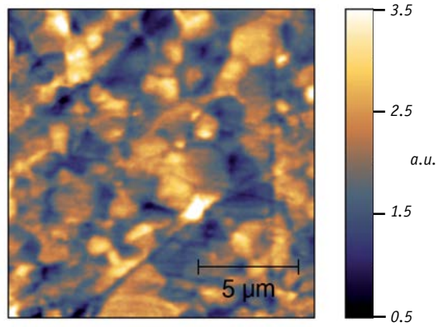

Figure 2: *Out-of-plane PFM amplitude of STO ceramics at 130 K. The PFM amplitude never exceeded 1 pm/V.*

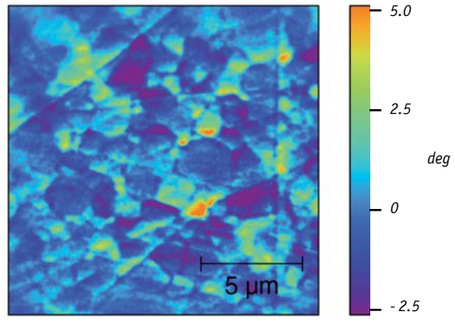

Figure 3: *Out-of-plane PFM phase of STO ceramics at 130 K.*

Scanning Tunneling Spectroscopy and Vortex Imaging on $NbSe_2$ with attoAFM III / STM I at 315 mK

Christian Debuschewitz
attocube systems AG, Munich, Germany

Scanning Tunneling Spectroscopy (STS) is a useful tool to characterize material properties, especially on superconductors at ultra low temperatures. In a series of experiments STS measurements as well as vortex imaging on $NbSe_2$ have been performed at a temperature of only 315 mK. The tests show excellent stability of the combined attoAFM/STM microscope setup as well as the possibility to apply stable voltages in the micro-Volt range.

An etched Platinum/Iridium tip was mounted on a tuning fork, thus allowing shear force measurements as well as STM type measurements. The setup including a small low temperature compatible trans-impedance amplifier was integrated in a 300 mK attoliquid3000 cryostat system (sample in vacuum) equipped with a 9 T magnet. To achieve the low noise and high stability required, the ANC250 voltage amplifier was used in combination with the ASC500 scan controller.

Typically, STS measurements involve the local measurement of the tunneling current versus the tip-sample bias voltage (see Figure 1) and measurements of the tunneling conductance *dI/dV* versus the bias voltage (as shown in Figure 2). In both experiments the superconducting gap can be clearly identified with 2Δ being 2.8 mV.

Additionally, an external field of 1 T was applied to generate a vortex pattern in the superconductor. Setting the bias voltage to a fixed value of ~1.4 mV, the typical hexagonal Abrikosov flux pattern (see Figure 3) was resolved. By analyzing the achieved image, the distance of the vortex centers were determined, in excellent agreement with the expected value for a magnetic field of 1 T.

These measurements prove the excellent mechanical and thermal stability of the setup. Hence, the combined tuning fork based attoAFM III /attoSTM I microscope system is the ideal instrument for analyzing and spatially mapping materials properties at low temperatures.

The sample was generously provided by of R. Kramer, Katholieke Universiteit Leuven, Belgium. The measurements were performed in the attocube application labs.

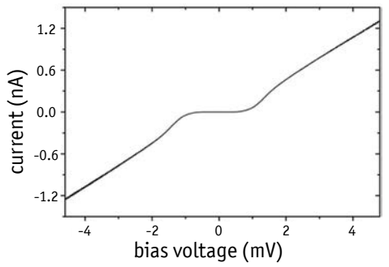

Figure 1: *Current-Voltage image of the superconducting $NbSe_2$ at 315 mK. The graph clearly shows the superconducting gap.*

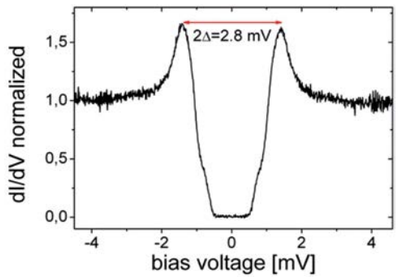

Figure 2: *dI/dV image of the superconducting gap. A fine structure of unknown origin at the side walls of the gap can be seen.*

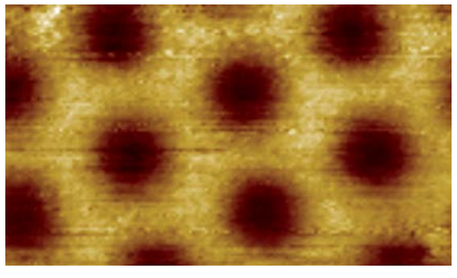

Figure 3: *Vortex imaging on $NbSe_2$ at 315 mK and 1 T external field. The image was taken at a bias voltage of 1.4 mV.*

In-situ characterization of exposed e-beam resist using an attoAFM III inside a electron microscope

Hans Koop, Christoph Bödefeld, Martin Zech
attocube systems AG, Munich, Germany

Pushing the size of e-beam lithography pattern to the nanometer range opens up new challenges for lithography apparatus and procedures. In order to achieve highest resolutions, a better understanding and control of the processes taking place on the nanometer scale in e-beam resists is crucial. In this application note, the impact of e-beam exposure on PMMA (poly-methyl methacrylate) is characterized by an in-situ application of attocube's attoAFM III in a Raith eLINE electron beam lithography (EBL) system (see also [1,2]).

Figure 1 shows the tuning-fork based attoAFM III in the configuration as used for these experiments. The setup is designed to fit into all standard SEM/EBL systems available and allows an operation in conditions ranging from ambient pressure to ultra-high vacuum ($1x10^{-9}$ mbar). A small tilt angle of the AFM tip with respect to the e-beam allows imaging every location on the surface with both AFM and SEM microsopes simultaneously.

In the experiment described, 60 nm thick PMMA A2 resist was spun onto a silicon substrate. Line-and-spaces pattern were subsequently exposed at different electron doses while keeping the acceleration voltage contant at 20 keV. Figure 2a) and 2b) show AFM phase and topography images of the resist as exposed to a 1 µm/2 µm line-and-spaces pattern at a dose of 190 µC/cm², indicating the shrinkage in resist thickness at exposed locations. In this specific example, exposed areas show a shrinkage of 0.45 nm compared to unexposed locations on the same resist. To demonstrate the vertical resolution/noise limit of the AFM apparatus, we have subtracted two neighboring topographic line cuts yielding a vertical noise figure of only 40 pm, see Figure 2c). In a separate set of experiments, the dependance of exposure dose on resist shrinkage was investigated. As can be seen in Figure 3, an increase in exposure dose yields an increase in resist shrinkage, with a roughly linear depenance between both figures (not shown).

In this application note, we have demonstrated a novel technique which allows the in-situ characterization of exposure processes of e-beam lithography processes, allowing a step-wise proximity correction and a reexposure of underexposed spots. Instead of the traditional approach of imaging the post-processed resist in a scanning electron microscope (SEM) as shown in Figure 1a), we have used an in-situ AFM to deliver more physically valuable information, such as polymer grain size and distribution.

(This work and the measurements were performed in collaboration with the groups of M.-C. Amann and A. W. Holleitner, Walter Schottky Institut and Physik-Department, Technische Universität München, Am Coulombwall, Garching, Germany).

[1] M. Zech, H. Koop, K. Karrai, D. Schnurbusch, A. Holleitner, M. Mueller, Microscopy and Microanalysis 16 (Suppl. 2), 476 (2010). doi:10.1017/S1431927610058988.
[2] H. Koop, M. Zech, K. Karrai, D. Schnurbusch, M. Müller, T. Gründl, M.-C. Amann and A. W. Holleitner, J. Vac. Sci. Technol. B **28**, 802 (2010). doi:10.1116/1.3457938

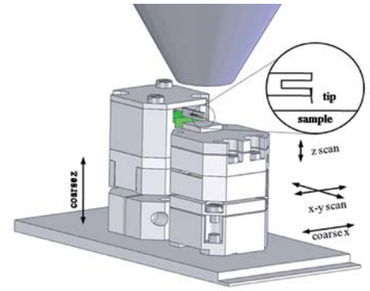

Figure 1: *Schematic drawing of the tuning fork-based attoAFM III as used inside a Raith eLINE EBL system. The system allows the in-situ characterization of the the quality of exposed ebeam resist without the need of a development process.*

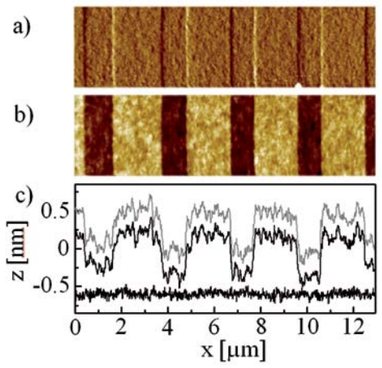

Figure 2: *Phase and topography image of an undeveloped resist measured in-situ by AFM. The topographic profiles of 2 neighboring lines cuts are shown in c). The two line cuts are shifted vertically for better visualization. The bottom graph shows the subtraction of the (non-shifted) line cuts, demonstrating a vertical noise of order 40 pm rms.*

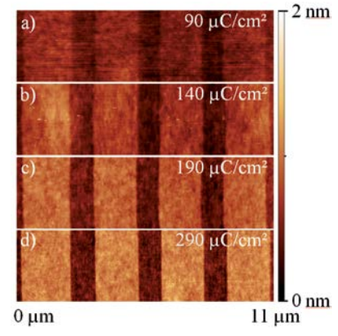

Figure 3: *Topographic images of undeveloped resist, exposed to doses ranging from 90 to 290 µC/cm². The dark areas are corresponding to exposed regions, where shrinkage of the PMMA has taken place.*

Low Temperature Raman Measurements on Layers of Graphene using the attoCFM I

Constanze Metzger, Sebastian Remi, Bennett Goldberg
Nanophotonics group, Physics Dept./Photonics Center, Boston University, MA, USA

In this report, we present Raman measurements on layers of Graphene performed with a modified attocube attoCFM I setup. Appropriate laser line filtering as well as an additional spectrometer were used in order to resolve the Raman spectra. The optical resolution of the setup is well below 1 µm, whereas the spectral resolution is better than 1 cm^{-1} at 633 nm.

The Graphene sheets were prepared by micromechanical cleavage, using scotch tape to peel off thin layers from a crystal of natural Graphite. Those layers were transferred to a Si wafer covered with 300 nm SiO_2. The sample was mounted into the attoCFM I and cooled down in a bath cryostat to $T = 4.2$ K with approx. 10 mbar of Helium as exchange gas. Figure 1 shows a confocal scan in reflection mode of the sample. Different regions with the bare SiO_2-substrate, or covered with single or bilayer Graphene can clearly be seen due to the optical contrast and can be distinguished using their different Raman spectra. Furthermore, the sheets are partly covering 20 nm deep holes, which were etched into the surface of the wafer. Figure 2 shows Raman spectra taken of the Graphene 2D band around $1/\lambda \approx 2650\ cm^{-1}$ at low excitation powers. A HeNe Laser was used as excitation source. The figure shows data from the single and bilayer regions of the sample. Clearly visible is the symmetric line shape of the single layers in contrast to the asymmetric line of the bilayer region allowing for a clear identification of the thickness of the sample. While staying in the single layer region, a spatial scan across one of the holes was performed (see red line in Figure 1) and the peak position of the respective Raman signal was recorded. The presence of the hole causes a very pronounced shift in the spectrum of about 12 to 14 cm^{-1}, consistent with strain induced Raman shift in the sheet [1].

In summary, Raman spectroscopy is a sensitive tool to distinguish between single and double layer sheets of Graphene. Additionally, a shift of the position of the single layer Raman peak has been shown in regions where the Graphene sheet covers the 20 nm deep holes. As a consequence it is concluded that this shift is due to mechanical stress in the layer, identifying regions with biaxial strain in the graphene sheet.

The data was generously provided by C. Metzger and S. Rémi from the Nanophotonics group of Prof. Bennett Goldberg, Physics Department / Photonics Center, Boston University, USA.

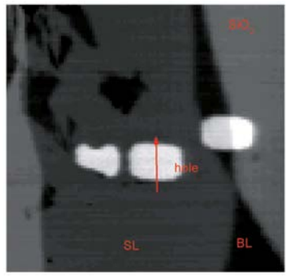

Figure 1: *Confocal scan of a sheet of Graphene on 300 nm SiO_2. The optical contrast allows identifying different regions as substrate (SiO_2), single layer (SL) and bilayer Graphene (BL), as well as three partly covered holes. Scan size: 30 x 30 µm², T = 4.2 K, Excitation = 632.8 nm.*

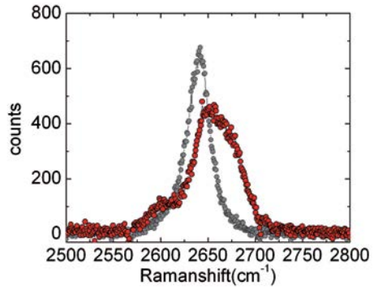

Figure 2: *Raman spectra of the Graphene 2D band for a single layer (black) and a bilayer (red). A HeNe laser was used for excitation, excitation power was P ≈ 200 µW.*

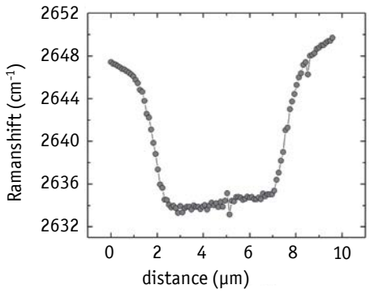

Figure 3: *Position of the 2D Raman band measured along the red line in Figure 1. There is a clear shift in the position of the Raman peak indicating e.g. stress in the sheet.*

References

[1] C. Metzger, S. Remi, M. Xiu, S.V. Kasminsky, A.M. Castro Neto, A.K. Swan, B.B. Goldberg, Nanodett., **10**, pp. 60-10 (2010).

Dynamic nuclear polarisation in GaAs/AlGaAs dots observed with the attoCFM I at 4 K

Evgueny Chekhovich, Maxim Makhonin, Alexander Tartakovskii
Department of Physics, Sheffield University, UK

In this note, nuclear spin effects are studied in individual quantum dots pumped by circularly polarised excitation using an attoCFM I. Spin is transferred from optically generated electrons to the system of about 10.000 nuclear spins. The effect of nuclear spin polarisation on the electron spin can be described in terms of effective nuclear magnetic field (also referred to as Overhauser field). Optically generated Overhauser fields of the order of several Tesla are observed localised in a single quantum dot of 4 x 20 x 20 nm³ in size (see Figure 1).

Optically pumped nuclear polarisation has striking dynamic properties: for example in electron-charged InP/GaInP dots a high nuclear spin polarisation can be excited in a few ms, but survives after the light has been switched off for hundreds of seconds with some background polarisation observed after two hours.

Additionally, optically detected nuclear magnetic resonance (ODNMR) spectra of a single quantum dot have been measured with this setup (see Figure 2). This allows insight into the local material composition on the nano-scale. This has been demonstrated only once before in 1997 by D. Gammon and co-workers [1]. The quality of data is considerably higher thanks to the stability of the attoCFM I.

Obviously, such measurements require exceptional set-up stability, since for each point in the decay curve (see Figure 3) a single dot is excited and probed by an individual pump-probe pulse pair. To remove uncertainty introduced by the noise in the CCD detectors, the whole decay curve has to be measured several times in the same conditions. Hence, the experiment is run for up to 25 hours, during which time the sample drift is considerably less than the 400 nm aperture size in the metallic shadow film through which the dot is optically excited.

Additional measurements of nuclear spin effects in charged and neutral quantum dots have been carried out with the setup (see [2]).

The following advantages of the attoCFM I setup seem to be crucial for these experiments:

- free space access conserving polarisation of light;
- exceptional mechanical stability both at zero and high magnetic fields;
- very small sample drift when scanning the field (<< 400 nm up to 2.5 T).

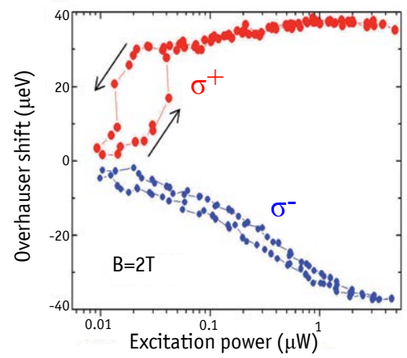

Figure 1: *Nuclear spin polarisation in interface GaAs quantum dots. The Overhauser shift increases with higher excitation power. Arrows indicate the direction of the sweep.*

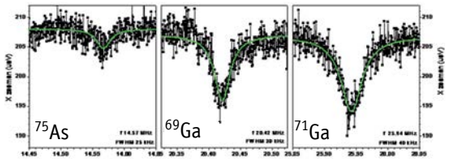

Figure 2: *Optically detected NMR (ODNMR) spectra of a single quantum dot. This allows to analyze the local material composition on the nanoscale.*

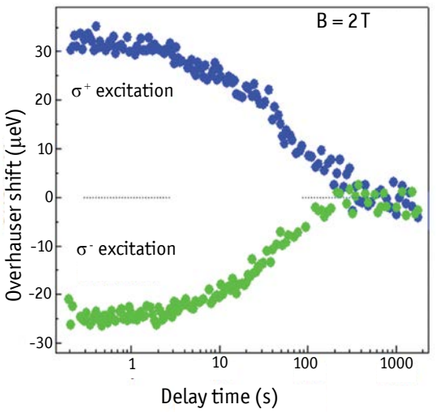

Figure 3: *Nuclear polarisation decay measurements in GaAs dots. A very smooth decay curve is observed, with the nuclear spin decay most probably caused by the nuclear spin diffusion in the semiconductor matrix surrounding the dot (see A. E. Nikolaenko, et al., PRB 79 1(R), 2009).*

References

[1] D. Gammon, *et al.*, Science **277**, 85 (1997).
[2] E. Chekhovich, *et al.*, submitted.

Stress-strain behaviour of fibrous biological material measured using an attoAFM/SEM

Fei Hang, Dun Lu, Asa Barber
Queen Mary University, London, UK

Christoph Bödefeld, Martin Zech
attocube systems AG, Munich, Germany

Bone is a complex composite material with a structural hierarchy from the millimeter down to the nanometer scale. On the latter, collagen fibrils - the building blocks of bone-form the predominant structural feature, significantly contributing to the overall performance of the bone. In order to understand the relationship between deformation at this fibrillar level and larger length scales, an investigation of the mechanical properties of the collagen fibrils becomes important.

In this application note, attocube's cantilever-based attoAFM I was used inside a FEI Quanta 3D Scanning Electron Microscope (SEM) to perform nanometer-scale tensile measurements of individual collagen fibrils [1]. The fibrils were extracted from the fractured surface of antler and were attached to the cantilever with the aid of a high vacuum compatible glue. The actual process of coating the silicon cantilever with glue is depicted in Figure 1a. After the collagen fibril was attached and the glue had hardened, the cantilever was slowly retracted while the force imposed on the collagen fibril was recorded. The latter measurement was achieved by interferometrically tracking the deflection of the cantilever (for the setup see Figure 1b). With a typical cantilever spring constant of only 0.2 N/m, a force resolution better than 100 pN was readily achieved in a 1 kHz measurement bandwidth.

Figure 2 shows the actual result of the stress-strain measurement conducted on a single collagen fibril. Up to a strain of 4%, the collagen fibril deforms elastically whereas higher strain values lead to strain hardening. It is interesting to note that the collagen fibril has a failure strain of 6% and an ultimate strength of 0.18 GPa. This makes the fibril half as strong as structural steel (ultimate strength typically 0.4 GPa) and indicates that the fibril has some degree of mineralization improving its overall performance.

Apart from the above measurements, Barber *et al.* have also addressed the question as to whether or not the vacuum conditions inside the SEM chamber alter the mechanical properties of the fibril. In this context, it was shown that vacuum exposure of less than an hour does not provide any degradation of the mechanical properties of the fibril. However, the ultimate tensile strength is reduced to 25% of its initial strength when exposed to vacuum for about 400 minutes. This decrease in strength is attributed to dehydration of the fibril.

In summary, attocube's attoAFM I was used inside an SEM chamber to measure the stress-strain behaviour of collagen fibrils, the building blocks of bone. With a force resolution of better than 100 pN, the cantilever-based attoAFM I allowed precise measurements of the mechanical behaviour of the fibrils, providing insight to their contribution to the overall mechanical performance of bone.

References

[1] A. Barber *et al.*, Mater. Res. Soc. Symp. Proc. **1187-KK06-06** (2009).

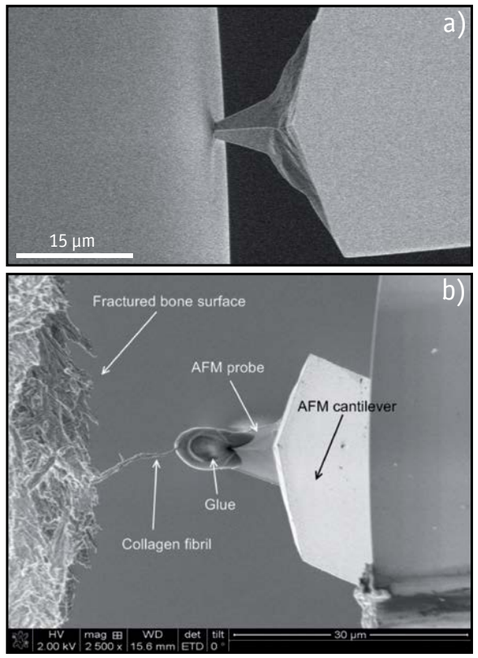

Figure 1: *(a) SEM image showing the AFM cantilever in touch with the vacuum compatible glue which is later on used to attach individual the collagen fibrils to the cantilever (b) after the glue is cured, the tensile measurement is initiated. The circular object to the right hand side is the optical fiber which is used to interferometrically measured the deflection of the cantilever during any experiment.*

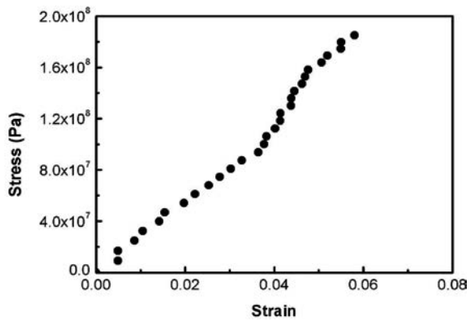

Figure 2: *Actual stress-strain measurement of a single collagen fibril. With an ultimate strength of 0.18 GPa, the tensile fibril is nearly half as strong as structural steel (0.4 GPa).*

APPLICATION NOTE

attoMICROSCOPY
Sophisticated Tools for Science

Optical absorption on a single semiconductor quantum dot with magnetic field applied in Voigt geometry

Martin Kroner, Khaled Karraï
Department of Physics, Ludwig-Maximilians University, Munich, Germany

The modular design of the attoCFM III represents a highly flexible and versatile system for high resolution spectroscopy. In these experiments, the setup has been modified to accommodate an inverted geometry. A special confocal objective was designed that redirects the incoming light by 90° to impinge onto the sample perpendicular to the externally applied magnetic field, i.e. in Voigt geometry (see Figure 1).

The measured spot diameter of ~1.5 µm is only slightly larger than that of a standard axial confocal objective. The light transmitted through the sample is measured by a photo detector directly behind the sample. All parts are made from Titanium, so that the microscope maintains its high stability during cool-down to cryogenic temperatures and exposure to magnetic fields of up to 8 T.

The optical setup allows performing high resolution laser spectroscopy on a single, self-assembled quantum dot (QD). Figure 2(a) shows the optical spectra of a QD charged with a single electron (X^{1-}), measured with different laser polarizations at 0.7 T in Voigt geometry. According to the respective optical selection rules, the unpolarized resonance line of the X^{1-} splits into four lines (see Figure 2a-i), where two transitions are mediated by linear polarized light parallel to the external magnetic field (π_0; see Figure 2a-ii), and two by light polarized perpendicular to the magnetic field (π_{90}; see Figure 2a-iii). Transmission spectroscopy allows direct probing of these optical selection rules.

In Figure 3, the magnetic field dispersion of all four resonances is shown as a function of the applied magnetic field. The ground states (one electron in the QD; electron depicted by a filled triangle; direction indicating spin arrangement) and excited states (two electrons with anti-parallel spin and one hole; hole indicated by an open triangle) are spilt according to their Landée *g*-factors. Optically allowed transitions connect all four levels leading to four resonances lines with comparable oscillator strength.

The presented experimental setup allows studying the anisotropic magnetic properties of single self-assembled quantum dots with high degree of precision (see Fig. 2(b)) [1]. Furthermore, the resonant optical pumping offers a spin shelving scheme for the resident electron in the QD [2,3], which was already demonstrated to be orders of magnitude more efficient if the magnetic field is applied in Voigt geometry rather than in Faraday geometry [3,4]. The equally strong coupling of the two Zeeman split ground states to either of the excited states opens the way for quantum optical coherent spin manipulation schemes as they are known from atom optics [3].

References

[1] M. Bayer, *et al.*, Physical Review B **65**, 195315 (2002).
[2] M. Atatüre, *et al.*, Science **312**, 551 (2006).
[3] M. Kroner, *et al.*, to appear in PRB.
[4] Y. Wu, *et al.*, Physical Review Letters **99**, 097402 (2007).

Sample courtesy of P. Petroff, UCSB, Santa Barbara, USA

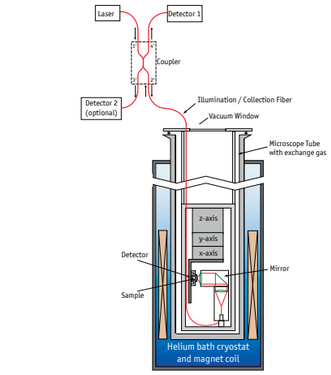

Figure 1: *Diffraction limited, fiber-based confocal microscope for high resolution spectroscopy in Voigt geometry, based on the CFM III design.*

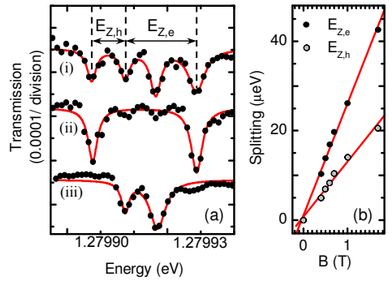

Figure 2: *(a) Transmission spectra of a single negatively charged quantum dot at a magnetic field of 0.7 T applied perpendicular to the quantum dot symmetry axis. The resonance line splits in four linear polarized lines (i). The outer resonances are resonant to light polarized parallel to the applied magnetic field direction (ii). The inner lines are polarized perpendicular (iii). (b) The Zeeman splitting of the electron ($E_{Z,e}$) and hole ($E_{Z,h}$) states of the quantum dot as a function of the magnetic field. The energies can be obtained directly from the spectra as shown in (a).*

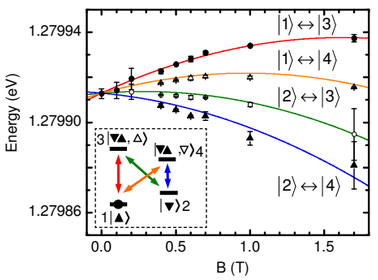

Figure 3: *Magnetic field dispersion of the X^{1-} resonance energies as a function of the magnetic field applied in Voigt geometry. The inset depicts the electronic and excitonic levels, interconnected by four optical transitions as indicated by the arrows.*

Tuning Fork based AFM Measurements of uncapped, stacked InAs Quantum Dots in a GaAs matrix

Claudio Dal Savio, Christoph Bödefeld
attocube systems AG, Munich, Germany

The attoAFM III is a tuning fork based setup for highly precise low temperature measurements. The non-optical design faciliates e.g. measurements on light-sensitive samples using conductive STM-type tips.

The distance feedback is done by detecting the tuning fork vibration using a Phase-Locked Loop (PLL) together with a feedback loop. The PLL tracks the resonance of the tuning fork, whereas the feedback loop keeps the z-distance in such way that the frequency shift (vs. the free oscillation) remains at a certain level. Deriving from the measurements which are presented in this application note, the z-noise (RMS) of such measurements is typically as low as 30 pm.

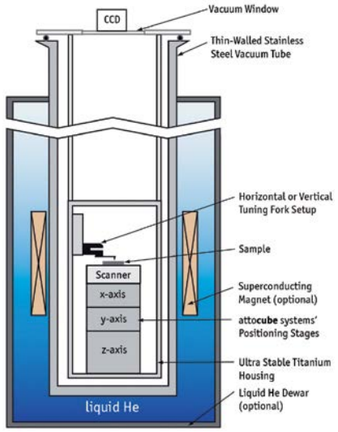

Schematic drawing of the attoAFM III

The sample under investigation features stacked, uncapped InAs quantum dots in a GaAs matrix (sample courtesy of P. Petroff, UCSB, Santa Barbara, USA). As can be seen from the topography image (Figure 1a), the dots are about 300 nm x 100 nm in size while having a height of about 4 nm (the scan size is ~2 x 2 µm²). Especially in the error image (Figure 1b), one can see atomic steps in the surrounding InAs.

On another spot of the sample, this has been investigated in more detail (Figure 2). Clearly spaced steps are visible in this graph. The height distribution is presented in Figure 3, showing atomic steps with a spacing of ~2.04 +/- 0.02 Ångstrøm. This corresponds to the atomic lattice constant of InAs of ~2.1 Å. The small difference is can be accounted to the scanner calibration.

As mentioned above the roughness analysis yields an RMS roughness value of 30 pm in this measurement, showing the excellent stability and low noise of the attoAFM III instrument.

The InAs QD sample is courtesy of P. Petroff UCSB, Santa Barbara, USA.

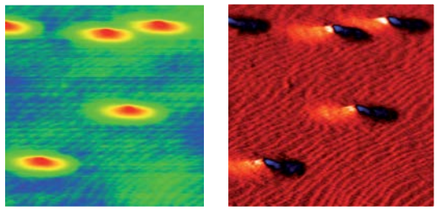

Figure 1: *Tuning fork AFM measurements of uncapped, stacked InAs Quantum Dots in GaAs at ambient conditions.*

Figure 2: *Detailed topographic image when performing a scan of 500 x 500 nm.*

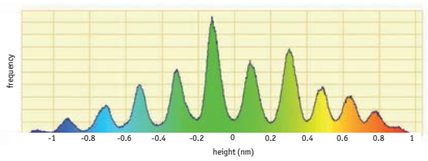

Figure 3: *AFM height distribution data extracted from Figure 2 yielding the atomic step height.*

attoMOTION
Piezo-based Nano Drives

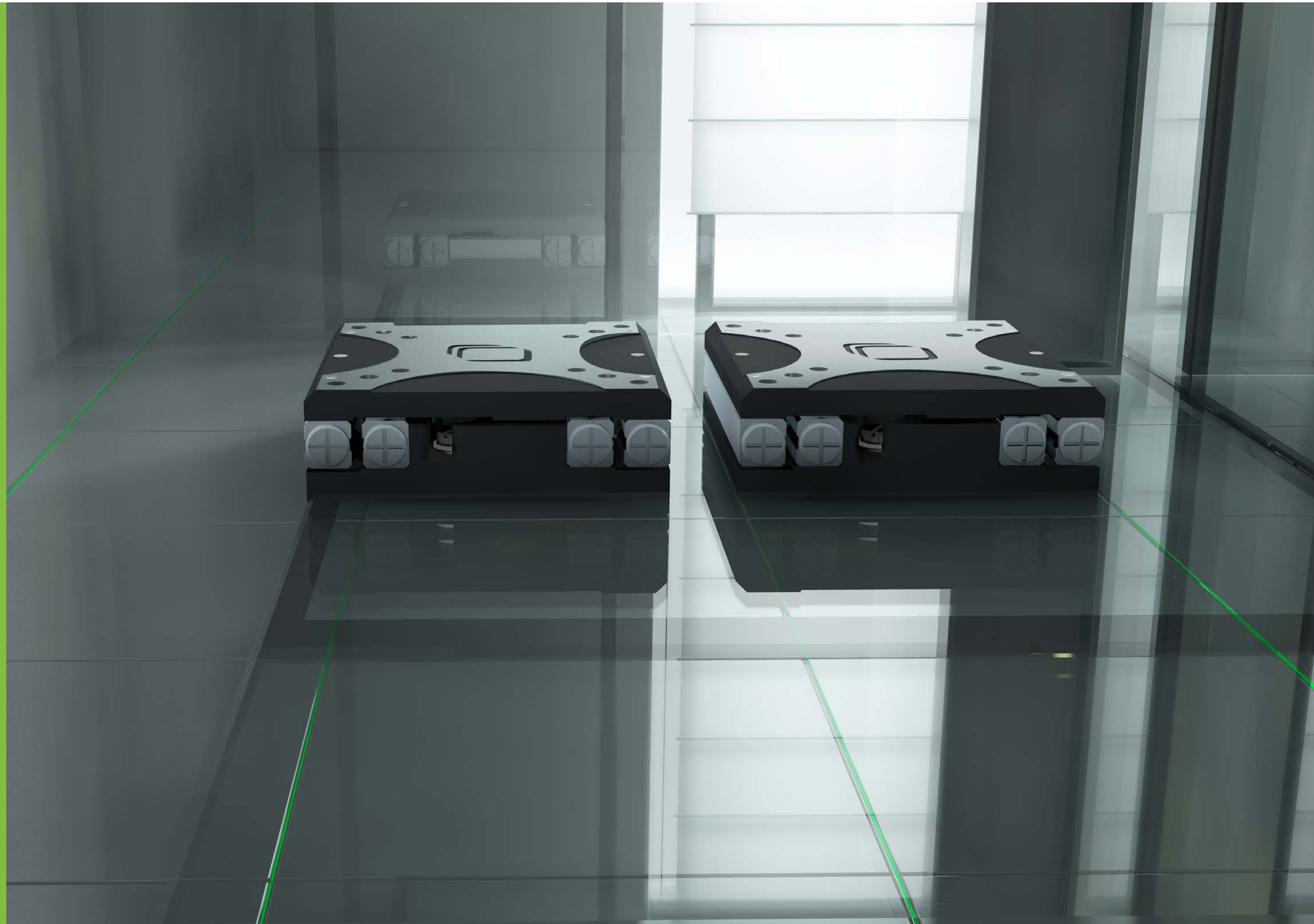

In situ Measurements of Irradiation-Induced Creep on Amorphous Micropillars

Sezer Özerinç, Robert S. Averback, William P. King
University of Illinois at Urbana-Champaign, Urbana IL, USA

Introduction

Cladding materials used in nuclear power plants experience irradiation-induced creep (IIC), due to combined irradiation damage and stress. Reliable design of the power plant requires a detailed understanding of the IIC. *In situ* creep measurements using high energy ion beams provide an accelerated way of characterizing IIC. In such experiments, heavy ions in the MeV energy regime are used to accurately simulate the damage conditions in a nuclear reactor environment. However, the penetration depth of MeV heavy ions is only about 1 µm; therefore, micron-sized specimens are required for direct measurements.

IIC measurements on miniaturized specimens are challenging due to the high force resolution (~1 µN) and displacement resolution (~1 nm) requirements. We have overcome this challenge by developing a micropillar compression apparatus that combines a microfabricated silicon transducer with an attocube ECS3030 nanopositioner and an FPS3010 interferometric displacement sensor [1]. We used the apparatus to measure the IIC of amorphous $Cu_{56}Ti_{38}Ag_6$ micropillars. Measurements show that the creep rate is proportional to the applied stress. The irradiation induced fluidity of the sample was measured to be 2.1 $dpa^{-1}GPa^{-1}$ (dpa: displacement per atom).

Setup Description

Fig. 1 shows a schematic of the measurement apparatus [1]. The micropillar is mounted on the nanopositioner and the laser spot of the displacement sensor is aligned with the center of the transducer. When the nanopositioner is moved, the micropillar specimen deflects the transducer. Once the required deflection (~1 µm) is reached, the nanopositioner keeps the micropillar stationary. The micropillar under compressive stress is then bombarded with 2.1 MeV Ne^+ ions. As a result, the micropillar experiences IIC, and its deformation corresponds to a decrease in the transducer deflection, which is monitored by the displacement sensor.

The apparatus has a force resolution of 0.2 µN using a transducer with a spring constant of 200 N/m. The deflection measurement can resolve displacements as small as about 1 nm. Thus for micropillars of 2 µm height, the strain resolution is 0.05%.

The silicon transducer is a doubly clamped beam with dimensions of 10 × 80 × 2000 µm³, and was fabricated using standard microfabrication techniques [1]. A 40 nm thick Al layer was sputtered on the sensor side of the transducer for high reflectivity. $Cu_{56}Ti_{38}Ag_6$ bulk samples were prepared by ball milling and micropillars of 1 µm diameter and 2 µm height were fabricated by focused ion beam. The amorphous structure of the sample was verified by X-ray diffraction analysis. Measurements were performed at room temperature in an irradiation chamber with vacuum level < 1×10^{-7} Torr. A Van de Graaff accelerator provided 2.1 MeV Ne^+ ions at an ion flux of ~1.7×10^{12} ions/(cm^2s).

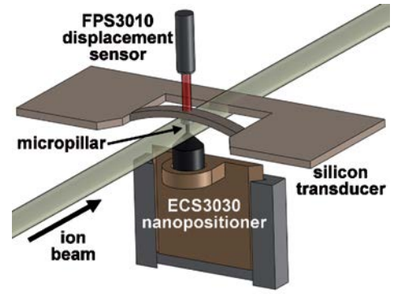

Figure 1: *Schematic of the measurement apparatus. Using the ECS3030, the micropillar is pushed against the transducer, resulting in its deflection. The micropillar is bombarded with 2.1 MeV Ne^+ ions, and its creep is measured through the change in the transducer deflection using an FPS3010 interferometer.*

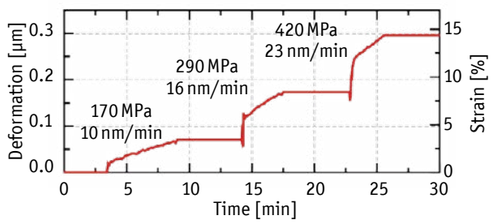

Figure 2: *Deformation of the micropillar as a function of time under irradiation. Micropillar stresses and corresponding creep rates are indicated for each loading.*

Measurement Results

Difference between the nanopositioner position reading and the displacement sensor reading provides information on the deformation of the micropillar. Fig. 2 shows the deformation of a $Cu_{56}Ti_{38}Ag_6$ micropillar under irradiation as a function of time [1]. The micropillar was loaded three times, with different transducer deflections, resulting in different stress levels. The results show that IIC rate is proportional to the applied stress, indicating Newtonian flow. This observation is consistent with previous measurements on other amorphous materials under irradiation [2].

Irradiation-induced fluidity of a material is defined as the inverse of the viscosity under irradiation normalized by the displacement damage rate. For the $Cu_{56}Ti_{38}Ag_6$ specimens, the fluidity was measured to be 2.1 $dpa^{-1}GPa^{-1}$ [1]. This value is close to results obtained using molecular dynamics simulations [3].

Summary

We have demonstrated *in situ* measurements of irradiation-induced creep (IIC) through micropillar compression. The attocube ECS3030 nanopositioner provided accurate control of micropillar position and transducer deflection, whereas the attocube FPS3010 displacement sensor has measured the deformation of the micropillar with excellent accuracy and precision. The apparatus provides a new and effective approach to IIC measurements for the accelerated evaluation of promising materials for future nuclear power plant applications.

References

[1] S. Özerinç, R. S. Averback, W. P. King, J. Nucl. Mat. **451**, 104 (2014).
[2] E. Snoeks, T. Weber, A. Cacciato, A. Polman, J. Appl. Phys. **78**, 4723 (1995).
[3] S. G. Mayr, Y. Ashkenazy, K. Albe, R. S. Averback, Phys. Rev. Lett. **90**, 055505 (2003).

Nanomanipulation of 1-D nanostructures using ECS3030 positioners inside an electron microscope

Rodrigo Bernal, Horacio Espinosa
Mechanical Engineering Department, Northwestern University, Evanston IL, USA

The characterization of 1-D nanostructures such as nanowires and nanotubes has recently become a topic of major interest, due to the potential of these nanostructures to be employed in the next generation of advanced materials and electronic devices. Due to their small characteristic size (<100 nm in diameter) and an increased surface to volume ratio, many nanostructures of a given material display significantly enhanced properties compared to the macroscale, bulk material. For example, zinc oxide (ZnO) nanowires, display a greater modulus of elasticity than bulk for diameters less than ~80 nm [1]. Similar behavior has also been discovered for other semiconducting nanowires such as gallium nitride (GaN) [2], and metallic nanowires such as silver [3].

The emergence of these size-effects in the properties of 1-D nanostructures has therefore elicited a need for the characterization and unambiguous measurement of these properties, as they are critical for the development, design and robustness of future applications employing nanostructures as their functional elements. However, the small size of the specimens imposes significant challenges for specimen preparation and testing. To overcome these difficulties, Prof. Horacio Espinosa's group at the Mechanical Engineering Department in Northwestern University, USA, has developed a microelectromechanical system (MEMS) that allows uniaxial mechanical testing of nanowires, with nanometer (nm) and nanoNewton (nN) resolution, therefore allowing the accurate measurement of mechanical and failure properties such as the elastic modulus, yield and fracture strengths [4] (see Figure 1). The system can also be employed to carry out simultaneous four-point electrical measurements as the mechanical straining is taking place, therefore allowing measurements of electromechanical properties of nanowires, such as piezoresistivity and piezoelectricity [5].

A critical step in these experiments is the sample nanomanipulation, where a nanowire must be transferred to the testing MEMS. This delicate procedure requires an instrument with capabilities of nm resolution in displacement, smooth movement to avoid any vibrations that may harm the sample, and seamless integration with an scanning electron microscope (SEM), to allow observation of the preparation process (an optical microscope lacks the needed resolution). A large range of total movement (> 1 mm) is also convenient to allow flexibility in the setup of the experiment. In recent experiments, the Espinosa group has employed an attocube Nanomanipulator, composed of three stacked ECS3030 positioners, one for each axes of movement, in order to accomplish this task. The nanomanipulator is positioned inside the SEM chamber and interfaced to the ECC100 piezo-controller, located outside the chamber, through vacuum feed-throughs. The controller is connected via USB to a laptop furnished with attocube software for controlling the manipulator.

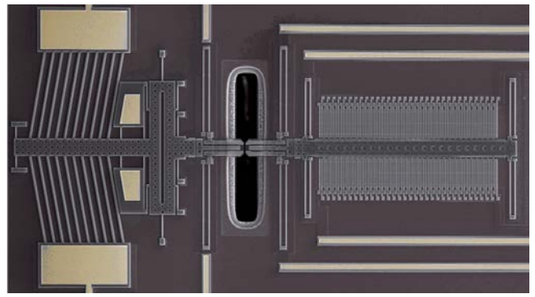

Figure 1: *MEMS device for the characterization of electromechanical properties of nanowires.*

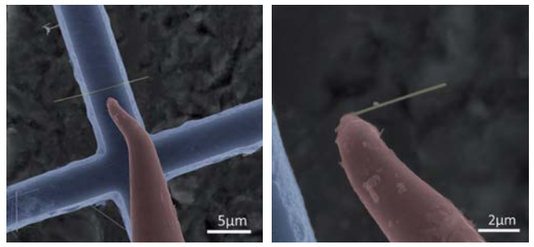

Figure 2: *Left side: Silver nanowire (yellow) laying on a copper TEM grid (blue) ready to be manipulated. The tungsten tip (red) attached to the nanomanipulator is used to approach finely to the specimen. Right side: Silver nanowire picked from the grid and ready to be mounted on the device of Figure 1. (Images manually colored for clarity)*

To perform the nanomanipulation, a sharp tungsten tip is attached to the manipulator (Figure 2, left side). Coarse-steps, of the order of µm, are used to approach the tip to the nanowire. Afterwards, fine steps with magnitudes controllable from sub-100 nm to few nm, are used to establish gentle contact between the tip and nanowire. Once the nanowire is picked (Figure 2 right side), a similar approach is used to position it on top of the MEMS device. Final attachment of the specimen is carried out by electron beam induced deposition of platinum (EBID-Pt) after which the tip is retracted from the area of interest.

References

[1] R. Agrawal, B. Peng, E.E. Gdoutos, and H.D. Espinosa, *Elasticity size effects in ZnO nanowires - A combined Experimental-Computational approach*. Nano Letters **8**, 3668 (2008).

[2] R.A. Bernal, R. Agrawal, B. Peng, K.A. Bertness, N.A. Sanford, A.V. Davydov, and H.D. Espinosa, *Effect of Growth Orientation and Diameter on the Elasticity of GaN Nanowires. A Combined in Situ TEM and Atomistic Modeling Investigation*. Nano Letters **11**, 548 (2011).

[3] T. Filleter, S. Ryu, K. Kang, J. Yin, R. Bernal, K. Sohn, S. Li, J. Huang, W. Cai, and H.D. Espinosa, *Nucleation-Controlled Distributed Plasticity in Penta-Twinned Silver Nanowires*. Small **8**, 2986 (2012).

[4] H.D. Espinosa, , Y. Zhu, and N. Moldovan, *Design and operation of a MEMS-based material testing system for in-situ electron microscopy testing of nanostructures*. Journal of Microelectromechanical Systems **16**, 1219 (2007).

[5] R.A. Bernal, T. Filleter, J.G. Connell, K. Sohn, J. Huang, L.J. Lauhon, and H.D. Espinosa, *In Situ Electron Microscopy Four-Point Electromechanical Characterization of Freestanding Metallic and Semiconducting Nanowires*. Small **10**, 725 (2014).

H.E. acknowledges funding from US Army Research Office through DURIP award No. W911NF-12-1-0366.

Transition from slow Abrikosov to fast moving Josephson vortices using the ANR31

Philip Moll, L. Balicas, V. Geshkenbein, G. Blatter, J. Karpinski, N. D. Zhigadlo, and B. Batlogg
Laboratory for Solid State Physics, ETH Zurich, Switzerland

In this paper, we report about an especially challenging transport experiment in a liquid Helium cryostat requiring milli-degree rotational accuracy and perfect angle stability over a wide range of temperatures (80 K - 2 K) and magnetic fields (±14 T), far beyond the capabilities of other rotators. Using the attocube ANR31 rotator, a precise nano-rotator setup was designed to fit on a small (25 mm diameter) standard sample carrier. It performed extraordinary well, extending our capabilities of research into areas where extreme angular precision and stability are required.

We have investigated the vortex matter of the iron-pnictide high temperature superconductors and the results were recently published in [1]. We studied the mobility of magnetic vortices in the layered superconductor SmFeAs(O,F) and could show an enormous enhancement of vortex mobility associated with a transition of the vortex nature itself, changing from Abrikosov to Josephson. The unit cell of SmFeAs(O,F) consists of layers of superconducting FeAs separated by non-superconducting Sm(O,F) layers. A perfectly in-plane Josephson vortex, centered in a "non-superconducting" Sm(O,F) layer, can only be weakly pinned and thus experiences the mentioned enhancement in mobility.

This feature, however, is immediately lost if the field is tilted out of the FeAs planes and even the smallest misalignment (<0.1°) completely destroys the effect as the misaligned vortex is not parallel to the crystallographic layers anymore. As mobile vortices cause dissipation, their mobility is observed as a very sharp spike in voltage as shown in Figure 1 (see also [1]). Therefore angular precision and stability is the key to observing this effect. In previous experiments using other rotators we missed this extremely sharp feature.

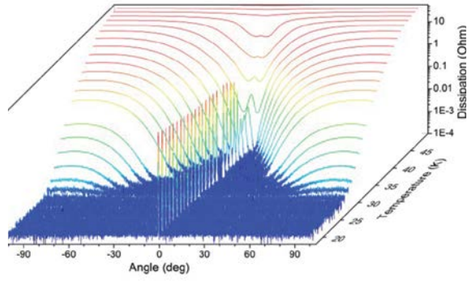

Figure 1: *Flux -flow dissipation as a function of the angle between the magnetic field (H=12 T) and the FeAs layers (=0°) for several temperatures. The main observation is the appearance of a sharp voltage spike (<0.1°) below a temperature T*≈42 K. This flux-flow voltage is caused by fast flowing in-plane Josephson vortices, remaining unpinned even down to the lowest temperatures.*

On the technical side, the rotator design addresses many issues:

- The ANR31 provides enough torque to turn even with 10(!) insulated Ag wires even at 1.9 K! These were guided as twisted pairs through the hole at the rotator axis. Hence, the rotator is more than sufficient for highly complex multi-channel transport experiments.
- The lack of angle encoding was overcome by two orthogonally mounted cryogenic hall sensors.
- The studied effect is extremely sensitive to even the smallest change in angle in the milli-degree range. Most amazingly, **no drift** on this scale has been observed even after a day when sweeping the temperature between 80 K and 2 K as well as ramping the field up to 14 T.

This unique study of the vortex nature in these high Tc compounds shows that its vortex matter still holds many surprises for us. The discovered Abrikosov- to Josephson transition was unexpected, as the materials' electronic anisotropy is low. Moreover, Josephson vortices are believed to be a feature of highly anisotropic superconductors. This finding challenges our "global" understanding of superconducting anisotropies and their relevance for the microscopic, intra-unit cell modulation of the order parameter.

References:

[1] P. J. W. Moll, L. Balicas, V. Geshkenbein, G. Blatter, J. Karpinski, N. D. Zhigadlo, and B. Batlogg, Transition from slow Abrikosov to fast moving Josephson vortices in iron pnictide superconductors, Nature Materials **12**, 134–138 (2013), DOI: 10.1038/NMAT3489.

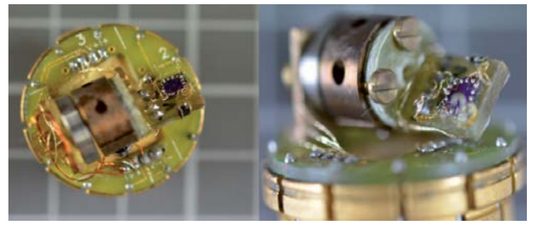

Figure 2: *Rotator setup showing the ANR31/LT rotator carrying the sample and two Hall sensors. The diameter of complete assembly is below 25 mm.*

ANPz51 Enabling Tuning of a Fabry-Pérot Resonator for High Field / High Frequency EPR

Petr Neugebauer, A.-L. Barra
High Magnetic Field Laboratory, LNCMI-CNRS, Grenoble, France

Thanks to the recent development of high field magnets, high-field/high-frequency electron paramagnetic resonance (HF-EPR) has seen a continuous growth in the last decades. One of the limitations that still exist is the relatively low power of high-frequency microwave sources of only a few milliwatts (as compared to the hundreds of mW of a usual X-band source). The standard method to enhance the microwave power on the sample is the use of a cavity. Unfortunately, the linear dimension of a cavity and its fabrication tolerances are mutually coupled and proportional to the wavelength. In the case of HF-EPR operating in the frequency range of 200-300 GHz, this translates to cavity sizes of one millimeter, which makes fabrication and sample loading very difficult.

The solution developed by Petr Neugebauer and co-workers [1] is to replace the single mode cavity with a broad band Fabry-Pérot (FP) resonator. The solution (with respect to single mode cavities) allows for measuring larger samples (crystals), easier loading, and also supports multi-frequency HF-EPR, hence measurements at several microwave frequencies. The FP resonator consists of two opposing mirrors: a semi-transparent, flat mirror (between the sample space and the corrugated taper - a gold mesh in this case) and a spherical one at the bottom of the resonator (see Figure 1).

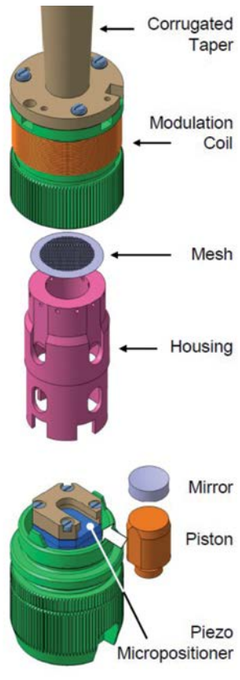

Figure 1: *The construction of the Fabry-Pérot resonator. The ANPz51 moves the mirror and hence, tunes the resonator.*

The figure of merit of a FP resonator is not the quality factor Q (as in case of a cavity), but the finesse F which is linked to the quality factor via $F = Q/n$ where n is the resonance mode. Choosing the right fine tuning of the resonator is critical, because the finesse strongly depends on it. Hence, a positioner with large working range, but very high precision is needed that can operate at low temperatures and high magnetic fields.

With the ANPz51 positioner, the group was able to move the spherical mirror of the resonator in a 3 mm range to find the right mode and fine-tune its position with a precision much better than 1 µm. The low temperature compatibility of the positioner allows the tuning procedure to be performed in situ at a certain measurement temperature and high magnetic field applied.

To demonstrate the performance of the setup they measured the cyclotron resonance on single crystal natural graphite. Figure 2 shows the results and illustrates well the increased sensitivity. In order to obtain signals with comparable intensity, it was necessary to use modulation amplitudes four times larger for the previously used transmission setup than for the Fabry-Pérot, resulting in overmodulated signals in the first case as indicated by the increased line width. More interestingly, weaker cyclotron-resonance harmonics could be observed at low field with the FP resonator. This allows approaching closer to the K point, a particularly relevant issue for better understanding of the properties graphite [2].

In summary, the use of a low temperature positioner with high precision over a long working range is essential for the realization of this new setup that increases the sensitivity of HP-EPR by at least a factor of four.

References:

[1] P. Neugebauer and A.-L. Barra, Appl. Magn. Reson. (2010).
[2] M. Orlita, P. Neugebauer, C. Faugeras, A.-L. Barra, M. Potemski, F. M. D. Pellegrino, and D. M. Basko, Phys. Rev. Lett. **108**, 017602 (2012).

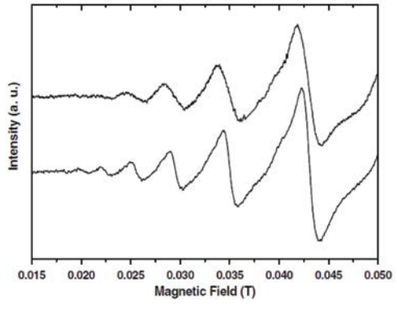

Figure 2: *Single-crystal cyclotron resonance of graphite at 283.2 GHz and 7.5 K for a magnetic field perpendicular to the carbon sheets. Upper spectrum recorded using a cavity in a transmission setup (modulation amplitude, 28 G); lower spectrum recorded with the Fabry–Pérot cavity (modulation amplitude, 6.8 G).*

Haptic 3D micromanipulation with optically encoded ANP101 positioners

Andreas Schmid, Mandayam A. Srinivasan
University College of London, UK

PD Stefan Thalhammer
Helmholtz Zentrum, Munich, Germany

Introduction

How can human touch be extended to enable manual exploration and manipulation of micro and even nano-structures? This is one of the key questions driving our research. M. A. Srinivasan of MIT, USA and UCL, UK, with support from TUM-IAS, Germany, has developed a micromanipulation system with a haptic interface to enable manual exploration, manipulation, and assembly of microstructures. In collaboration with A. Schmid of UCL, London, S. Thalhammer of Helmholtz Zentrum, Munich, and R. Yechangunja of Yantric, Inc., USA, he has demonstrated manual grasping and moving of 10 to 100 µm sized objects with direct haptic feedback of the gripping force in real-time, so that the objects can be placed in three dimensions with nanometer precision [1].

Setup Description

Our Master-Slave micromanipulation system consists of an haptic interface (Master), taking human position commands and displaying interaction forces and the robotic micromanipulator (Slave). The devices are connected through a control-ler PC. A stereomicroscope at the slave end enables visualization of the micro-objects.

Slave system:

For the micromanipulator a force-sensing microgripper with 100 µm opening is mounted onto two attocube's ANPx101/NUM and one ANPz101/NUM for xyz positioning. Additionally an ANR101/NUM rotator can adjust the tilt angle. Using the ANC350 controller box, the positioners are run in closed-loop mode with the control command continuously updated by the master commands.

Master system:

The demanded 3D-position is read by the Phantom haptic interface (in the centimeter range), scaled down and sent to the controller (micro/nanometer range). On the slave side, the force measured by the microgripper in the micro-Newton range, is scaled up to the Newton-range and exerted on the operator's fingers through the haptic interface.

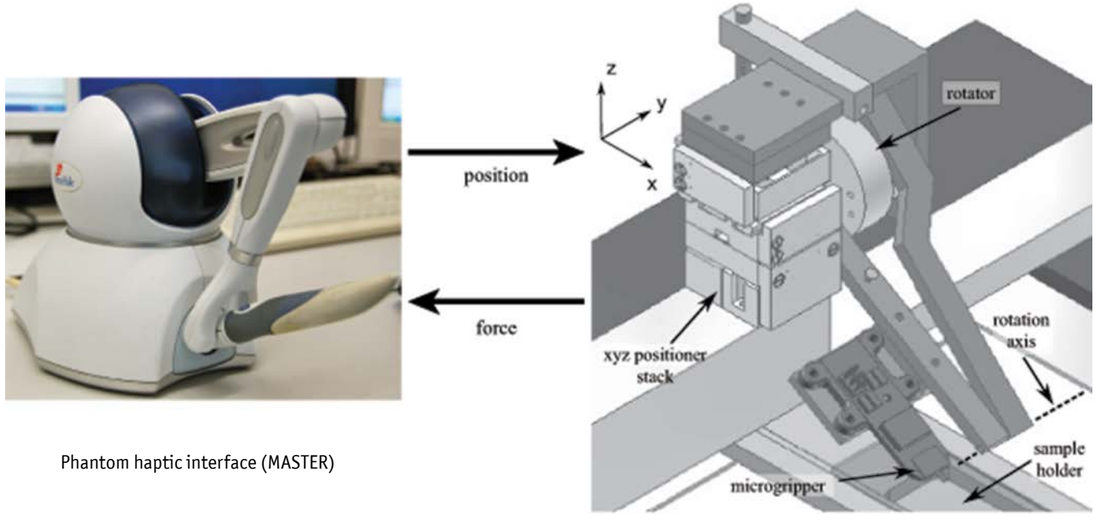

Phantom haptic interface (MASTER)

Micro-manipulator (SLAVE)

Figure 1: *Haptic interface (left) and positioner arrangement for the micromanipulator (right).*

Results

For validation of the tracking behavior and the force measurement capabilities of the manipulator, it was employed in a model scenario: to approach a glass slide from above. Performing an operator controlled, oscillating movement in y-direction (Figure 2a) the gripper was carefully moved downwards (Figure 2c) while the measured force of the gripper sensor (Figure 2d) was scaled up and presented to the operator. This force was caused mainly by friction of the tip touching the glass surface. In Figure 2e it can be seen how this force increased. With decreasing height, this force increases, which can be observed in Figure 2e.

The 3D manipulation capabilities are assessed by performing the task for stacking four 45 µm diameter polystyrol beads into a two-layered pyramid. The resulting structure is shown in Figure 3. Each bead was lifted up from the ground, moved to a target position, precisely put down and released. The human operator commanded the opening of the gripper through the Phantom device while the measured force was scaled up and displayed to the user on the device. This gives the operator a direct "feeling" for the bead.

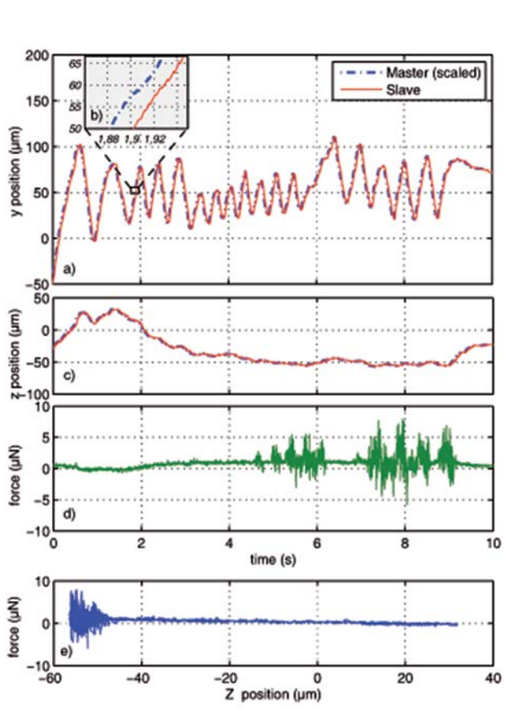

Figure 2: *Tracking behavior and force measurement during surface approach: a) y position of oscillating gripper (slave) compared to scaled master position with b), zoomed view on position trajectory, c) z position of gripper and master, d) measured force, e) measured force over z position.*

Summary

The major purpose of the presented teleoperation setup was to build a tool for human experimenters which provides them with direct and intuitive capabilities to explore and assemble micro-structures. The applied gripping force on the object could be controlled through a haptic feedback loop. This does not only prevent fragile objects from damage but actively helps reducing adhesion during contact manipulation.

Our human-in-the-loop system gives scientists a versatile tool for micro-assembly and characterization at hand.

References

[1] A. Schmid, R. Yechangunja, S. Thalhammer, and M. A. Srinivasan, Proceedings of the IEEE Haptics Symposium, 517-522 (2012).

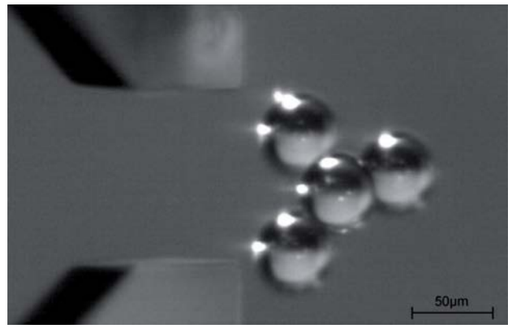

Figure 3: *Microscope image of a pyramid of four 45 µm beads as a result of 3D assembly done using the microgripper whose tips are also visible in the image.*

pioneers of precision

Controlling Electron Emission in Space and Time with ANPxyz101 positioners

Michael Krüger, Markus Schenk, Peter Hommelhoff
Max Planck Institute of Quantum Optics, Garching, Germany

Attosecond science (1 attosecond = 10^{-18} s) has enabled insights into ultrafast fundamental processes in atoms and molecules [1,2]. It is based on the steering of electrons with the electric field of ultra-short, intense laser pulses. Usually, atoms or molecules in the gas phase are used as electron source. Recently it was shown that the regime necessary for attosecond science can also be reached with nanometer-scale metal tips [3]. In this application we have investigated the dynamics of electrons emitted from a sharp tungsten tip triggered by femtosecond laser pulses [4]. The setup consists of a sharp tip which is mounted on a stack of UHV compatible attocube systems' positioners and brought into the prealigned focal spot of an off-axis-parabolic mirror (see Figure 1).

The whole setup is situated in an UHV chamber at $p = 10^{-10}$ mbar pressure. The tungsten tip has been produced from single crystal tungsten wire by electro-chemical etching and has a radius of curvature at the apex of about 10 nm (as confirmed by SEM imaging). Using attocube's positioners in scan mode (applying DC voltages), the tip can be positioned to test and measure the focal spot of the laser beam in situ. Its size is typically about 2.4 µm ($1/e^2$ intensity radius).

At a laser intensity of 4×10^{11} W/cm², photoelectron spectra are recorded with a spectrometer. The phase between carrier wave and intensity envelope (carrier-envelope phase, see explanation in Figure 2) is varied in small steps. Figure 3 shows two electron spectra, recorded with a phase difference of 180 degrees. In a), pronounced peaks are visible caused by interference of two electron wave packets emitted during subsequent optical cycles. In b), no peak structure is visible; only one electron wave packet contributes. This energy domain effect allows conclusions about the time dynamics of the electrons. By shaping the laser electric field with the carrier-envelope phase, the dynamics of the electrons can be controlled with attosecond precision. Semiclassical calculations confirm this notion [4].

In summary, an experimental setup for studying ultrafast electron emission from a sharp metal tip is described in this application note. The presented system enables control over photoelectrons from a metal tip in space (nanometer scale) and time (attosecond scale). The spatial confinement is enabled by the size of the electron emission area and the precise positioning control provided by attocube systems' positioner stack.

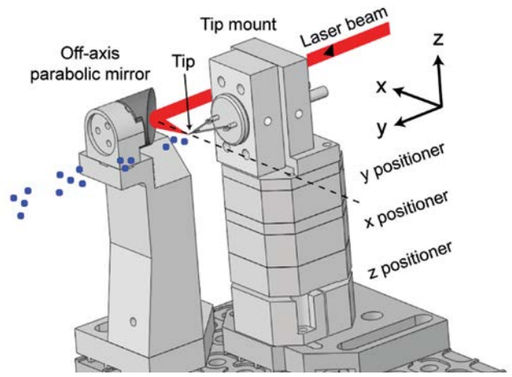

Figure 1: *Sketch of the experimental setup. The tungsten tip is irradiated by femtosecond laser pulses (red) and electrons (blue) are photoemitted from the tip. An electron spectrometer (not shown) records photoelectron spectra. The tip is positioned in the microscopic focal spot of the off-axis parabolic mirror with a set of xyz-positioners.*

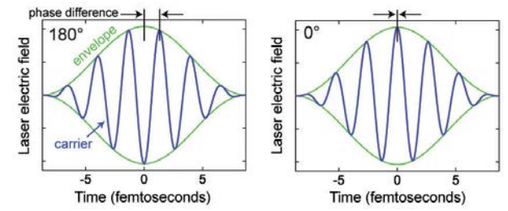

Figure 2: *Electric field of a few-cycle femtosecond laser pulse. The phase difference between the maximum of carrier wave and envelope is the carrier-envelope phase.*

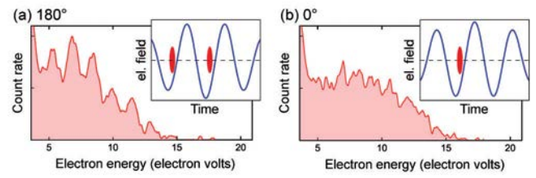

Figure 3: *Electron spectra for two different carrier-envelope phases. Peaks are visible in a) due to two interfering wave packets generated during the pulse (marked in red in the inset), whereas in b) no interference peaks are visible.*

References

[1] P. B. Corkum and F. Krausz, Nat. Phys. **3**, 381 (2007).
[2] F. Krausz and M. Ivanov, Rev. Mod. Phys. **81**, 163 (2009).
[3] M. Schenk, M. Krüger, and P. Hommelhoff, Phys. Rev. Lett. **105**, 257601 (2010).
[4] M. Krüger, M. Schenk, and P. Hommelhoff, Nature **475**, 78 (2011).

© attocube systems AG, 2014. All rights reserved.

Polycapillary X-Ray optics alignment in confocal micro-XRF using ANPxyz101 positioners

Stephan Smolek, Christina Streli
Atominstitut of the TU Wien, Austria

Micro x-ray fluorescence analysis (micro-XRF) is a well established tool to determine the spatial distribution of major, minor, and trace elements in a sample. It is widely used to investigate samples from different fields (biology, geology, life science, etc.). The method is nondestructive, requires little sample preparation, and allows simultaneous multi-element detection if an energy dispersive (EDX) detector is used. Most available micro-XRF spectrometers operate in air which does not allow the analysis of low-*Z* elements. Therefore, a special micro-XRF spectrometer has been installed at the Atominstitut of the TU Wien [1]. The key component in this spectrometer is the polycapillary x-ray optics which focuses the x-rays from the x-ray tube to a small spot (31 µm FWHM for Mo-Kα) on the sample. The optics needs to be aligned in two ways. First, the entry focus of the x-ray optics has to be matched with the focal spot on the anode of the x-ray tube. Second, the sample has to be aligned in respect to the optics to achieve minimum spot size. Due to the fixed focal length of the optics and the fact that the whole setup is inside a vacuum chamber, the positioners to align the optic have to be very compact.

A further extension of micro-XRF is confocal micro-XRF. Therefore, a second polycapillary optic (a half lens) has to be installed in front of the EDX detector. The second optic needs to be aligned in a way that the focal spots of both (primary and secondary) optics overlap to create a well defined measurement micro-volume. This enables us to determine the elemental distribution inside a sample in three dimensions by moving the sample relative to the measurement volume. Two xyz-stacks consisting of four ANPx101 and two ANPz101 are used to align the optics. Figure 1 shows the confocal setup inside the vacuum chamber. The positioners' travel range of a few millimeters as well as sub micrometer resolution is required for our purposes. Long time stability is also very important as ideally an alignment must not change over time. The attocube positioners easily fulfill both these requirements. A 2D scan with the primary beam polycapillary across the focal spot of the x-ray tube (Figure 2) shows a clear maximum of intensity (optimum alignment). The optic in front of the detector is aligned in a similar way. Figure 3 shows a 3D measurement of a cross made from 10 µm copper wire which is placed on an x-ray screen and fixed using adhesive tape. This clearly demonstrates our ability to measure elemental distributions in three dimensions on the micrometer scale.

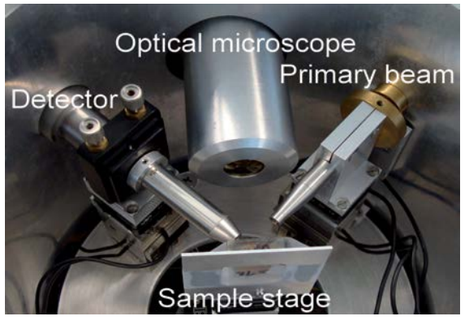

Figure 1: *Photograph of the confocal µXRF setup. The incident beam impinging from the right induces fluorescent radiation in the sample, which is collected by the detector on the left. An attocube xyz-positioner stack is placed underneath each polycapillary optics.*

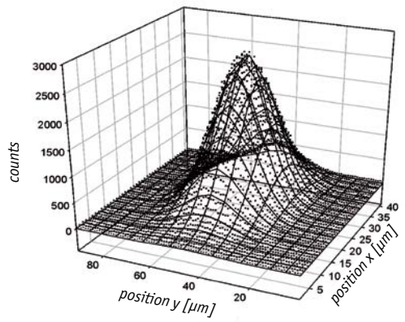

Figure 2: *2D scan of the primary polycapillary showing the point of optimum alignment (peak maximum).*

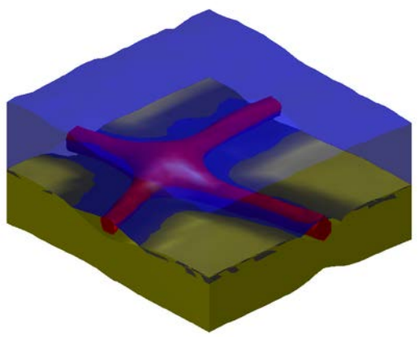

Figure 3: *3D scan of a 10 µm copper wire cross (red) on x-ray screen (yellow) fixed with adhesive tape (blue).*

References

[1] S. Smolek, C. Streli, N. Zoeger, and P. Wobrauschek, Rev.Sci. Instr. **81**, 053707 (2010).

Mapping and Manipulation of Leakage Currents in a Nanostructure with ANP101 positioners

Magdalena Huefner, Bruno Kueng, Stephan Schnez, Thomas Ihn, Klaus Ensslin
Solid State Physics Laboratory, ETH Zürich, Switzerland

Transport phenomena in nanostructures rely on charge flow of charge carriers in real space. In order to receive spatially resolved images of transport processes in certain nanostructures, we employ scanning gate microscopy (SGM). Here we show how this method has been used to spatially image and manipulate undesired electrical leakage currents in a nanostructure.

In this application note, attocube's smallest titanium positioners (ANPx51/RES and ANPz51/RES) are used as part of an atomic force microscope (AFM) inside a Janis ^{3}He cryostat with a base temperature of 280 mK (see Figure 1a). The setup is a combined low temperature AFM and scanning tunneling microscope (STM), which we employ to carry out SGM experiments on various nanostructures. In these measurements we use attocube systems' positioners to move the metallic tip directly above the nanostructure predominantly at 4.2 K but also as low as 280 mK.

In a SGM experiment, we use the tip as a flying nano-gate to locally induce a potential perturbation in the sample (see Figure 1b). Here we show how this method was used to investigate and manipulate the undesired leakage currents occurring between two insulating terminals of a nanostructure fabricated via local anodic oxidation [1] in a two-dimensional electron gas (2DEG) (see Figure 2a) when a voltage above a certain threshold is applied to one terminal of the structure [2].

To record a current map, we measure the current through the nanostructure in dependence of the tip position. When investigating the leakage currents in this nanostructure, we find that the current map is flat except for a single point of suppressed current (Figure 2b). We therefore conclude that the leakage current crosses the barrier not homogeneously along the whole extent of the barrier but rather at one single point. Crossings of two oxide lines are especially prone to the occurrence of leakage currents, as at those points the effective writing distance during sample processing is increased. By scanning the tip over the defected region in feedback mode, we can temporarily decrease the leakage current appearing at this point by more than a factor of two due to electrostatic alterations in the sample as shown in Figure 3.

In summary, attocube systems' positioners were used in a low temperature AFM-STM setup to coarse-position a metallic tip reliably close to the nanostructure under investigation. The setup was used to investigate the flow of leakage currents in a 2DEG-based nanostructure. We could show, that leakage currents cross oxide barriers at isolated points and how we can temporarily suppress these leakages. Additionally, the setup has successfully been used to investigate the positions of double dots in a 2DEG based structure, where we could use this technique to image and manipulate the apparent positions of both dots in real space [3].

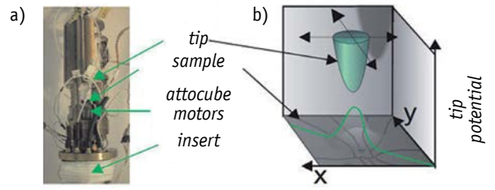

Figure 1: *a) Photograph of the microscope head. b) Schematic principle of scanning gate microscopy.*

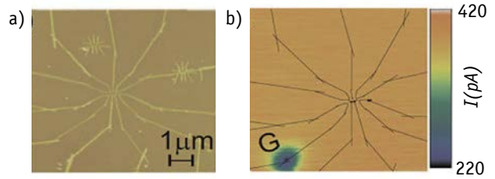

Figure 2: *a) AFM scan of the sample. The bright protrusions correspond to the electrically insulating oxide barriers. The regions below the dark brown areas are electrically conducting. b) Current map of the leakage current when a large enough voltage is applied to the terminal labelled G. The oxide lines are indicated as black lines.*

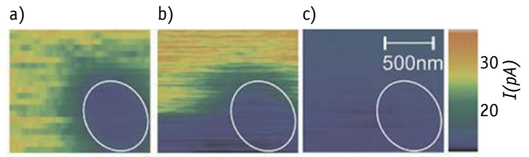

Figure 3: *a) Current map to localize the leakage current occurring at one specific point. b) Current map recorded while scanning the tip in feedback mode over the same position. c) Current map recorded at the same setting and position as the map displayed in b) recorded after the current map shown in b).*

References

[1] A. Fuhrer, A. Dorn, S. Luescher, T. Heinzel, K. Ensslin, W. Wegscheider, and M. Bichler, Superlattices and Microstructures **31**, 19 (2002).
[2] M. Huefner, S. Schnez, B. Kueng, T. Ihn, M. Reinwald, W. Wegscheider, and K. Ensslin, Nanotechnology **22**, 295306 (2011).
[3] M. Huefner, B. Kueng, S. Schnez, T. Ihn, M. Reinwald, W. Wegscheider, and K. Ensslin, Phys. Rev. B **83**, 235326 (2011).

3D g-factor mapping of single quantum dots utilizing an attocube ANPxyz50 positioner stack

Matthias Ediger, Richard T. Phillips
Cavendish Labs, University of Cambridge, UK

In this application, we report on a novel fibre-based confocal microscope [1] to investigate the properties of nanostructures such as InGaAs quantum dots (QDs) via magneto-photoluminescence (PL). The design allows them to turn the samples to arbitrary angles of tilt and rotation with respect to a magnetic field of up to 10 T at low temperatures, while maintaining focus on a single QD. Modelling the exciton emission [2] they can extract the full 3-dimensional g-factor tensors for the electrons and holes and their exchange parameters. The new method improves upon the first studies of this type [3,4] by allowing dots to be selected in the microscope using the positioning capability.

An integral part of this setup is a stack of four attocube nanopositioners consisting of an ANPz50, an ANR50 and two ANPx50's; this stack is fixed to a rotatable mount by a gear mechanism (see Figure 1). The ANR50 and the mount provide the two axes required to allow exploration of all orientations with respect to an applied magnetic field. Ediger & Phillips are able to make full use of the high spatial resolution of the positioners at any angle, which allows them to correct efficiently for the effects of gravity or diamagnetic shifts during parameter change in the experiments. On the other hand, the high stability of the motors is demonstrated by the ability to study the same structure at any angle over extended periods of time without loss of focus. The only effect of tilt on the operation of the motors is the transfer of the slight preferential down movement of the ANPz50 due to gravitation to one of the ANPx50.

The example data in Figure 2 shows the emission of the neutral exciton of a single InGaAs quantum dot tilted to 45° with respect to a magnetic field of 0 to 10 T at a temperature of 4 K. The intense upper doublet belongs to the bright exciton states, while the faint lines emerging at about 2 T stem from predominantly dark transitions that only become visible due to a field-induced mixing with the bright states. For standard magneto-PL in Faraday geometry (0° tilt) this mixing would not appear for rotationally symmetric dots.

An obvious feature for tilt angles around 45° is the anti-crossing of the dark and bright states, which in this case happens at about 5 T. The size of this splitting, as obtained from precise modelling shown in the Figure 3, is dominated by and gives direct access to the in-plane hole g-factor [5], an important parameter for the emerging idea of quantum information processing using long-lived hole spins. This effect is again typically not visible in standard magneto-PL setups in either Faraday or Voigt (90° tilt) geometry, respectively.

This technique is adaptable to a host of different nanostructures giving access to wealth of detailed information about the wave functions, the bright and dark spin states, as well as structural information by probing the 3D confinement properties of the respective nanostructure.

References

[1] T. Kehoe, M. Ediger, R. T. Phillips, and M. Hopkinson, Rev. Sci. Instrum. **81** 013906 (2010).
[2] H. W. Van Kesteren, E. C. Cosman, W. A. J. A. Van der Poel, and C. T. Foxon Phys. Rev. B **41** 5283 (1990).
[3] A. G. Steffan and R. T. Phillips, physica status solidi a 190 541-545 (2002); Physica E **17** 15-18 (2003).
[4] R. T. Phillips, A. G. Steffan, S. R. Newton, T. L. Reinecke and R. Kotlyar physica status solidi b **238** 601-606 (2003).
[5] I. Toft and R. T. Phillips, Physical Review B **76** 033301 (2007).

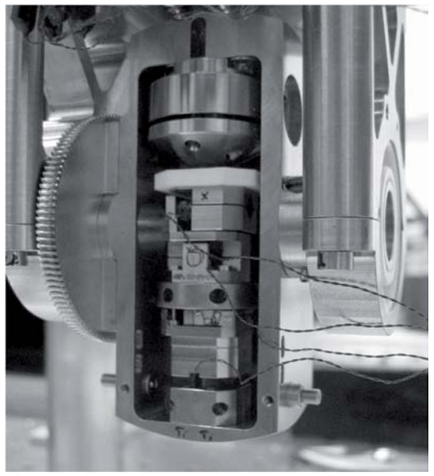

Figure 1: *Photo of the experimental setup. The positioner stack is mounted in a rotatable cage. The rotator ANR50 is mounted onto the ANPz50.*

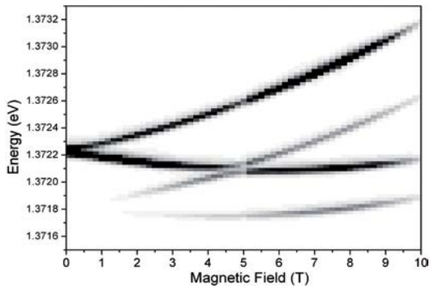

Figure 2: *Photoluminescence data from a single quantum dot in a magnetic field at 45° inclination to the surface.*

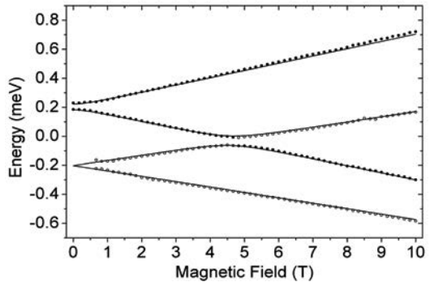

Figure 3: *Model of the anti-crossing data shown in Figure 2. Emission energy and diamagnetic shift have been subtracted in this model.*

Figure 1-3 courtesy of M. Ediger and R. T. Phillips, University of Cambridge.

Dissipation in Optomechanical Resonators measured using a setup based on ANPxyz51 positioners

Garrett D. Cole, Markus Aspelmeyer
University of Vienna, Austria

Quantum optomechanics [1-3] is a rapidly expanding field of research, combining quantum optics with optomechanical coupling in order to generate and detect quantum states of micro- and nanomechanical devices. Recent experiments have demonstrated mechanical laser cooling down to the level of only a few thermal quanta [4-8] and theory predicts that the quantum ground state can be reached with this method [9-11]. At present, however, the rate of thermalization prevents laser cooling to the vibrational ground state. In order to overcome this barrier, the impact and sources of mechanical damping in these devices must be quantified.

In this application, we have analyzed the acoustic disspiation of microresonators using a cryogenic interferometry setup, see Figure 1. In detail, their system utilizes a continuous flow ^{4}He cryostat as sample chamber equipped with a stack of attocube's ANPxyz51 positioners for aligning the sample with respect to an optical fiber. This fiber is part of a homodyne interferometer, allowing high signal-to-noise measurements of the eigenmodes of the resonator (Figure 2) while keeping disturbances due to radiation pressure and optical fluctuations at a minimum. The turbo-pumped cryostat enables interrogation from room temperature (RT) to 20 K, and from atmospheric pressure to vacuum levels of 2.5×10^{-7} mbar.

Cole & Aspelmeyer take advantage of a piezoelectric disc to excite the optomechanical resonator, either broad band by white noise or resonant at a specific frequency. While the first method allows to characterize the resonance spectrum of the resonator, the second accurately yields the ringdown time for a single resonance and therefore its quality factor Q. Figure 3 depicts this information for a resonator eigenmode with a frequency close to 4 MHz, demonstrating a Q factor of 8×10^4. To simultaneously achieve high Q and high reflectivity, the optomechanical resonators are fabricated from an epitaxial $Al_xGa_{1-x}As$ Bragg reflector. This technique results in reflectivities exceeding 99.98% at 1064 nm, providing the basic requirement for optical ground-state cooling.

In summary, an experimental setup used to characterize the properties of a micro-optomechanical resonator with resonance frequencies of up to 4 MHz and Q-factors as high as 8×10^4 is described in this application note. A stack of attocube ANPxyz51 positioners is used to precisely position the resonator with respect to an optical fiber, forming one arm of a homodyne interferometer.

References

[1] M. Aspelmeyer and K.C. Schwab, New J. Phys. **10**, 095001 (2008).
[2] T. J. Kippenberg and K. J. Vahala, Science **321**, 1172 (2008).
[3] F. Marquardt and S. M. Girvin, Physics **2**, 40 (2009).
[4] S. Gröblacher, J. B. Hertzberg, M. R. Vanner, G. D. Cole, S. Gigan, K. C. Schwab, and M. Aspelmeyer, Nature Phys. **5**, 485 (2009).
[5] A. Schliesser, O. Arcizet, R. Rivière, G. Anetsberger, and T.J. Kippenberg, Nature Physics **5**, 509 (2009).
[6] T. Rocheleau, T. Ndukum, C. Macklin, J.B. Hertzberg, A.A. Clerk, and K.C. Schwab, Nature **463**, 72 (2010).
[7] ...er, J.B. ... A.
[8] ...eid-
[9] ...rg,
[10] ...ys. Rev.
[11] ...leyer,

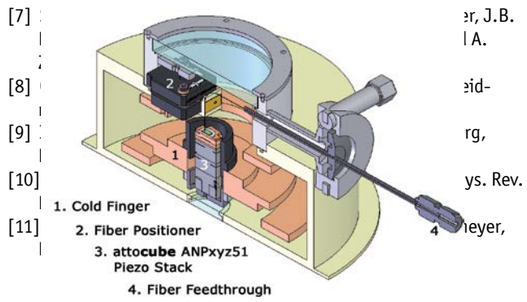

Figure 1: *Schematic of the experimental setup: the sample chip (green) is placed in a continuous flow ^{4}He cryostat and positioned underneath an optical fiber using an ANPxyz51 positioner stack. The resonator is piezoelectrically excited and its vibrational modes are detected using homodyne fiber interferometry (not shown).*

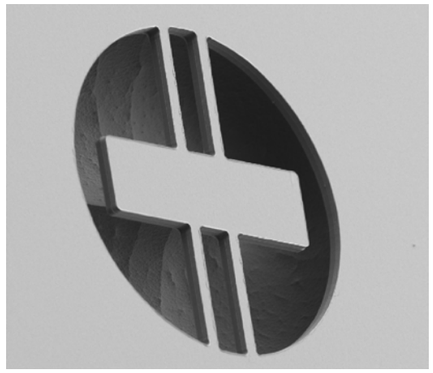

Figure 2: *Scanning electron microscope image of the optomechanical resonator, fabricated from epitaxially grown $Al_xGa_{1-x}As$.*

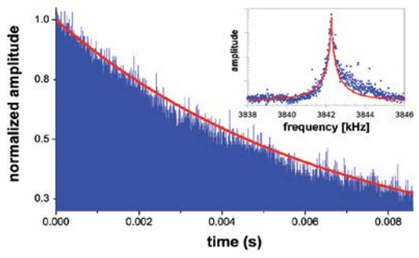

Figure 3: *Experimental ringdown of a 100 x 50 µm² resonator stack measured at 20 K and 2.5 x 10^{-7} mbar. The exponential fit (red) yields a Q value of ≈ 80000.*

Figure 1-3 courtesy of G.D. Cole/M. Aspelmeyer, Univ. of Vienna.

Scanning Hall Probe Microscopy down to 300 mK based on ANP positioners

Volodya V. Khotkevych, Milorad V. Miloševi□, Simon J. Bending
Department of Physics, University of Bath, Claverton Down, Bath, UK

The magnetic properties of superconducting (SC) and ferromagnetic materials at ultra-low temperatures represent some of the most interesting contemporary problems in condensed matter physics. These properties are typically investigated using a magnetic force microscope (MFM) or a scanning Hall probe microscope (SHPM). In this note, we report on a self-built SHPM capable of working at temperatures as low as 300 mK and magnetic fields of up to 10 T, while still having sub-micron lateral spatial resolution.

The scanner head is depicted in Figure 1. The setup consists of a three-axis attocube systems ANPxyz100 nanopositioner set (see no. 1,2, and 3 in Figure 1(b)) that enables precise *in situ* adjustment of the probe location within a 5 x 5 x 5 mm³ space, carrying a 2 inch piezoelectric tube (no. 4) to scan the SHPM head (no. 5) over ranges up to 22 x 22 x 0.6 µm³ at 4.2 K. A readily exchangeable microfabricated Hall probe maps the local magnetic induction at the sample surface (no. 6), while the tip-sample distance is controlled using an integrated scanning tunnel microscopy (STM) tip. Advanced lithographic patterning is used to reduce the active Hall cross area down to typically ~0.4 x 0.4 µm² with the STM tip positioned as close as possible to the Hall effect sensor.

Hence, the instrument is capable of simultaneous tunneling and Hall signal acquisition with minimum detectable fields ≥ 10 mG/Hz$^{1/2}$. It is possible to use the instrument in fixed height as well as constant distance modes with the scan speed in fixed height mode being as fast as 300 µm/s. The whole setup is mounted on the cold flange of a commercial ^{3}He-refrigerator and operates between room temperature and 300 mK.

The potential of the system is illustrated with images of SC vortices at temperatures down to 300 mK. Figures 2(a),(b) show vortices at the surface of a sputtered 700 nm SC Nb thin film at temperatures of 1.575 K and 372 mK, respectively [1]. Figures 2(c),(d) show lower contrast vortex structures at the cleaved surface of a single crystal of the unconventional SC Sr_2RuO_4 (T_C = 1.5 K) captured at 303 mK with somewhat higher spatial resolution (courtesy of V. V. Khotkevych, P. J. Curran & S. J. Bending (Univ. of Bath) and A. S. Gibbs & A. P. Mackenzie (Univ. of St. Andrews). The scan height of the SHPM sensor was set in the range 0.7 - 0.9 µm for the Nb film and less than 0.5 µm for the Sr_2RuO_4 single crystal.

In summary, a versatile and stable SHPM has been built using attocube systems nanopositioners. The microscope is operational in temperatures down to 300 mK and magnetic fields of up to 10 T.

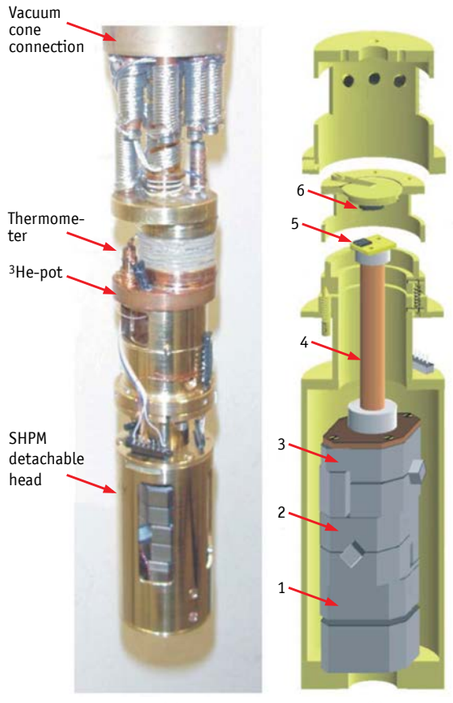

Figure 1: *Photograph (a) and sketch (b) of the LT compatible SHPM scanner head (see text). For a more complete description of all details, refer to [1].*

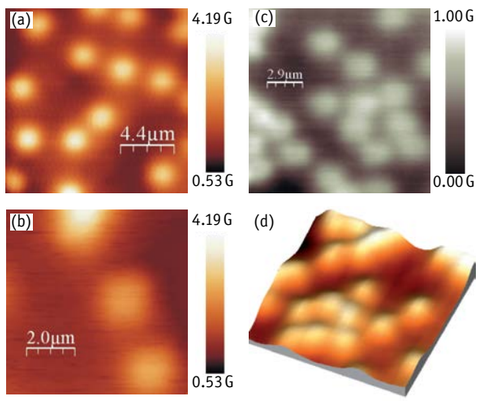

Figure 2: *SHPM images of SC vortices. (a),(b) Vortices in a 700 nm thick Nb film at (a) T = 1.575 K and (b) T = 372 mK. (c) Disordered vortex structures at the cleaved surface of a single crystal of the unconventional SC Sr_2RuO_4 at T = 303 mK. (d) 3D view of (c).*

References

[1] V. V. Khotkevych, M. V. Miloševi□, and S. J. Bending, Rev. Sci. Instrum. **79**, 123708 (2008).

Angle-dependent magneto-transport measurements at mK temperatures with an ANR30/LT

A. Jos M. Giesbers, Ulrich Zeitler
High Field Magnet Laboratory, Nijmegen, The Netherlands

Based on an attocube systems rotator ANR30/LT (see Figure 1) a rotation stage for angle-dependent transport measurements in magnetic fields up to 33 T and temperatures down to 40 mK was built at the user facility of the High Field Magnet Laboratory in Nijmegen.

The mixing chamber of the commercially available dilution refrigerator from Leiden Cryogenics offers only a limited space of 17 mm in diameter. Hence, the ultra compact attocube rotator ANR30/LT is the positioner of choice for this task. Figure 2 shows the rotator which is fixed on a plastic (Hysol) dilution refrigerator insert.

The angular movement of the ANR30/LT is transmitted via a thin copper wire (100 µm diamter) to a rotating sample stage with a home-made 20-pin spring-contact socket for samples mounted into standard LCC-20 packages. The contacts are connected to a fixed 40-pin connector of the dilution refrigerator using copper wires with a diameter of 30 µm to minimize the mechanical load on the rotator. The voltage pulses which are needed for driving the rotator are supplied via the same 40-pin connector using two parallel wires for each contact. Due to the small capacitance of the ANR30/LT of only 14 nF at low temperatures, the relatively high resistance of the cabling of approx. 36 Ohm in total does not raise a problem for the rotator. The additional LEDs which are also marked in Figure 2 enable excitation of additional carriers in semiconductor samples.

A GaAs-heterostructure Hall-bar was mounted onto the described insert and the angle dependent Quantum Hall Effect between 0 and 52 degrees was measured at a temperature of 40 mK (see Figure 3). At $q = 0°$ the sample is oriented perpendicular to the magnetic field. A driving voltage of 70 Volts at f = 1000 Hz was used to rotate the sample. During a typical rotation by a few degrees, lasting several seconds, the dilution refrigerator warmed up only a few tens of mK and its temperature never exceeded 100 mK (independent of rotation time). The step size at these low temperatures and the conditions above was measured as 0.6 +/- 0.05 millidegrees. The angle covers a range from +110 degrees to -50 degrees, only limited by the contact wires' mechanical load.

Figure 1: *Ultra compact attocube rotator ANR30/LT with 10 mm diameter and 9 mm height.*

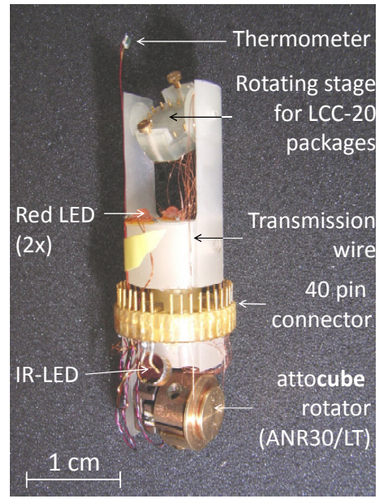

Figure 2: *Setup for angle dependent transport measurements with an attocube rotator ANR30/LT which is inserted in a dilution refrigerator.*

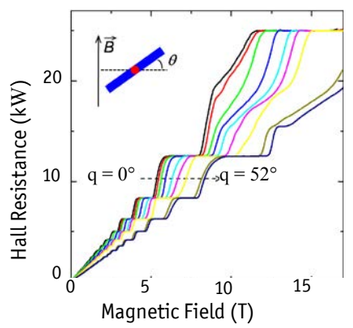

Figure 3: *Angle dependent measurements of the Quantum Hall Effect in an AlGaAs two-dimensional electron gas.*

UHV-Compatibility of encoded attocube rotator ANR101/RES/UHV with vacuum of up to 8*10^{-11} mbar

Christian Kalus, Stefan Eisebitt
Bessy GmbH, Berlin, Germany

Christoph Bödefeld
attocube systems AG, Munich, Germany

Experiments in Ultra High Vacuum (UHV) conditions require highest precision and care in manufacturing of the respective equipment. The outgassing behavior is a crucial factor when researchers decide for new instruments in their setups. This application note describes measurements of the outgassing data of an attocube rotator with an integrated resistive encoder ANR101/RES/UHV (see Figure 1). The tests were carried out at the BESSY synchrotron facility in Berlin, Germany.

Figure 1: *Ultra compact attocube rotator ANR101 with 30 mm diameter and 15.2 mm height.*

The tests were split in two parts:

a) Measurement of the reference mass spectrum of the empty vacuum chamber (green curve in Figure 2)

b) Measurement of the mass spectrum of the vacuum chamber after inserting the attocube rotator (blue curve in Figure 2).

The vacuum chamber was baked out for three days at a temperature of 180°C. The turbo pump used had a pumping power of 180 l/s for N_2. After cooling down to room temperature a pressure of 7.3*10^{-11} mbar was measured and a mass spectrum was taken.

Afterwards the rotator ANR101/RES/UHV was inserted into the vacuum chamber and baked out again for three days at 100°C. Due to this procedure an end pressure of 8*10^{-11} mbar could be achieved. The measured mass spectrum is shown in Figure 2 (blue curve).

The third (brown) curve in Figure 2 illustrates the difference between both mass spectra. This curve shows emissions added by the rotator; these are at remarkably small levels. The peaks that are visible in the spectrum mainly refer to H_2O, CO, N_2, and CO_2, i.e. elements that were present in the chamber before. It is expected that these peaks can be further reduced by an increased bake out temperature and duration. In summary , this means that the positioner is perfectly suited for UHV use.

These experiments are an example for the outstanding UHV compatibility of the attocube systems positioning systems which are specified to pressures down to 5*10^{-11} mbar.

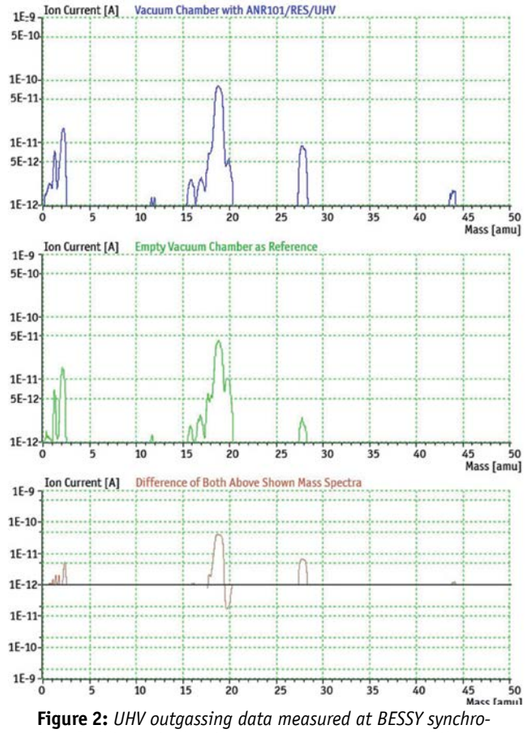

Figure 2: *UHV outgassing data measured at BESSY synchrotron facility in Berlin. Blue curve: mass spectrum of the vacuum chamber with an ANR101/RES/UHV inside. Green curve: reference mass spectrum of the empty vacuum chamber. Brown curve: Difference of both mass spectra. The peaks refer to additional emissions caused by the ANR101/RES/UHV.*

The data was generously provided by Christian Kalus (christian.kalus@bessy.de) and Stefan Eisebitt (eisebitt@bessy.de), BESSY GmbH, Albert-Einstein-Str. 15, 12489 Berlin, Germany.

Magnetic Resonance Imaging of Nanoscale Tabacco Mosaic Virus at 300 mK using ANPx51 positioners

Martin Zech
attocube systems AG, Munich, Germany

Magnetic Resonance Force Microscopy (MRFM) is a three-dimensional imaging technique derived from classical magnetic resonance imaging (MRI). In an effort to increase the resolution of MRI from the millimeter to the sub-micrometer range, MRFM uses a cantilever for signal detection instead of a coil as used in classical MRI apparatus. A recent experiment by C. L. Degen, now at ETH Zürich, and his colleagues at IBM Almaden demonstrates improvement of MRFM imaging resolution to length scales of a few nanometers, representing a 100-million fold increase in volume resolution over conventional MRI [1]. In the setup used for these groundbreaking experiments, two attocube ANPx51 positioners played the crucial role of coarse positioning the sample over the nanoscale magnetic tip, see Figure 1. The experiment was conducted inside a dilution refrigerator at a temperature of 300 mK.

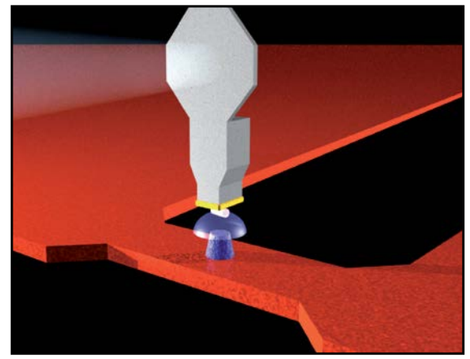

Figure 1: *Schematic drawing of the MRFM setup showing the ultra-sensitive cantilver (grey), tobacco virus (white), and magnetic tip (blue). Magnetic resonance is achieved within the resonant slice (faint blue), where the gradient magnetic field of the tip and the rf magnetic field created by the microwire (red) satisfy the Larmor condition. The microwire and magnetic tip are brought to close proximity with the cantilever by taking advantage of two attocube ANPx51 nanopositioners.*

For their nanoscale imaging experiment, Degen and coworkers attached Tobacco Mosaic Virus particles to the tip of an ultra-soft cantilever in vertical orientation (Figures 1, 2). The cantilever end was then positioned in close proximity to a tiny magnetic tip providing a strong and inhomogeneous magnetic field. With a typical separation of only several tens of nanometers, a highly accurate and robust positioning process was crucial. In Degen's experiment, two attocube ANPx51 nanopositioners carried out this positioning process with highest precision and reliability.

Underneath the magnetic tip, a copper nanowire was used to generate an *rf*-magnetic field with a center frequency of 114.8 MHz. At this frequency, the Larmor resonance condition is satisfied at a magnetic field of approximately 2.7 T. Due to the strong position dependence of the magnetic field created by the conical magnetic tip, resonance only occurs in a spherically shaped "resonant" slice (see Figure 1). With magnetic field gradients exceeding 106 T/ m, the resonant slice can be as thin as a few nanometers, defining the imaging resolution of the MRFM apparatus. A magnetic resonance signal is generated by periodically inverting the nuclear spins in the slice at the mechanical frequency of the cantilever. These nuclear spin inversions present an oscillating force to the cantilever, typically of order attoNewton rms, resulting in a small mechanical oscillation of the cantilever that is proportional to the number of nuclear spins in the resonant slice. By scanning two-dimensional slices at different tip-sample separation while simultaneously recording the amplitude of the cantilever motion, information on the ^{1}H spin distribution of the sample was obtained. The recorded data were subsequently transformed into a real-space 3D image by means of a sophisticated software algorithm, see Figure 3.

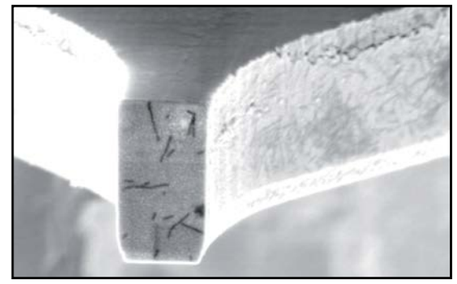

Figure 2: *SEM image of the tip of the ultra-sensitive silicon cantilever used for the MRFM experiment, clearly showing several Tobacco Mosaic virus particles.*

In summary, attocube's ANPx51 positioners were used in an MRFM setup with the task to precisely and reliably position a magnetic tip and a copper nanowire to close proximity of an ultra-sensitive cantilever. The MRFM setup was used to investigate and reconstruct the ^{1}H spin distribution of Tobacco Mosaic Virus particles, representing a 100-million fold improvement in volume resolution over conventional MRI.

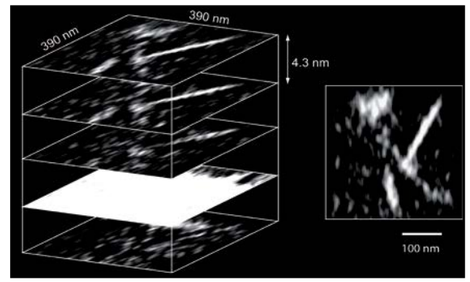

Figure 3: *Three dimensional reconstruction of the ^{1}H-spin distribution of a virus particle sitting on an adsorbed hydrocarbon layer. The insert shows a representative horizontal slice located 13 nm above the hydrocarbon layer.*

References

[1] C. L. Degen, M. Poggio, H. J. Mamin, C. T. Rettner, and D. Rugar, PNAS 106, 1313 (2009). doi:10.1073/pnas.0812068106

Performance Test of the ANPz30/LT at 35 mK and 15 Tesla

Jeroen Custers
Institute for Solid State Physics,
Vienna University of Technology, Austria

The precise performance of nanopositioning elements is of great importance in order to realize instrumental setups which work reliably under extreme environmental conditions. Although attocube systems' positioners have been tested at low temperatures down to 10 mK and at high magnetic fields up to 28 Tesla, their successful performance has never been demonstrated when both environmental conditions were simultaneously applied. A real challenge, furthermore, is to carry out such a test in a ^{3}He/^{4}He environment due to the fact that ^{3}He carries a magnetic spin which becomes polarized in magnetic fields. This influence on the positioner's operation has so far not been investigated. Furthermore, the required low-resistive wiring of the positioners becomes challenging under these conditions.

Due to the size of the ANPz30 positioner (see Figure 1), the heat input is considered to be very low which makes these units particularly suitable for the application in the mK range. The experiments were performed in a commercially available top-loading cryostat equipped with a 18 T magnet. The cooling power at T = 100 mK is 370 µW and the base temperature without any insert is around 12 mK. In order to confirm the movement of the positioner a small switch was placed on top of the ANPz30/LT which was activated after a travelled distance of 1 mm. For the wiring, a twisted pair of copper wires with a diameter of 90 µm were used for the most part, but from the 1K–pot downwards NbTi–superconducting wires were applied in order to reduce heat leakage via the copper wires. With the inserted setup as shown in Figure 2a base temperature of 35 mK was reached. Two different temperature sensors have been applied to monitor the possible warming up of the ^{3}He/^{4}He–mixture when operating the ANPz30/LT.

The experiments reveal that the stepper positioner works reliably when applying both, temperatures in the low mK regime and magnetic fields up to 15 Tesla. Exemplary, Figure 3 shows the temperature measured before ($T_{7,START}$) and after ($T_{7,END}$) moving the positioner downwards for 30 sec. The jump in temperature which is observed when the field changes from B = 0 T to 1 T is due to the high current in the leads of the superconducting magnet. The plot clearly shows, that operating the positioner at any field does not affect the base temperature, that means almost no or only little heat is produced. Furthermore, no considerable heat release was detected when moving the positioner even when the step frequency was increased up to 73 Hz.

These successful tests open up the door to a wide range of new cryomagnetic experiments and applications.

The data was generously provided by Dr. J. Custers from the Institute for Solid State Physics, Vienna University of Technology, Austria.

Figure 1: *Photo of the ANPz30, the smallest positioner offered by attocube systems providing high resolution z-positioning over 2.5 mm.*

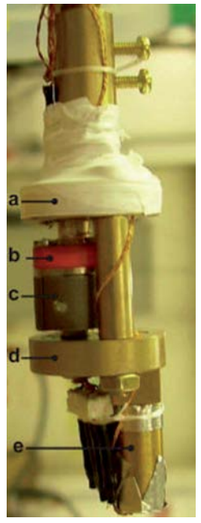

Figure 2: *Photo of the setup:*
(a) upper platform with heater and thermometer
(b) plastic disc
(c) ANPz30/LT movable platform
(d) lower platform
(e) second thermometer

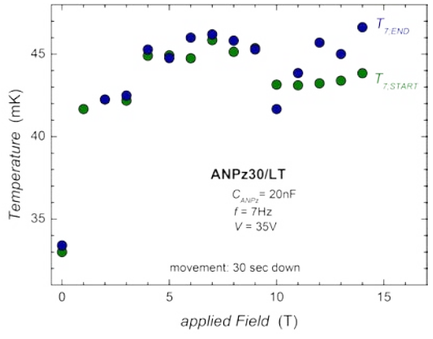

Figure 3: *Heat release due to the downwards motion t = 30 sec at base temperature in various magnetic fields.*

ANP100 positioners for photoluminescence measurements in magnetic fields up to 28 T

Aadm Babinski, Marek Potemski, Christoph Bödefeld
attocube systems AG, Munich, Germany

The attocube systems positioners ANPxyz100/LT have been used in a setup for optical measurements in LHe temperature and magnetic fields up to 28 T at the Grenoble High Magnetic Field Laboratory. In the setup laser excitation is delivered using a single-mode fiber and is focused onto the sample with two microlenses. A multimode fiber is used for photoluminescence (PL) collection. The estimated laser spot size was 20 µm and its position over the sample is controlled by an attocube systems ANPxyz100/LT set of positioners. The setup has been placed in a non-magnetic steel tube of 32 mm diameter and immersed in liquid Helium. The 1.8 m long tube can be mounted in a Helium cryostat. The cryostat can fit in the bore of a resistive magnet in the Grenoble High Magnetic Field Laboratory, which supplies continuous magnetic field up to 28 T. The PL spectra were dispersed by a 1 m double grating monochromator and focused onto a CCD. Both, Ar^+ laser and Ti:Sapphire tunable lasers were used for the measurements. A general view of the setup is shown in Figure 1. One can see the fixed fibers and lenses (middle part of the Figure) and the sample, which is mounted onto the set of attocube systems x, y, and z piezostages (right-hand side of the Figure). During measurements the setup is immersed in liquid Helium and subject to magnetic fields up to 28 T.

Properties of the setup can be presented in an example measurement of the near-edge photoluminescence of an epitaxial layer of GaAs (see Figure 2) excited with laser light of 796 nm. A broad PL band around 825 nm is due to the recombination of bound excitons in GaAs. The relatively long wavelength of the excitation light permits its penetration into the bulk GaAs, which results in the seen broadening of the spectrum. Dips in the spectra around 816 nm result from a reabsorption of the light emitted from bulk GaAs by free excitons in the epitaxial layer of GaAs. Its dependence on the actual position on the sample reflects most likely a strain distribution in the epitaxial layer.

The setup has also been successfully used for single-dot spectroscopy measurements in high magnetic fields. The number of semiconductor self-assembled quantum dots is limited by mesa-patterning of the sample (submicron sized mesas are used for measurements on a single quantum dot). An example of the obtained results is presented in Figure 3. A series of emission lines due to recombination of excitons in a single quantum dot can be followed in magnetic fields up to 26 T. A diamagnetic shift as well as the splitting of lines can be seen in the trace of the emission lines versus magnetic field. The emission lines are due to excitons involving the carriers from the ground state ("s"-shell) of a single quantum dot.

References

[1] A. Babinski, S. Awirothananon, J. Lapointe, Z. Wasilewski, S. Raymond, and M. Potemski, Physica E **26**, 190–193 (2005).

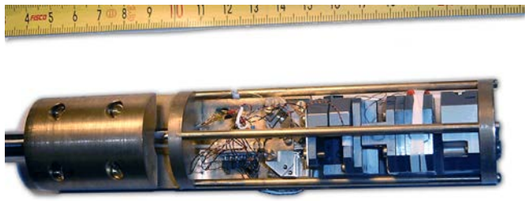

Figure 1: *Photo of the setup.*

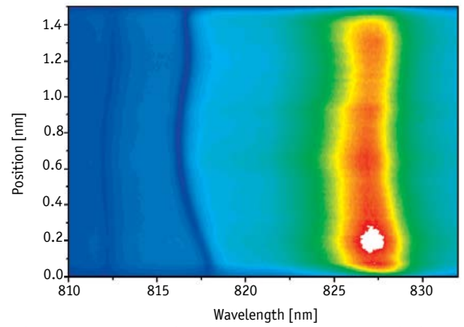

Figure 2: *Scanning photoluminescence spectrum of a bar-like sample of epitaxial GaAs.*

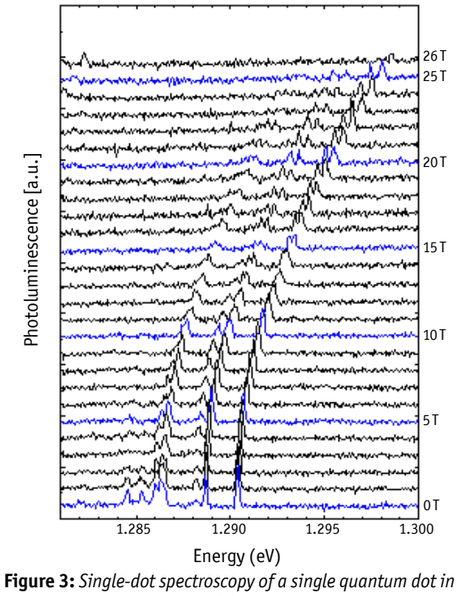

Figure 3: *Single-dot spectroscopy of a single quantum dot in high magnetic field of up to 26 T.*

attoSENSORICS
Ultra Precision Sensors

attoSENSORICS
Ultra Precision Sensors

FPS1010

FPS3010

FPS Individual

attoSENSORICS
Ultra Precision Sensors

Contactless Frequency Analysis of Motor Vibrations with the Ultra Precise FPS3010

pioneers of precision

Pierre-François Braun, Matthias Handloser
attocube systems AG, Munich, Germany

Machine vibrations induce errors in parts manufacturing. Tiniest vibrations of a milling machine produce erratic motions of the workpiece with regards to the cutter and hence, may lead to contouring errors or bad surface finish. Yet, in state of the art mechanical manufacturing allowed tolerances are constantly narrowed down. Indeed, misshaped components can jeopardize the whole system's assembly or safe operation. In the end, such parts may fail quality criterions such as the 6-sigma standard – this quality process ensures that only two out of a billion manufactured parts may be outside the specifications. attocube now provides a perfect tool to efficiently and precisely characterize vibrations.

A few months ago, a customer needed to test a rotating motor embedded in his system. Simulations emphasized that the maximum vibration amplitude of the motor housing should not exceed 100 nm to comply with the overall system error budget. As the development project was approaching a deadline, our customer required a fast and accurate method to characterize the machine vibrations. But how to measure these?

Even minimal mass variations may induce dramatic shifts in vibration frequency / amplitude signature. This discards any contact sensing solutions (such as CMM probe calibration spheres or optical encoders). Moreover space configuration in our customer's setup imposed a cylindrical geometry for the motor housing, hence prohibiting the use of capacitive sensors. In fact, only a non-contact, high accuracy interferometric technology could work.

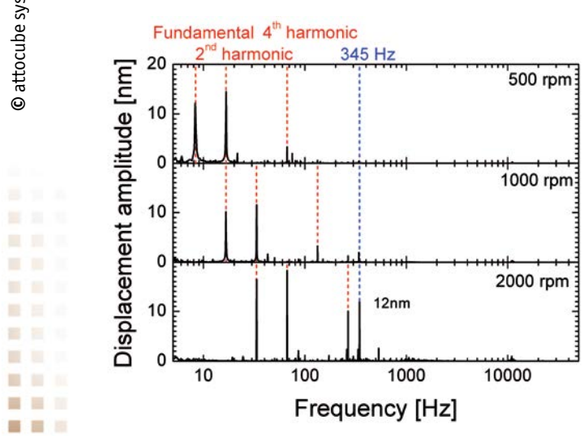

Figure 2: *FFT of the displacement signal monitored in a 100 kHz bandwidth. The spindle of the motor was rotated at 500 rpm (top), 1000 rpm (middle), and 2000 rpm (bottom). We evidenced vibrations at the fundamental rotation frequency as well as replicas at the 2nd and 4th harmonic (red dashed lines). At 2000 rpm, the 345 Hz (blue dashed line) system resonance is highly amplified.*

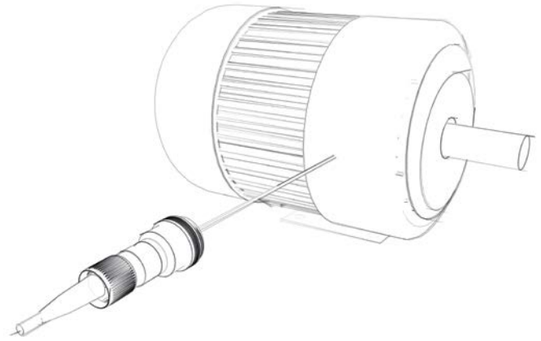

Figure 1: *Schematic setup for measuring an vibrating object. As the motor is actuated, its position changes, hence vibrations are monitored by the laser interferometer. Note that different sensor heads are available for objects of different size and different sensing distances.*

attocube then offered to perform a fast test measurement with its easy to use sensing solution (see sketch in Figure 1). We mounted our non-contact probe within less than five minutes and started recording the displacement of the motor housing. Our sensor's remote electronics performed a live Fast Fourier Transform (FFT) of the signal and allowed us to monitor the assembly's vibrations on the fly. Figure 2 shows the results of the measurements with the motor spindle rotating at 500, 1000, or 2000 rotations per minutes (rpm).

For the lower two rotation velocities, the system complied with the requirements. However, at 2000 rpm, the total vibration exceeded 150 nm overall amplitude. With our frequency analysis feature, we assessed that the system triggered vibrations not only at the fundamental frequency but also at its second and fourth harmonics (see Figure 2). We evidenced that when rotating at 2000 rpm, the motor generated vibrations at 270 Hz which in turn amplified a system resonance at 345 Hz, and therefore drastically increased the overall vibration amplitude. With this crucial information, our customer could take action (modify the design of the holder) to minimize the system response to vibrations and prevented potential failure.

The ease of use of attocube's sensor initiates in situ fast monitoring of vibrations even by non-experts in laser interferometry. The frequency analysis tool of the FPS3010 allows on-the-fly diagnosis of a machine in a production line: Hence, production managers can trace back unbalanced, misaligned, damaged, or loose components and trigger service or maintenance on time. This not only improves part quality, but also minimizes machine downtime. attocube's compact sensor design and high integration qualifies for the "Industry 4.0" challenges.

More detailed documentation on the FPS3010 can be found at www.attocube.com.

attocube
pioneers of precision

Using the FPS3010 Optical Interferometer in Quality Control of a Nanopositioner

Daniel Schiessl, Christoph Bödefeld
attocube systems AG, Munich, Germany

Confidence is built on quality

Despite all efforts, in real-life production processes errors that lower product quality are still possible. Such errors generate additional costs and in the worst case customer confidence can be damaged. Optical sensing in quality control can help to reduce these risks to a minimum by achieving high quality standards. The FPS series of optical displacement measurement sensors with its broad range of optical collimators is ideally suited to detect and limit errors to a minimum in various applications.

For attocube, the precise determination of a positioner's repeatability is one important parameter for characterizing its performance during a standard quality check. This note describes the implementation of the FPS3010 interferometer sensor into a quality control setup to characterize the repeatability of a standard positioner.

The FPS3010 offers quick and highly precise relative measurements of targets at up to 1 m distance moving with 2 m/s maximum velocity. One major benefit of these robust sensors is their capability to measure also in extreme conditions, such as vacuum, cryogenic temperatures as well as in high magnetic fields. This is especially important here, as thermal drifts can be reduced by introducing the whole test setup into a vacuum chamber.

Fully automated testing

The positioning repeatability of an ECS3030 closed loop positioner controlled by an ECC100 closed loop controller was measured in ambient as well as in vacuum conditions. Only the measurements in a vacuum of 4×10^{-7} mbar are shown here.

The ECS3030 positioner features an internal optical encoder with a resolution of 1 nm. Together with the ECC100 controller, the setup is capable of positioning over 20 mm with a specified repeatability R of (better than) 50 nm.

To check the latter specification, the position of the motor was externally referenced by a FPS3010 interferometer arranged on the same breadboard as the motor. The sensor was mounted on a flange made from aluminium. To minimize the effect of thermal fluctuations, the measurements were performed in vacuum.

For the test, the motor was programmed to repeatedly approach random positions distributed along nearly the full travel range (some space was left free to the positive side of the travel range). After approaching one such position, the motor was moved away by 1 mm, then programmed to go back to the same position again. Using the FPS3010 as external reference, the difference in "real" position of these two successive approaches was measured. 1 s of waiting time before each measurement was introduced to keep errors to a minimum due to residual vibrations.

Encouraging Measurement Results

The result of the test shows a homogeneous distribution of the difference in position over the full travel range (see Fig. 1). A slight increase towards both ends of the travel range can be seen from the graph.

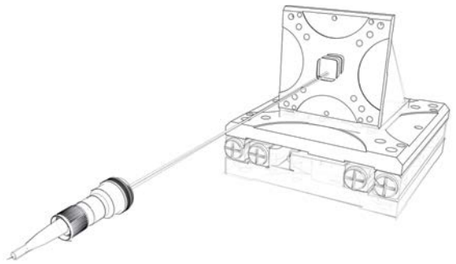

Figure 1: *Sketch of the setup. The sensor head of the interferometer is used to externally reference an ECS3030 positioner in a repeatability measurement setup.*

The histogram of the data is plotted in Figure 2. The deviation σ can be calculated to 13.2 nm RMS. The slight asymmetry and the displacement of the center by $\Delta \approx 9$ nm arises from the fact that the intermediate displacement was always performed towards positive side, hence the shift is only measured for approaches from the positive direction. From this data, one can see that the repeatability criterion of $R < 50$ nm is well accomplished.

Conclusion

We implemented an FPS3010 to automatically characterize the repeatability of an ECS3030 as a part of our quality control process. The simple and robust alignment of the sensor allows for direct integration in production as well as for high throughput in quality control.

More information can be found on www.attocube.com.

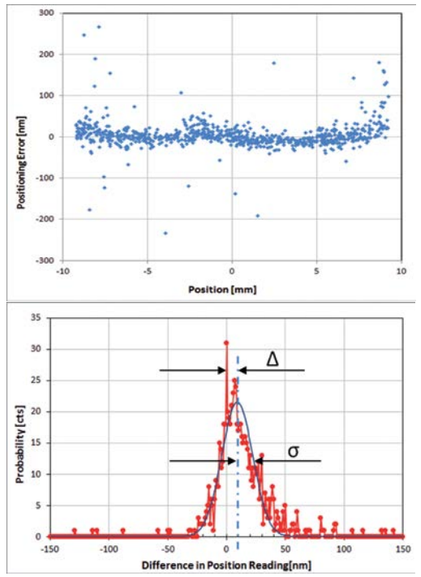

Figure 2: *Top: Difference in position measurement along the axis of an ECS3030 positioner. Each dot represents the position difference of two successive approaches towards the same position, measured using an external FPS3010 interferometer.*
Bottom: Histogram of the data. The standard deviation σ is evaluated numerically to 13 nm.

Laser Interferometry in Radiation Harsh Environments using the FPS3010

Markus Brugger, Mario Di Castro, Alessandro Masi, Roberto Losito
Engineering Department, CERN

Christoph Bödefeld
attocube systems AG, Koeniginstrasse 11a, Munich, Germany

Introduction

Synchrotron applications can nowadays be found in areas as diverse as biosciences (e.g. protein crystallography), medical research (e.g. microbiology), engineering (e.g. imaging of evolution of cracks with high resolution), and research on advanced materials (e.g. nanostructured materials). In many of these applications, highest resolution in the nanometer regime is desirable when positioning objects such as lenses, Bragg reflectors, slits, or targets. These mechanical setups should be compact and stable as to reduce thermal drifts and positioning errors. Additionally, the masses of moved parts should be kept low in order to improve the mechanical behavior, as well as to minimize positioning errors.

With regards to the applications discussed above, this means that position encoding has to happen in close vicinity of the moved objects, hence, encoders need to be placed inside irradiated areas, if not even on-axis with a focused X-Ray or particle beam.

attocube's FPS3010 laser interferometer featuring picometer resolution, compatibility with vacuum conditions, and remote readout electronics is the tool of choice for such applications. Here we show that the FPS3010 can operate under extreme radiation opening ways to use interferometric systems and subsystems close to synchrotron beams and beamlines, or other environments with high radiation.

Among the existing sensor portfolio, the "M12" sensor heads have been qualified for the operation in radioactive environments at radiation doses of up to 10 MGy. This study focusses on the radiation hardness of these new sensors under irradiation from a ^{60}Co source (1.17 MeV / 1.33 MeV γ- and 0.31 MeV β-rays). We demonstrate that the heads show no significant deviations in the readout during the irradiation of up to 3 MGy. In a second test the heads did not show any significant deviations in position when measuring the fixed target before and after irradiation of the sensor heads up to 10 MGy.

Setup

Two attocube UHV compatible M12-type sensor heads (one with an AR-coated lens and one without AR coating), connected to polyimide fibers were placed in the irradiation area at places with a dose rate of 1 Gy/s. Both heads were mounted in aluminum supports, which were expected to cause a position drift over temperature of 20 nm/°C. The cavities of 3 mm distance were built using radiation hard mirrors that were gold coated to avoid solarisation.

The FPS3010 controller was placed outside the chamber and located in a temperature controlled chamber located in a non-radioactive zone. The temperature stability inside the chamber was better than 1°C during the complete measurement cycle. The total cumulated dose at the end of the measurement was 3.024 MGy in water equivalent.

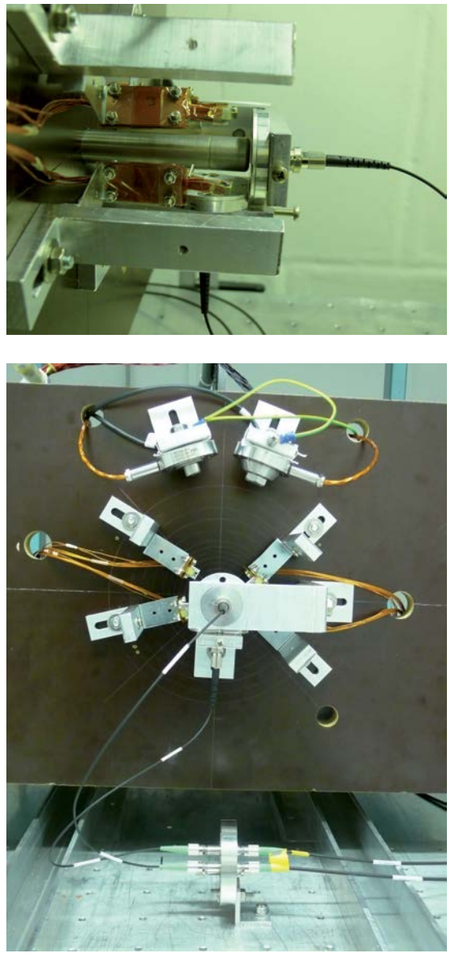

Figure 1: *Side and front-view of the setup. Upper Image: Side View. One sensor is positioned axially to the source, one sensor is positioned below the source. The source in the middle radiates homogeneously. Lower Image: Front View of the setup. Note the vacuum feed-through below the setup, which was also irradiated.*

Measurements

Figure 2a shows the measured positions during the measurement campaign. The sampling rate of the encoder positions was set to 1 kHz. Each point in the graph represents an average over 100 individual measurements. The position drift observed over the full period of 34 days and a cumulated dose of 3 MGy was only 150 nm with the coated sensor head and 400 nm with the uncoated one. The uncertainty of the positions (standard deviation) was always better than 10 nm, due to the fact that a good signal could be retained throughout the measurement.

On the non-coated sensor head, the drift increased a bit after 2 MGy of total cumulated dose (22.5 days). Until this point, the performance of the two sensor heads was comparable. The graph in Figure 2b shows the temperature drift at the encoder (red) and at the controller positions (blue) which was within 1°C during the whole time.

Summary

This note shows results of radiation tests on two attocube M12 sensor heads for the FPS3010 laser interferometer. The setup and installation were proven to be robust in terms of mechanical vibration, giving a position uncertainty of less than 10 nm over a measurement period of 34 days. The measured positions were stable within a few 100 nm during the whole time.

This qualification for radiation harsh environments opens up new applications and advancements. Measurement of beam collimator displacement, Laue-Lens position and many others in radiation harsh environments – inside the ultra-high vacuum assembly – become hence possible.

The work was accomplished by CERN and the radiation tests performed at the Fraunhofer Institute.

References

[1] S. K. Höffgen, M. Di Castro, *Co-60 Irradiation of Optical Sensor Heads*, Cern Report, EDMS Id 1337167 v.1, 2013.
See https://edms.cern.ch/file/1337167/1/

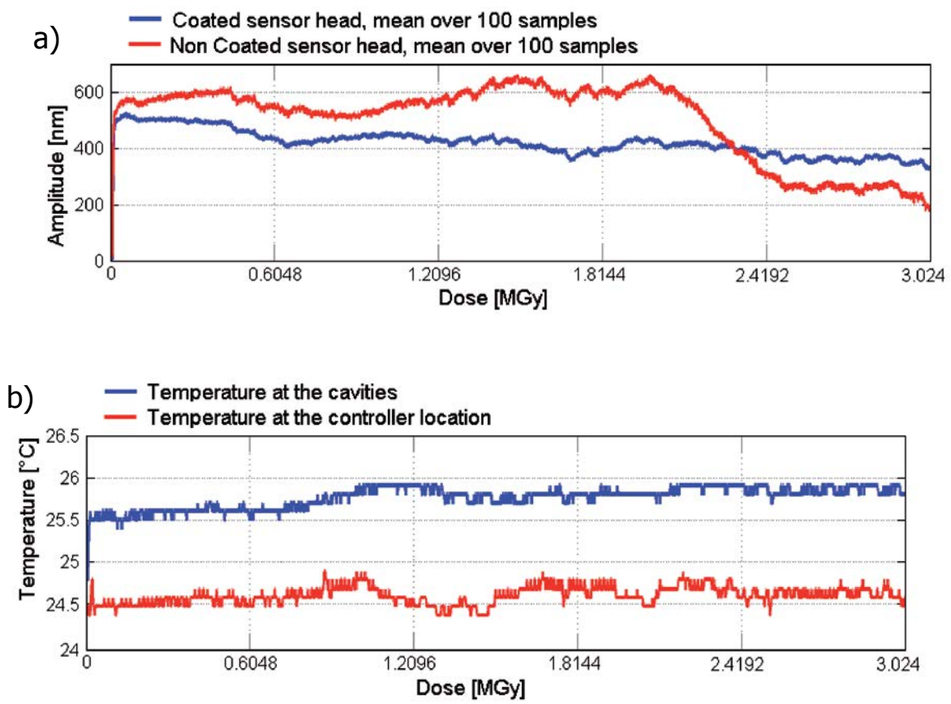

Figure 2: *a) Sensor heads comparison (34 days span). Each sensor position point is a mean over 100 samples.*
b) Measured temperature at the position of the encoders and in the chamber with the FPS3010 controller.

pioneers of precision

Long distance and high-speed displacement measurements using the FPS3010

Thomas Ch. Hirschmann, Klaus Thurner
attocube systems AG, Munich, Germany

attocube's fiber-optic based Fabry-Pérot sensor (FPS) interferometer allows the user to measure a target's relative displacement with sub-nm resolution and real-time position output at 10 MHz bandwidth. Various applications in industry as well as in science and research and development require the precise detection of a target's position at high velocities as well as long distances. As shown below, the FPS3010 is now able to measure displacements at distances of up to 1 m and velocities of up to 2 m/s.

In these tests, an FPS3010 interferometer was equipped with attocube's M12-type sensor head and a retroreflector as target. Figure 1 illustrates the setup including sensor head and reflector. To realize reproducible displacement measurements of the target a commercial linear motor stage was utilized. Moreover, by using a retroreflector instead of a plane mirror the alignment process was very fast: the reflector can be tilted by more than 4 degrees with respect to the detection direction without losing the signal. This is due to the geometrical construction of the reflector, which is based on three perpendicular mirrors. The high stability of the signal guarantees that the FPS3010 can be calibrated at any position along the full length, making it extremely user-friendly and easy to use.

For the first test measurement, the target was set at 1.0 m distance from the sensor head. This first measurement consisted of an oscillation of the target with 0.9 m displacement amplitude and velocities of up to 1.0 m/s. Figure 2(a) shows the position measurement and the derived speed of the target during this oscillatory movement.

Figure 2(b) depicts the measurement during a high-speed movement over a distance of 0.5 m with a velocity of up to 2.0 m/s. As can be seen from the blue curve, the maximum stage acceleration is limited: it needs more than 10 milliseconds to realize the speed of 2 m/s as well as another 10 ms to slow down before the programmed end position is reached.

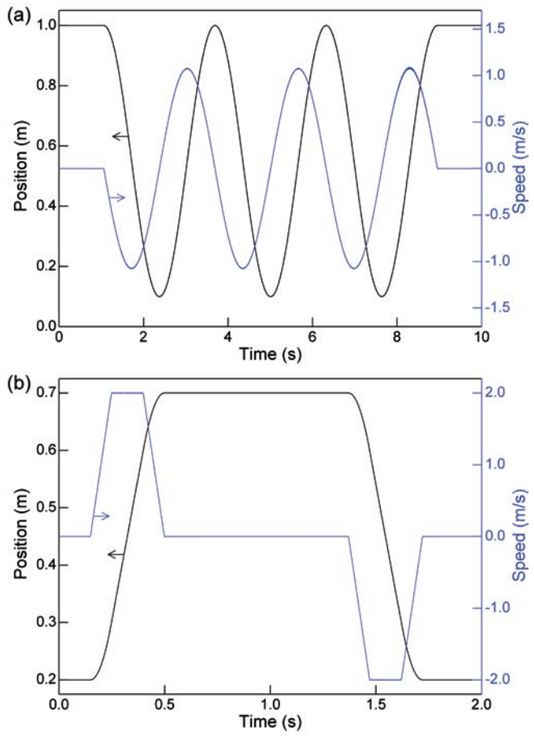

Figure 2: *(a) Displacement measurement of an oscillating target. The resulting speed was calculated from the position data. (b) Displacement measurement while moving the target with a maximum velocity of up to 2 m/s to different positions.*

This Application Note demonstrates the capability of the attocube's FPS3010 interferometer to measure displacements at large distances of up to 1 m with sub-nanometer resolution even at a target's velocity of up to 2.0 m/s.

For more information on the FPS3010, please visit our website: www.attocube.com.

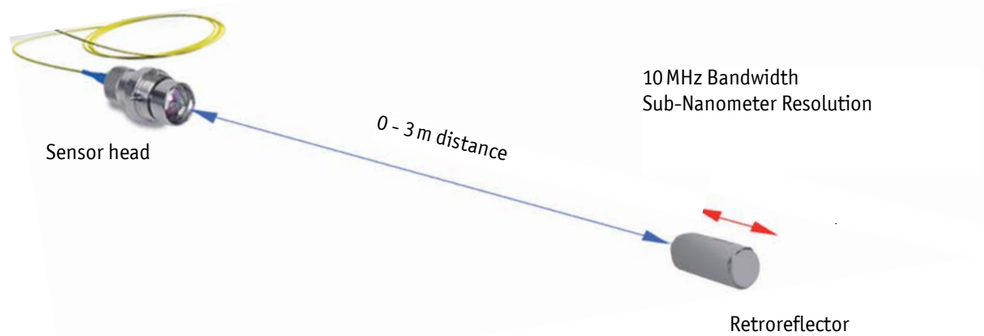

Figure 1: *Sketch showing the setup including attocube's M12 sensor head together with the retroreflector, which can be displaced with 2 m/s velocity over a distance of up to 1 m.*

Ultra precise contactless detection of bearing errors with the FPS3010

Pierre-François Braun, Matthias Handloser, Thomas Sieben, Markus Huber
attocube systems AG, Munich, Germany

Error motions of rotating objects are of major interest in high precision mechanical engineering. In case of a high speed spindle, even sub-nm deviations from a perfect rotation can create undesired vibrations or error movements. Monitoring error motion with sub-nm resolution is therefore of prime necessity from state of the art mechanical engineering to nanotomography research. The main challenge always remains: how to minimize the error motion? attocube's interferometric plug-and-measure solution now answers this unmet need!

In any application requiring the rotation of a mechanical part or sample with highest accuracy, the major problem is always the same: is the error motion of the rotation axis – see Figure 1 – well defined and known?

A typical application is to consider the concentricity of a drive spindle for manufacturing purposes: A shaft eccentricity directly creates imbalance. As soon as the mass and/or the rotational speed increases, not only the accuracy of the machined parts is jeopardized, but instrument instability may also lead to increased wear and tear. The same goes for nanotomography: a typical high resolution crystallographic analysis in a synchrotron requires perfect knowledge of the crystal center of rotation. Any errors or drifts lead to significant inaccuracies in data analysis [1].

To solve the issue, get to know it.

In order to eliminate inaccuracies, first they need to be characterized. The ideal measurement scheme exploits a non contact, compact, plug-and-play solution. Usually for linear displacement sensing, the first choice is an interferometric approach due to its long range, sub-nm accuracy. However, it typically requires flat target implementation whereas monitoring rotation means measuring on curved surfaces. Therefore, up to now, error motion characterization setups consist of invasive sensing solutions – e.g. capacitive sensing for nanotomography or even contact CMM characterization for mechanical engineering. Thanks to recent innovations, attocube further enlarges the traditional linear displacement interferometric sensing field to strongly curved surfaces.

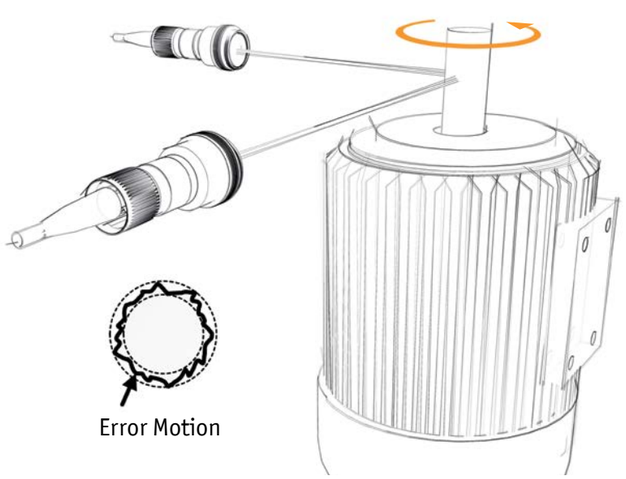

Figure 1: *Schematic setup for measuring error motions of a rotating object. A shaft is rotated while its error motion perpendicular to the rotation axis is simultaneously monitored by two interferometer heads. Note that different sensor heads are available for objects of different size.*

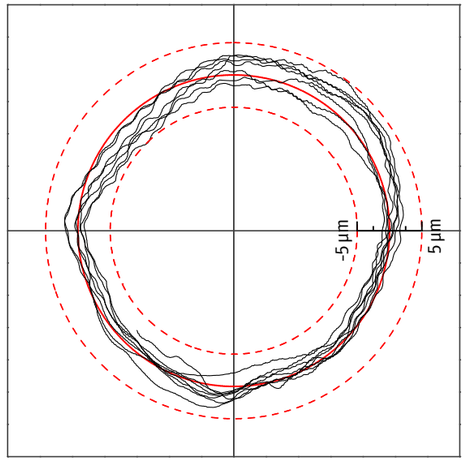

Figure 2: *Error motion (black) measured while rotating the cylinder, showing errors over µm range with sub-nm resolution. The central red line indicates the average position (corrected for eccentricity), while the dotted lines indicate an error of 5 µm each.*

attocube's non-contact sensing solution

In the following, the in-plane displacement of the 10 mm diameter shaft of an electromagnetic motor is monitored. On the drive shaft, a commercially available fine polished cylinder is mounted. Thanks to its high alignment angle tolerance, two attocube interferometric sensor heads are easily aligned and the characterization can start immediately. On top of that, the fiber based XS sensor heads allow *in situ*, space restricted, and extreme environment operation.

In this application, an electrical motor is driven at 2160 rotations per minute (RPM) and the two attocube interferometers measure the error motion of the cylinder perpendicular to the rotation axis. After correcting the data for the eccentricity of the rotation axis, synchronous and asynchronous errors can be directly characterized as in Figure 2.

attocube's FPS3010 user-friendliness finally opens up sub-nanometer error motion correction even to non-experts in interferometry. More detailed documentation on the attocube FPS3010 laser based interferometer system can be found at www.attocube.com.

References

[1] Jungdae Kim, *et al.*, Rev. Sci. Instrum. **84**, 035006 (2013).

Fiber based laser interferometry stimulating the development of highly precise micro manufacturing

Silka Grimske, Nanxi Kong
Helmut-Schmidt-Universität, Hamburg, Germany

Martin Zech
attocube systems AG, Munich, Germany

In micro manufacturing, ever increasing requirements for precision and size of machined parts have, in recent years, driven the development of highest-precision machining tools. A potentially highly rewarding approach is the so called "Square Foot Manufacturing", which is based upon the standardized usage of miniaturized, modular machining units. As every unit has to be working with highest precision, the interferometric measurement of positions and angles of moveable components is of utmost importance.

The mechanical tolerances needed in metal cutting manufacturing technology have reduced significantly due to very high requirements coming from the different application fields such as medical engineering, optics, bio-technology, fluidics, and (micro-) mould and tool making. Consequently, a new research field, analogous to precision engineering has emerged, with micro-machining technologies as its main focus.

A new potentially highly rewarding approach in this field of highest precision machining is being currently developed at the Helmut-Schmidt-University in Hamburg. The Square Foot Manufacturing (SFM) concept separates well-known machining centers into small-sized sub-groups (micro machining units - MMU) that can be combined in nearly any possible way. This separation allows not only for the integration of new production methods in the future, but, due to the small dimensions of the diverse MMUs, also allows for the use of materials and technologies that have not been used in such machining centers before, hence leveraging big advantages for production. The MMUs have standardized interfaces not only for power supply and data transmission but also for the transmission of processing forces and moments.

In this respect, a new mechanical interface was developed that enables reproducible mounting and exchanging modules such as machining tools. High frequency bearing spindles driven by pressurized air, laser heads, or grinding tools of a new kind may be connected to these interfaces (see Figure 1). To measure the reproducibility of these interfaces, attocube systems' miniaturized fiber interferometer FPS3010 was employed (see Figure 2). A special differential technique allows for precise characterization of translational and rotational errors, which, in this case, are better than 0.16 µm and 8.22 arc seconds (3 sigma) respectively.

Laser interferometry also plays a key role in the feed units of this concept: Instead of traditional positioners and spindle drives, a monolithic, piezo-based design with integrated flexure hinges is employed. In this way, the system can address up to 2300 × 1015 µm². The intrinsic reproducibility of the system is about 360 nm (open-loop), yet closed-loop operation with interferometric sensors promises to bring this down to a few nanometers.

More information on „Square Foot Manufacturing" can be found at www.hsu-hh.de/laft as well as in [1-4]. More detailed documentation on attocube systems' laser based fiber interferometer „FPS3010", that was recently recognized by the R&D100 award, may be downloaded from www.attocube.com/attoMETROLOGY/introduction.html.

References:

[1] S. Grimske, N. Kong, B. Röhlig, and J. P. Wulfsberg, Square Foot Manufacturing – Advanced Design and Implementation of Mechanical Interfaces, Proceedings of the 11th euspen International Conference, Como, Italy, p. 313 (2011).
[2] N. Kong, S. Grimske, B. Röhlig, and J. P. Wulfsberg, Flexure Feed Unit – A Progress Report, Proceedings of the 11th euspen International Conference, Como, Italy, p. 331 (2011).
[3] S. Grimske, B. Röhlig, N. Kong, and J. P. Wulfsberg, Repeatable Positioning Accuracy of Mechanical Interfaces for Micro Manufacturing, Proceedings of the 12th euspen International Conference, Stockholm, Sweden, p. 209 (2012).
[4] N. Kong, S. Grimske, B. Röhlig, and J. P. Wulfsberg, Flexure Based Feed Unit for Long Feed Ranges: Concept and Design, Proceedings of the 12th euspen International Conference, Stockholm, Sweden, p. 403 (2012).

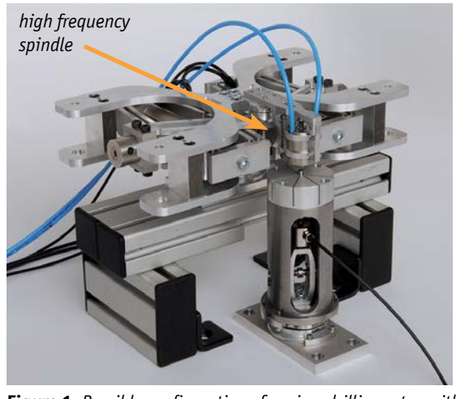

Figure 1: *Possible configuration of a micro drilling setup with a high speed spindle and miniaturized mounting brackets.*

Figure 2: *attocube's 3-axes real time interferometer, the FPS3010, features 25 pm resolution and a measurement bandwidth of 10 MHz. The fiber based measurement heads are available in sizes from 4 to 14 mm diameter dependent on the application. These heads are also compatible with ultra-high vacuum as well as cryogenic conditions.*

attocube systems AG | Königinstrasse 11a | D - 80539 München | Germany
Tel.: +49 89 2877 809 - 0 | Fax: +49 89 2877 809 - 19 | info@attocube.com
www.attocube.com

Application Note Brochure version: 2015 - 01